AN INVESTIGATION OF CTOL DUAL-MODE PAVE CONCEPTS

by

James F. Marchman, III, Nanyaporn Interatep, Eugene Skelton, and William H. Mason
Aerospace and Ocean Engineering Department
Virginia Tech, Blacksburg, VA

A REPORT TO NASA - LANGLEY RESEARCH CENTER

PERSONAL AIR VEHICLE EVALUATION PROJECT

NASA GRANT NAG-1-01100

Virginia Tech AOE Report 276

January 2002

TABLE OF CONTENTS

EXECUTIVE SUMMARY	3
INTRODUCTION	5
A Primary Roadability Consideration: 3 or 4 Wheels	9
SENSITIVITY AND CONSTRAINT ANALYSIS	10
PAVE Mission Requirements	10
Sensitivity Study	12
PAVE DESIGN RECOMMENDATION	13
Initial Weight Estimation for Redesigned Pegasus	14
Wing Design	14
Inboard Box-Wing/Winglet Concept	15
Outboard Wing Stowage Design	16
Outboard Wing Concepts	16
Lift Coefficient Calculation for the New Wing Concept	20
Power Selection	21
Pusher Propeller	22
Predicted Noise Calculation	24
Component Weight Analysis	25
Performance Estimates	26
ROADABILITY	27
CONCLUSIONS AND RECOMMENDATIONS	27
REFERENCES	29
FIGURES	30 - 38
APPENDIX A: Comparator Aircraft Performance and Sizing Data	39
APPENDIX B: Analysis of Comparator Aircraft	46
APPENDIX C: Roadability Evaluation from Reference 2	65

AN INVESTIGATION OF CTOL DUAL-MODE PAVE CONCEPTS

by

James F. Marchman, III, Nanyaporn Interatep, Eugene Skelton, and William H. Mason
Aerospace and Ocean Engineering Department
Virginia Tech, Blacksburg, VA

EXECUTIVE SUMMARY

A study was conducted to assess the feasibility of the dual-mode concept for a personal air vehicle, to determine how constraints differ between the dual-mode concept and a CTOL general aviation aircraft, to recommend a dual-mode vehicle concept, and to recommend areas where further research can contribute to the successful development of a viable PAVE vehicle design.

Beginning with the evaluation of 17 existing general aviation "single-mode" aircraft and of 4 dual-mode (roadable aircraft) concepts the study examined the sizing requirements for a PAVE vehicle and looked at the design revisions needed to make the Virginia Tech "Pegasus" dual-mode concept conform to the size and mission requirements established for the PAVE program. Narrowing the scope to the assessment of two existing and successful four passenger general aviation aircraft, the Cessna 182 and the Cirrus SR22, and to two dual-mode concepts, the resized Pegasus (Pegasus II) and the LaBiche design, the performance of these four vehicles was evaluated for the defined mission and sensitivity studies were done to better define the factors which must be optimized in a dual-mode design.

The results of this study are almost pre-ordained by the additional requirements placed on a dual-mode concept when compared to a single-mode general aviation vehicle. A dual-mode vehicle with four wheels must meet all DOT and EPA safety and emission requirements for automobiles and a three-wheeled vehicle is speed limited on the ground. Meeting the DOT and EPA requirements as well as satisfying the handling and stability needs of a highway vehicle results in a heavier vehicle than a comparable single mode aircraft. While this extra weight can be considerably offset with the use of modern light weight materials and construction techniques, the additional requirement for some means of folding, retracting, stowing, or towing wings and perhaps canards or tail surfaces also contributes to a heavier vehicle, especially if the transition between road and flight modes is accomplished with a motor driven automated system.

In addition to weight, a second constraint unique to the dual mode vehicle is a result of dimensional limits in size. U. S. and EU roadway width limitations specify vehicle widths under eight feet unless a "wide load" permit is used when on the highway. PAVE size limits were set at seven feet in order to fit a home garage. This essentially means that the wing for a dual mode vehicle has as its "base" a seven foot mid section width. Any wing span beyond seven feet must be folded, retracted, or removed and stowed in some manner to fit within the allowable 7' x 7' x 20' PAVE "box". Further, a PAVE program goal is to have any transition between highway and flight modes be automated.

The need for a unique wing design results in two constraints for a dual-mode concept. Either a very low aspect ratio wing/fuselage design must be employed, imposing serious aerodynamic performance penalties or a complex and heavy motor driven wing folding/retracting/stowing system must be incorporated into the design.

The primary conclusion/recommendation of this study is that a thorough evaluation of the wing design is essential to the optimization of any dual-mode PAVE design. As noted above, any dual-mode CTOL concept must have as the primary basis of its wing design a highly effective, low aspect ratio, inner wing. It is proposed that the "box-wing" design, shown by Kroo[1] to be an optimum non-planar wing configuration, be further evaluated as this base wing design. It is further recommended that the proper placement of a propeller at the rear of the forward (lower) component of the box wing can enhance the flow over that wing and improve its performance and that this needs to be evaluated in further research.

Since it is almost certain that a low aspect wing alone will not suffice in giving the desired performance for the CTOL dual-mode PAVE vehicle it is recommended that further research needs to be done to ascertain the best form of wing extension which can provide optimum synergy with the inner, box-wing configuration. The emphasis in this research should be the development of an outer wing which will result in the least complex, lightest weight flight-mode/road-mode transition requirement.

It is suggested that synergy between the outer wing and an inner box-wing arrangement is one in which the vertical stabilizer elements connecting the upper and lower box-wing segments are designed as winglets which utilize the inner/outer wing junction vortices to produce a thrust (often viewed as a reduction in induced drag). Further study should examine the best configuration for these vertical box-wing elements to optimize this "inboard winglet" effect.

It is obvious that the simplest design for any "outer" folding, retracting, stowing wing will be one which requires a minimum number of transition actions; i.e., a single fold, a single retracting segment. If automation of transition is sought this will result in the lowest weight design. However, it is also recommended that the lifetime cost of wing transition automation be evaluated since a non-automated transition will provide significant weight savings. Given the small fraction of total vehicle use time involved in the road/flight mode transition process and the penalties that the extra weight and complexity of an automated transition system would impose on the vehicle's flight mode performance we believe it is worth considering a manual transition concept design.

Finally, we have recommended a unique inboard/outboard wing design which can greatly simplify the road/flight mode transition process and result in a minimal wing weight if a manual transition process is utilized. This design is illustrated in the figure below.

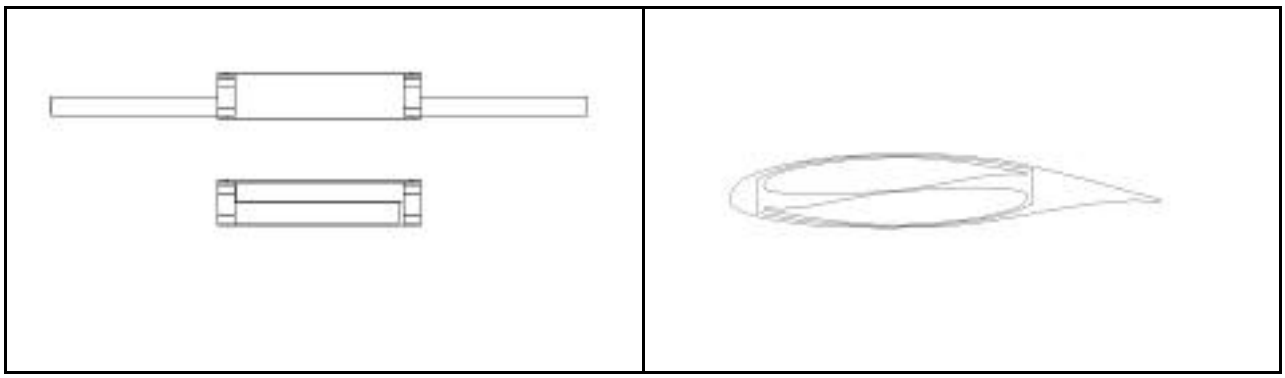

Figure 1: Inboard/Outboard Wing Stowage Concept

(Note: all other figures at the end of the text)

INTRODUCTION

The “flying car”, “roadable aircraft”, “personal aeronautical vehicle”, or “flying fliver” is a concept which has intrigued travelers since the advent of both the automobile and the airplane (Figure 2). Yet, despite the attempts of many, from crackpot backyard inventors to well financed major corporations, no such vehicle has ever succeeded in the marketplace. Many combination highway/skyway vehicles have reached prototype and even production over the last century but none have succeeded; however, people keep on trying to find the right combination of capabilities and cost which can make the flying car a commercial reality.

Inherent in this investigation is the perceived need for an individual mode of transportation which will carry its user from doorstep to doorstep over any desired journey at any time and in any weather in as little time as possible. The two factors which drive the quest for the flying car are the desires for individual freedom of travel and for minimal travel time from departure point to destination. There certainly exist other means of travel over both short and long distances, many of which involve combinations of personal transport and mass transport. It is then important to consider the extent to which these other modes of transportation ranging from walking, to bicycle, to automobile, to private plane, to bus, to train, to chartered plane, to ship, to airliner, might impact the need for some type of flying car. What does the potential traveler consider when assessing the best means of making a given journey?

Some of the considerations are the same now as they have been since long before either the car or plane existed. These are convenience, time, and cost. Two hundred years ago the choice was between going on foot (walking), riding an animal, or riding in a carriage or wagon pulled by animals. The time difference among these modes of transportation was not as significant as the factors of cost and convenience. The slightly faster time in route afforded by the horse or horse-drawn carriage or wagon was probably not as significant as the added ease of travel to those making the choice. But that added convenience came at a significant cost; the expense of housing, feeding, and caring for a horse or mule and possibly of owning a wagon or carriage. These factors played a strong role in stereotyping the chosen means of travel as an indication of social and financial status. This added cost included solving the problem of what to do with the animal and cart at one’s destination and caring for the animal along the way on longer journeys. If these costs or inconveniences were too great the traveler might opt for some means of “mass” transportation such as the stagecoach or later the train, in which the passenger paid others to do the work necessary for the upkeep of the transportation system. When faced with a need for travel one needed to make a choice between going on foot, riding or being pulled by one’s own animal, or paying the cost of traveling with others via coach, wagon, or train. The chosen mode of travel might depend on one’s personal wealth, the importance of the journey, and the convenience of the schedule of the public transit system.

The above factors have not changed significantly in the past 200 years even though the vehicles used for transportation and their speeds have changed greatly. For all but the shortest trips the choice of modes of travel today include the automobile (or motorcycle), the bus, the train, private aircraft, charter aircraft, and the airlines. If overseas travel is excluded, the automobile obviously offers the most freedom of movement, allowing the traveler to make the trip at any desired time and providing a valuable means of transportation at the point of destination. None of the other modes of travel offer these two advantages.

Busses, trains, and scheduled airlines may offer more comfort on a long trip than a car and the airliner offers more speed but the traveler must give up the luxury of travel on demand and must find a second mode of local transportation at his or her destination. And with some of these modes of public transport the traveler's desired departure point and destination may differ from the end points of the commercial system, necessitating the need for multiple modes of travel.

Charter aircraft and privately owned general aviation aircraft offer some of the speed of the commercial airlines, and their ability to operate from hundreds of smaller airfields may actually make the desired trip time shorter than that offered by the airlines while bringing the traveler closer to his or her actual destination. Still the traveler must get from home or office to the local airport and from the destination airfield to the destination itself, requiring the use of up to three vehicles for the trip. The use of general aviation aircraft also exposes the traveler to greater risk of delay caused by bad weather and the cost is substantially higher than that of traveling by commercial aircraft.

In general the choice of transportation mode depends on the length of the trip. Most would agree that for trips of 100 miles or less nothing beats the automobile, which can make the journey as quickly as any other mode and offers true door-to-door travel. For journeys of over 1000 miles the speed of the commercial airliner offers enough advantages to outweigh the multi-mode hassles of the trip for everyone who isn't fortunate enough to have access to a corporate jet.

The 100 to 1000 mile trip then is up for grabs. This is the range of trip where the general aviation aircraft could offer travelers some real advantages, provided its use was both convenient and affordable.

Cost and the "hassle" factor are probably the two major reasons that the vast majority of travelers would not even consider the use of general aviation aircraft for a trip. One can take a lot of round-the-world airline trips for the purchase price of a popular, single engine, GA aircraft. Just getting a private pilot's license can cost more than some new cars and with the money spent on the annual maintenance of a GA plane one could easily trade for a new car every year.

Even when one owns a general aviation aircraft it may not offer the most convenient means of travel on 100 to 1000 mile trips. Weather is without doubt the major factor in the "go" or "no-go" decisions of private pilots every time they plan a trip. There isn't a private pilot alive who hasn't spent hours agonizing over whether to fly or drive or cancel the travel plans when weather looks "iffy", or who hasn't spent many nights in strange motels waiting for unforseen weather to clear and permit the trip home. As the old saying goes, "flying is the quickest way to travel, provided you have an unlimited amount of time".

Conventional wisdom among private pilots who have instrument flight ratings and who thus think everyone else should also have one is that having this rating will take much of the unpredictability out of general aviation travel, but statistical evidence might show that the results aren't all that clear cut. Even with a well equipped GA plane the instrument rated pilot still must observe instrument minimums for airfields and he or she can only do that if legally "current" in instrument flight experience, a condition most instrument rated GA pilots probably do not meet. Also the requirement for instrument operations eliminates the use of many smaller airports with no established instrument approaches, and few GA planes and pilots are equipped or rated to allow operation in "zero-zero", Category III conditions open to many airliners. Further, GA flight over long distances also sometimes falls victim to lines of thunderstorms which will block even instrument rated flyers from reaching their destinations.

Hence general aviation finds itself between the proverbial “rock and a hard place” in trying to claim the 100 to 1000 mile trip as its natural operating territory. GA is a “fit” for this range of travel only for those wealthy enough to own a plane and have a pilots license and with enough spare time to allow travel on unplanned, alternate dates. For the other 99 % of the population the automobile, bus, regional airline, and, in rare cases in the United States, the train, must come to the rescue and these often provide a much more reliable and always less expensive means of travel than a general aviation airplane.

This is, however, the place where the flying car, roadable aircraft, or personal aeronautical vehicle, can potentially offer huge advantages over all other modes of travel. The roadable aircraft is a means of transportation which can be used for any trip regardless of the weather or airport location. Except in rare cases (earthquake, hurricane, flood, etc.) the user of a roadable aircraft can depart for a trip in any weather and at any time of day or night. If the weather at home is bad the trip can begin on the highway and then proceed by air from the most convenient airport en-route after the weather clears. In the case of bad weather en-route or at the destination an intermediate landing can be made and the trip completed or bad weather bypassed by road. Upon reaching the destination there is no need for a taxi or rental car. And one need never worry about being stuck hundreds of miles from home when making the return journey.

The roadable aircraft has the potential of, at long last, making general aviation a dependable means of efficient travel in the 100 to 1000 mile trip range. Why then have “flying cars” never caught on? Not because none have been built because many, including several relatively good ones, have been on the market over the past 100 years. The primary obstacles to successful roadable aircraft seem to have been cost of purchase and cost of ownership.

In reality, much of any potential market for roadable aircraft is voided by the need for a pilot’s license. With a couple of weeks behind the wheel with instruction from a friend almost anyone can learn to drive a car and earn their driver’s license, but it takes lots of money and determination to get a pilot’s license. Thousands of dollars are required to pay for ground instruction, flight instruction, airplane rental, a medical exam, and flight planning supplies and there are many long hours of frustration while waiting for an airplane and instructor to be available at the same time that the weather and one’s work schedule allows a lesson. Most who start lessons never finish and many who finish take years to complete the task. Even then, many, if not most who get their private pilots license will never use it for significant travel, preferring to use their ticket primarily for weekend joy rides around the local airport. Hence, of the millions of people who will make 100 to 1000 mile trips in any given week only a tiny fraction could take advantage of a flying car even if it was available and free.

Several aspects of the recent AGATE program and the successor SATS program have been aimed at solving some of the problems above. These include lowering the cost of aircraft and simplifying the pilot licensing process. Many people, especially present pilots, remain skeptical about the potential for success of these programs, noting that as long as there are strict and time intensive certification standards for GA aircraft and the lack of the economy of scale enjoyed by the automotive industry, airplane prices are likely to remain at or near present levels. And many would question the viability of the semi-autonomous flight capabilities required of GA aircraft for effective implementation of SATS plans.

Some of the proposals and experiments coming out of the AGATE program have been aimed at simplifying the licensing process and streamlining instruction or toward combining private pilot and instrument rating instruction into a single process. The goals of these proposals appear to be to encourage all private pilots to get an instrument rating as part of their initial licensing more than to reduce the cost or time required to become a licensed pilot. While these proposed instructional methods may well increase the percentage of instrument rated private pilots it remains to be seen if there will be any resulting increase in the percentage of the general population which actually become pilots. The trend in the last 40 years has been for a general decrease in the percentage of the population with a pilots license. At best these proposals may succeed at bringing the level of interest in flying among the general public back to the levels seen in the 1950's.

Aircraft acquisition and operating costs are the other big obstacles which must be overcome. For those who could make use of a roadable aircraft; i.e., licensed pilots, the question has always seemed to come down to the expenses of purchase and ownership, and the ability to get insurance at a reasonable price. Flying car designs have usually ended up being much more expensive to buy and operate than regular general aviation aircraft of comparable size and capability.

While some have speculated that owning a roadable aircraft is the equivalent of owning an airplane and a separate private car and, hence, that a vehicle costing the same as the sum of the two is reasonable, this is really not true. The owner of a roadable aircraft must still own a separate private car even though the aircraft can be driven on the highway. One is simply not going to drive the roadable aircraft to the grocery or the mall or to and from work. The $500 fender-bender accident in the mall parking lot too easily becomes the $50,000 repair job to the vehicle's retracted wing mechanism or propeller crankshaft. It is no wonder that both aircraft and automobile insurers have refused to insure flying cars in the past. Aircraft insurance companies know that operating the vehicle on the highway greatly increases the chance for an expensive accident (and every accident in an aircraft is much more expensive than one in a car). Automobile insurers also don't want to mess with cars that fly for similar reasons. The roadable aircraft enthusiast community must change its thinking about acceptable pricing and realize that for the flying car to be successful it must cost no more than a comparable GA aircraft. And the insurance industry, perhaps with government backing, must create a special category of coverage which perhaps limits the highway use of such vehicles to travel which is tied to a flight.

Another factor dictating that the flying car not be used for everyday road travel is the vast difference in usable lifetimes of aircraft and cars. The average lifetime of an aircraft is up to ten times that of a car, but if the aircraft is operated like a car its lifetime will be greatly reduced, making it an unwise long term investment. Most aircraft owners would not want their on-the-road engine use to count against their TBO time for an aircraft engine. It is to the owner's advantage to limit the roadable portion of vehicle operation to the minimum needed to facilitate trips by air.

The conclusion that one must draw is that the roadable aircraft may well be the answer to the problem of making general aviation an attractive option for 100 to 1000 mile personal travel. However, the cost of vehicle purchase and long term ownership, including insurance, and the hassles of earning a pilot's rating continue to limit this opportunity to a very small percentage of the population. This becomes a classic "chicken and egg" problem. There won't be more GA pilots until the cost of ownership comes down and the cost of ownership won't come down until more people become pilots.

The proven formula for manufacturing costs is that the selling price of a product is cut in half for every tenfold increase in production. Hence, if a company now makes 500 airplanes a year (a very big number by today's standards) and the plane costs $200,000, to get the cost of the airplane into the range of even a very expensive automobile, say $50,000, the company would have to manufacture some 50,000 planes a year. And, after that there would have to be someone to insure them at a reasonable cost. This is a tall order indeed!

This report seeks to examine some of the technical and performance factors which must be tackled in designing a roadable aircraft or personal aeronautical vehicle, especially those factors which will ensure that the roadable aircraft will be able to at least match the performance of comparable general aviation airplanes. It also examines the requirements for acceptable on-road operation. The report will conclude with a recommendation for a concept vehicle based on the "Pegasus", a roadable aircraft conceptual design developed by a team of undergraduate students at Virginia Tech and Loughborough University (UK) which was selected as the winner of the 2000 NASA/FAA General Aviation Design Competition[2].

A Primary Roadability Consideration: 3 or 4 Wheels

Prior to examining the factors which will affect the design of a roadable aircraft from a flying perspective it is appropriate to take a brief look at an important issue related to the on-the-road operation of the vehicle. The primary issue here is whether a roadable aircraft will have four wheels or only three. Most aircraft have three wheels while all cars but an occasional automotive oddity have four wheels. There are significant advantages to the designer of a roadable aircraft in creating a vehicle with three wheels instead of four in that the three wheeled road vehicle is legally classed as a motorcycle rather than as an automobile. Motorcycles are exempt from many of the safety and environmental regulations which currently apply to automobiles, and these requirements inevitably add significant complexity and weight to the four wheeled vehicle. As a result, some current designers of roadable aircraft have chosen to limit their designs to three wheels.

The penalty one pays with a three wheeled road vehicle is primarily found in the automobile's turning capabilities and stability. In many ways the three wheeled automobile is simply not as safe as the four wheeled vehicle and this lack of safety would probably be accentuated when the vehicle is operated at highway speeds by someone who normally drives a regular four wheeled car. For this reason, laws have limited the speed of 3-wheelers and many researchers and designers have ruled out the three wheel option, preferring to pay the weight penalty of the extra wheel and of meeting the added DOT and EPA requirements to ensure that the operator of the roadable aircraft will have a vehicle with familiar and safe on-road handling.

Before the three wheel option is rejected out of hand, however, one should examine the capabilities of modern automated stability augmentation systems to transform the three wheeled vehicle's handling characteristics into the familiar feel and safety of a four wheel system. The cost and weight of such a stability augmentation system may only prove a fraction of those of going to a four wheel vehicle design.

Nonetheless, the requirements of this study were to look at four wheeled concepts and that is what follows.

SENSITIVITY AND CONSTRAINT ANALYSIS

The first phase of our work was to review the performance specifications and calculations for four CTOL vehicles, two roadable vehicles and two conventional aircraft. A wide range of general aviation aircraft and roadable aircraft were initially examined. The conventional aircraft assessed included the Cessna 172, Cessna 182, Cirrus SR20, Cirrus SR22, Lancair Columbia 300, Diamond DA40 180, Luscombe Spartan Model 11E 185, Luscombe Spartan Model 11E 210, Piper Archer III, Piper Warrior III, Piper Arrow, Socata Aircraft Tampico, Socata Aircraft Tobago, Tiger AG-5B, Commander 115, Mooney Eagle 2, and the Mooney Ovation 2. Data for all of these aircraft are given in Table 1 of Appendix A. Four proposed dual-mode vehicles or roadable aircraft were initially examined: the Virginia Tech Pegasus, the Aeromaster Innovations Synergy, the AFA Sokol A400, and the LaBiche Skycar. Data for these are also shown in Appendix A in Table 2.

All of the above single and dual-mode vehicles and concepts were examined using conventional aircraft performance analysis methods and equations. These methods are described in Appendix B.

Based on our analysis of the above vehicles or concepts and information given us about another dual-mode concept design, the LaBiche flying car[3], and the limited time available for this project, the scope of our study was narrowed to an examination of four vehicles, two conventional GA aircraft and two dual-mode concept proposals, all of which were capable of meeting or exceeding the defined PAVE performance and mission requirements. The selected vehicles were the Cessna 182, the Cirrus SR22, the LaBiche flying car, and the Pegasus II flying car. The Pegasus II is an 87% scale modification of the original Pegasus design with a redesigned outboard wing and wing stowage system and with an engine based on the GAP turboshaft engine.

PAVE Mission Requirement

The mission specified for the PAVE study consisted of the following requirements and flight segments:

- Range 400 nm
- Loiter 45 min
- Takeoff/landing distance to clear 50 ft 3000 ft
- Payload 800 lb
- Cruise Speed >100 kt
- Dimension restriction (highway mode) 7’ x 7’ x 20’
- FAR 23 and FMVSS part 571 compliance

The required flight performance requirement is illustrated in Figure 3.

The only requirements above which represent a significant challenge to the aircraft designer are the restricted vehicle dimensions set for on highway use and compliance with the motor vehicle regulations. The size limitations essentially dictate either a very low aspect ratio wing design or a concept in which the wing(s) is (are) folded, rotated, or collapsed to a stowed position or detached and towed for highway travel. This requirement has, since the advent of flight, represented the most interesting challenge to the dual-mode vehicle (flying car) designer and the publications such as that of Palmer Stiles[3] provide interesting documentation of the myriad approaches to the solution of this problem.

Motor vehicle regulations which impose constraints on the dual-mode aircraft designer include requirements for crash protection (airbags, bumpers, etc.) and environmental emissions restrictions, all of which essentially present a weight penalty.

Perhaps a more difficult obstacle than the motor vehicle requirements for the designer is the difference in the needs for longitudinal stability between road vehicles and aircraft. This is essentially an issue of center of gravity placement relative to the wheels (landing gear). In a road vehicle the ideal is for the center of gravity to be mid-way between the front and rear wheels with a long wheel base (distance between front and rear wheels) desirable for a comfortable ride and stability. For an aircraft the center of gravity is normally placed near the vehicle's aerodynamic center and slightly behind the center of lift for positive pitch stability and good handling in flight and placed slightly in front of the rear or main landing gear on a typical tricycle gear aircraft or slightly behind the main gear on a "tail-dragger" design. Such placement of the center of gravity on an aircraft allows easy rotation (increase in wing angle of attack) for takeoff. These are therefore, conflicting requirements. A good "car" design in terms of *CG*/wheel placement may make an aircraft impossible to rotate for takeoff if normal aerodynamic methods for rotation are employed. A good airplane *CG*/wheel placement will result in a vehicle which is very difficult to handle and perhaps dangerous on the highway, particularly if flow over the vehicle tends to lift its front end (the classic Corvair problem). This problem was addressed in the Pegasus' redesign, as it has been by others, with a variable height front suspension used with conventional automobile placement of the vehicle's wheels.

Details of the Pegasus' redesign and vehicle specifications will be presented in a later section of the report, following this review of the sizing and sensitivity analysis. The above discussion, however, reflects the central issues which come to the forefront in a sensitivity analysis of dual-mode vehicles. A dual-mode vehicle design will probably differ from a conventional aircraft in the following ways:

- A dual-mode vehicle will probably weigh more than an equivalent conventional aircraft.
- A dual-mode vehicle will probably be limited in takeoff rotation capability.
- A dual-mode vehicle will probably have a limited wing span and aspect ratio.

All three of the above factors will increase the takeoff distance required for the dual-mode vehicle compared to a conventional aircraft and the first and third of these factors will decrease climb rates, cruise distance, and glide distance.

To look at these factors calculations were performed using standard aircraft performance relationships for the four vehicles mentioned earlier (C-182, SR22, LaBiche, Pegasus II) to look at predicted performance for the defined PAVE mission and sensitivity studies were conducted looking at the effect of ten-percent variations in such things as engine power, specific fuel consumption (SFC), maximum lift coefficient (C_{Lmax}), vehicle empty weight, and the vehicle's zero lift drag coefficient (C_{D0}).

Table 1 shows the calculated performance of the four vehicles for the specified PAVE mission. The "gross weight" given in the table is not the maximum gross weight but is the weight with the specified 800 pound mission payload and including enough fuel to fly the specified 400 nautical mile mission. It is seen that the two dual-mode vehicles perform comparably to the two conventional aircraft and that all meet the mission requirements. The LaBiche vehicle has a higher cruise speed

and rate of climb due to a significantly larger engine power than the other aircraft. The Pegasus II also has a high rate of climb resulting from its large engine but its smaller aspect ratio wing and increased induced drag limits its cruise speed more than the LaBiche wing. The higher (nearer the FAR limit) stall speeds for the dual mode vehicles result from the use of stall speed as a constraint on wing area and the desire to limit the wing area on these designs.

TABLE 1

	Pegasus II	**LaBiche**	**SR22**	**Cessna 182**
Gross Weight (lb)	2766	3440	3285	2945
Takeoff Distance (ft)	1033	1272	1380	975
Landing Distance (ft)	1730	1511	1451	1096
Stall Speed (kts)	60	61	58	48
Cruise Speed (kts)	180	258	185	137
Rate of Climb (fpm)	2259	2638	1400	924

All tabulations based on 400 nm range and 800 lb payload.

It should be noted that the LaBiche takeoff distance reflects its claimed ability to accelerate on the ground using wheel drive as well as propeller thrust. Achieving this requires a drive coupling system capable of transferring power as needed from wheels to prop or visa-versa. Other dual-mode vehicle designers have proposed doing this using systems such as those used on all-wheel drive automobiles which claim to transfer power to the wheels that need it, as required. However, the use of such a system in an application where virtually 100% of the power must be transferred instantly from wheel to prop on liftoff, or of more concern, from prop to wheels on touchdown in landing remains unproven.

Sensitivity Study

A sensitivity analysis was performed to try to better understand the role of typical design parameters in the performance of conventional and dual-mode vehicles. For clarity, the results of this study will be presented only for the higher performing conventional design, the Cirrus SR22, and for the Pegasus II. As mentioned above, five design factors were examined, the vehicle empty weight, the engine power, the zero-lift drag coefficient, the specific fuel consumption, and the maximum lift coefficient. The study looked at the effect of varying each of these factors by 10% with reductions in C_{D0}, empty weight, and SFC, and with increases in power and C_{Lmax}, all of which should result in performance improvements. It was hoped that this study would reveal whether a dual-mode vehicle is any more sensitive than a conventional aircraft to any of these factors. The results are shown as bar graphs in Figures 4 - 7.

Figure 4 shows the effect of the above 10% variations on the takeoff ground roll for the two vehicles. The results are not surprising in that they show takeoff distance to be more dependent on empty weight, power, and maximum lift coefficient than the other two parameters. The primary conclusion is that for the dual-mode Pegasus II the takeoff ground run distance is less sensitive to variations in weight, power, and C_{Lmax} than for the SR22.

Figure 5 examines the effect of 10% changes in these same parameters on stall speed. Of course, only empty weight and C_{Lmax} will have any effect on stall speed and the calculations show that the SR22 would benefit much more from an increase in C_{Lmax} than the Pegasus II.

Figure 6 looks at cruise speed sensitivity to changes in these same five factors. Obviously the maximum lift coefficient has no effect on cruise speed and, as expected, the most sensitivity was to C_{D0} and engine power with the Pegasus II exhibiting higher sensitivity to these two factors than the SR22. Interestingly, the cruise speed is much more sensitive to changes in empty weight with the Pegasus than for the SR22.

Figure 7 also shows the rate of climb of the Pegasus II to be more sensitive to changes in all relevant parameters than the rate of climb of the SR22, with the greatest effects seen for changes in empty weight and engine power.

It appears that the differences in performance related sensitivities between the SR22 and the Pegasus II are due primarily to the smaller wing span (aspect ratio) of the latter vehicle. The Pegasus II performance also appears more sensitive to weight even though it is a relatively light weight dual mode concept. These are not unexpected results. Vehicle weight impacts almost all aspects of aircraft performance and decreases in aspect ratio result in increased induced drag which also impacts many aspects of flight, especially those such as climb which require increased lift. The reduced wing span of the Pegasus is the result of the need to collapse or fold the wing in the road mode to meet width requirements and of the desire to greatly simplify the wing design needed to meet this constraint.

These sensitivities are also evident in a constraint analysis comparison of these same two vehicles shown in Figure 8. This constraint diagram, based on the defined 400 nm mission requirement shows that the single mode (SR22) constraints are easier to meet.

These analyses show that the selected dual-mode vehicle concept, the Pegasus II, can operate competitively with conventional general aviation aircraft, even when compared to new technology designs such as the Cirrus SR22. We will now take a look at the Pegasus II design and the factors and innovations which we believe enable it to be a successful dual-mode vehicle.

PAVE DESIGN RECOMMENDATION

Since the Pegasus roadable aircraft[2] was the basis for our being part of the PAVE project it seemed reasonable that we begin our study with that design. The Pegasus was the result of an undergraduate student design project collaboration between Virginia Tech and Loughborough University (UK). This collaboration was between the Department of Aerospace and Ocean Engineering at Virginia Tech and the Department of Aeronautical and Automotive Engineering at Loughborough and made use of the automobile expertise of the latter institution which has a close relationship with Ford, UK. The resulting design won first place in the 2000 NASA/FAA General Aviation Design Competition. This design was shown in Figure 9.

The Pegasus design had several unique features which enabled it to meet the need for flying performance comparable to competitor GA aircraft and to simultaneously meet all US and EU automobile requirements. In this study it seemed desirable to continue to employ these features in a PAVE concept. There were also questions raised about the Pegasus design which needed to be addressed in this project. Primary among these were concerns about the structural integrity of the

telescoping wing system and the flowfield seen by the pusher prop. The latter concern relates to both the effectiveness of the propeller in generating thrust and the noise generated by the prop.

The guidelines established for the PAVE project also required a downsizing of the vehicle from the Pegasus design. The Pegasus dimensions met all US and EU vehicle size limitations but the PAVE guidelines were more restrictive. Hence the design was revised to meet these guidelines and all issues related to that downsizing were addressed.

Figure 10 shows the design for the Pegasus II, our PAVE concept recommendation. The new configuration meets the 7' x 7' x 20' limitation of the PAVE program and presents a slightly reformulated shape for the vehicle while still retaining the basic features of the original Pegasus. It should be noted that the outboard wings of the Pegasus II are not segmented like the original Pegasus wings. The redesign of the wing stowage system for the vehicle represents an important change in the design and the exploration of a new two piece wing stowage system for which a Patent application is being prepared.

Initial Weight Estimation for Resized Pegasus

Typical initial aircraft weight estimations are based on statistical data from existing airplanes. Nevertheless, despite all the curve regressions between the takeoff gross weight (TOGW) and required empty weight (REW) provided in several databases, none matches the roadable aircraft category since there are insufficient samples to assess these weight trends. Hence, a first approximation for the weight estimation for the Pegasus II is found by considering the variation of structure weight as a function of volume. Starting without any change in the configuration, downsizing the vehicle to 87% of the original would decrease its weight to 66%. It was assumed that the engine used and hence its weight was unchanged from the original design.

$$REW = \left[\left(W_O - W_{EO} \right) \times \gamma^3 \right] + W_{EN} \qquad (1)$$

where

REW	required empty weight, lbs
W_O	original empty weight, lbs
W_{EO}	original engine weight, lbs
W_{EN}	new engine weight, lbs
γ	reducing size factor

This weight estimation, 1533 lbs, provided a starting point for performance calculations and configuration development.

Wing Design

Without a doubt the most significant distinction between a CTOL single-mode and dual-mode vehicle (airplane and roadable aircraft) is the need to restrict the wing span for highway use. This must be done either by employing a very low aspect ratio wing or by in some way folding, detaching and towing, or retracting part of the wing if the vehicle is to remain a single unit in all modes of travel (i.e., unless part of the vehicle is to be left at the airport). History shows a wide variety of systems which have been devised to meet this requirement[3]. Although many of these past wing span reduction systems have required manual transition from road to flight mode or visa-

versa, there is a natural desire to automate such a device even though automation inevitably results in much higher weights.

The original Pegasus wing design was unique in that the wing is composed of distinct inboard and outboard wing sections. This concept is retained in the Pegasus II design but the mechanism for stowing the outboard wing section is completely redesigned.

The inboard/outboard wing design is the result of the need for a vehicle which will meet the width requirements for highway travel. In the Pegasus design the team decided to employ a unique inboard wing design and to combine this with a smaller outboard wing section. The telescoping wing design proposed with the Pegasus is one which has appeared in several forms before[3] but is also one which inevitably raises questions about its structural integrity and weight.

Let us first examine the inboard wing concept which is retained in the Pegasus II design.

Inboard Box-Wing/Winglet Concept

The inboard section of the Pegasus and Pegasus II wings was designed to utilize several concepts brought together to provide a synergy which would enhance the performance of the vehicle. The inboard wing is really part of a small aspect ratio, box-wing configuration combining wing and horizontal tail and vertical stabilizer/rudder/inboard winglets. These elements also enclose the vehicle's pusher prop, providing both a noise shielding effect and enhanced flow over the wing due to the propeller flow.

Past studies by Kroo[1] have shown that the box-wing configuration is superior to almost any other non-planar wing arrangement in spanwise efficiency. The closest non-planar wing concept to the box configuration in spanwise efficiency is the "c-wing" which is essentially a winglet-on-winglet design that doesn't offer the structural integrity of the box wing. This advantage in spanwise efficiency is important because of the small span of the inboard wing. The box-wing represents a way to optimize the performance of a wing that is, of necessity, very low aspect ratio.

In addition to the box-wing efficiency, the Pegasus and Pegasus II inboard wing design employs a slight twist in its vertical sections which allows those sections to act as winglets which further enhance the performance of the inboard wing. A low aspect ratio wing has more intense vortices than a more conventional wing and even though an outboard section of wing will be added to the inboard wing for flight, there will still be a significant vortex shed at the inboard/outboard wing junction. The inboard winglet provides a means of using the energy in these wing junction vortices to enhance the performance of the vehicle. In the design report on the original Pegasus[2] calculations were presented analyzing this winglet-induced performance enhancement and showing it to give improvements of 5.5% in lift-to-drag ratio. This important feature of the Pegasus design was retained in the Pegasus II and the calculated performance enhancements were included in the assessment of vehicle flight capabilities.

The placement of the propeller within the box wing enclosure also provides at least two benefits over normal propeller placement. The propeller will induce increased flow speeds over the inboard wing's upper surface, enhancing its lifting capabilities at low vehicle speeds and reducing the wing area and extent of flap deflection or auxiliary circulation control needed for takeoff.

The box wing's partial enclosure of the propeller also helps lower the noise footprint of the propeller and engine. Covering the relevant surfaces of the wing and inboard winglets/vertical

stabilizers with appropriate sound absorbing materials offers the opportunity to further reduce the takeoff and in-flight noise, an important environmental consideration.

Outboard Wing Stowage Design

One questionable aspect of the original Pegasus design was its use of telescoping outboard wings. While there are other options for the removal, stowing, folding, towing or otherwise dealing with the need to eliminate these wings for on-road use of the vehicle, the completely automated stowage concept of telescoping wings was attractive to the Pegasus student design team. Unlike the obvious options of either folding the outer wings along the side of the vehicle or of removing and stowing them over or under the fuselage or of towing them on a trailer, the internally stowed outboard wings appeared to be an option which would appeal to buyers. On the other hand it is obvious that such a system is going to add considerable weight and complexity to the vehicle and the structural integrity of any telescoping system is one of the first things questioned by any engineer who looks at the design. The fact that telescoping wings have been analyzed structurally in the past and that several such concepts have been patented does little to allay such concerns.

Outboard Wing Concepts

In the re-examination of the Pegasus design, several alternatives to the telescoping wing system were studied. The following outboard wing concepts and their means of transition from flight to highway mode were briefly assessed.

1. *3-section Telescoping Wing* – A reduction in telescoping sections by one to simplify construction and operation.

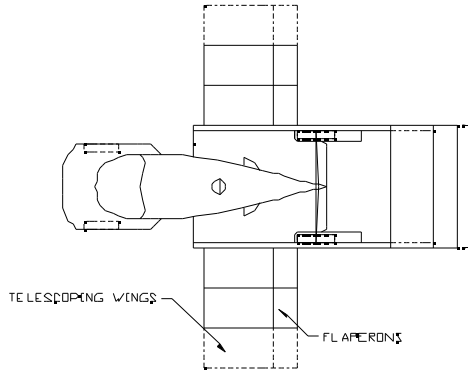

Figure A: Telescoping Wing Concept

1. *2-section Telescoping Wing* – Similar to the 3-section concept, another alternative if its smaller wing area is enough to carry takeoff gross weight.

1. *Overlap Wing* – The idea is for one side of outboard section slides into the inboard wing section while the other folds underneath the fuselage.

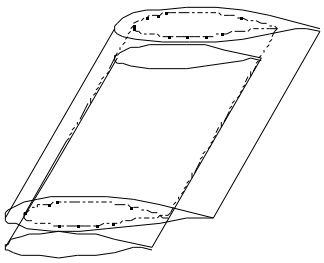

Figure B: Overlapping Wing Concept

1. *Half-half Wing* – Both outboard wing sections, having a span approximately half of inboard wing span entirely retract into inboard wing.

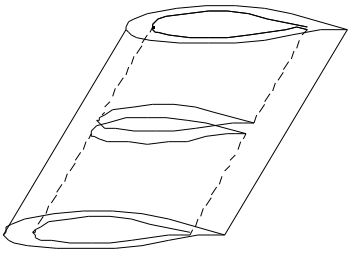

Figure C: Half/Half Outer Wing Concept

1. *Folding Wing Concept* – Wing sections are folded parallel to a fuselage and attached to tail section. This idea, however, proves to be unsuitable for the Pegasus configuration.

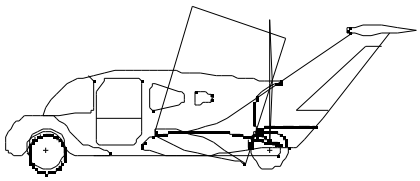

Figure D: Folding Wing Concept

Table 2 indicates results of performance evaluations for the first 4 concepts above. The problems with all of these low wing span and area concepts are that the resulting stall speed is somewhat too close to FAR part 23 requirements and increased engine power is needed to overcome increased induced drag.

Table 2: Variations of Outboard Wing Concept and Performance Results

Description	3 section telescoping wing	2 section telescoping wing	Overlap concept wing	Half-half concept wing
Takeoff gross weight (lbs)	2446	2450	2446	2493
Fuel weight (lbs)	239	270	238	314
Wing area (ft^2)	110.55	89.20	111.45	87.97
Engine HP	250	250	250	250
Wing loading (lb/ft^2)	22.1	27.5	21.9	28.3
Power loading (lb/hp)	9.8	9.8	9.8	10
Takeoff ground roll (ft)	637	824	631	875
Takeoff with 50 ft clear (ft)	1309	1408	1306	1588
Landing ground roll (ft)	596	724	591	742
Landing with 50 ft clear (ft)	1329	1638	1319	1820
Service ceiling (ft)	22283	16593	22503	11290
Absolute ceiling (ft)	23645	17764	23873	12331
Max cruise at 80% power (kts)	165	160	165	(Not enough HP)
Stall speed w/flap at sea level (kts)	54	61	54	62
Stall speed clean at cruise alt. (kts)	69	77	69	79
Max rate of climb (fpm)	2011	1673	2023	1258

An examination of these concepts led us to believe that an entirely new outer wing concept was needed. The resulting outer wing stowage system developed to replace the telescoping wing is, we believe, unique in its simplicity both in design and in user utility. We are, hence, in the process of applying for a patent on the concept.

This new outboard wing stowage concept represents a complete reversal of the reasoning behind the original choice of a telescoping outer wing. Instead of complete automation and its accompanying complexity and extra weight, the new concept allows a much lighter wing and vehicle and relies on a very simple, manual system of outer wing removal, stowage, and attachment. With this new design we are able to realize significant weight savings over the original system at the cost

of a few minutes of manual labor. The only other “penalty” of this design is a limitation in outboard wing chord and span imposed by the maximum on-road vehicle width and the stowage volume available in the inboard wing section.

The new “inboard/outboard” wing stowage design is shown in Figure 11. The outboard wing sections are designed to be manually inserted in a vertically stacked arrangement for stowage inside the enlarged structural wing box of the inboard wing. At the wing junction end of each of the outboard wings there is a larger section shaped to completely fill the inboard wing tip stowage opening and to extend far enough into that opening in the in-flight configuration to easily handle the aerodynamic loads of the outboard wing. The moments from the spanwise load on the outboard wing sections are transmitted to the inboard wing box via the close fitting junction box of the outboard section and/or through other attachment devices such as bolts, screws, or even simple latches which are also used for proper positioning and laterally securing the outboard wings for flight. As seen in the figure, the resulting outboard wings have a semi-span of slightly less than the width of the inboard wing.

The main inboard wing has 7-feet span to meet the width requirement for the vehicle in road mode and 8.5-feet chord with a GA(W)–1 airfoil untwisted section. Its main structural elements, being different from conventional wing structure[2], enclose a box in which the outboard sections are stowed. The permissible inner wing box size placed a constraint on the span and chord of the outboard wings. As a result, a 13-percent thick airfoil, GA(W)–2 section was selected to give the outboard wings which are as thin as possible and still create impressive aerodynamic characteristics. This gave an outboard wing semi-span of 5 feet and a chord of 5.2 feet. Unlike the telescoping wing concept, the outboard wing stowage concept has only one outboard segment on each side. The inner end of the outboard wing section is a one-foot span (width) structure that fits into the junction box of the inboard wing and transmits loads from the outboard section to the inboard wing box. During the road mode vehicle operation, each outboard wing is manually pulled out, reversed in spanwise direction, and inserted into the inner wing box in the position indicated in the side view of Figure 11 with one outboard wing inserted upside-down. In road travel the outboard wings are completely concealed inside the inner wing box. The conversion would only take a short time and is easily done by one person unless there are significant winds.

This design limits the ultimate span of the total wing to slightly less than three times the roadable width of the vehicle, but any resulting loss in aspect ratio compared to telescoping wing systems is more than compensated by its much lighter weight. The outboard wing sections, made of light-weight aluminum, will weigh less than 40 pounds each, easily handled by most adults.

During the PAVE review two questions were raised about this design. One concerned the manual transition requirements citing a PAVE program desire for automated transition between road and flight vehicle configurations. The other question related to the difficulty of performing the transition on a windy day.

There is no question that a totally automated system for flight/road transition would be desirable. There is also no question that any such system is going to be complex, heavy, and expensive, imposing significant performance, handling, and operational cost penalties when compared to a very simple manual system.

We believe that this combination of the inboard “box” wing design, inboard winglets, and a simple, stowable outboard wings is uniquely suited to PAVE designs and deserves further study and

development even though its transition between highway and flight modes is not automated. The further study should include an assessment of lifetime cost differences between manual and automated wing transition systems to evaluate the true costs of automated convenience which may be more than many people realize.

Lift Coefficient Calculation for the New Wing Concept

As stated above, this new wing concept used a GA(W)–2 airfoil. It was chosen for the outboard sections so that the wing can be properly inserted in the inboard section and still have sufficient wing area. These 3 segments of wing, an inboard and 2 outboard wings, were integrated to produce the main lifting surface for the vehicle. To analyze the aerodynamic performance of this wing combination 2 assumptions were made for lift coefficient prediction.

1. The lift distribution of the inboard section was considered to resemble that of a 2-dimensional airfoil due to the effect of the vertical stabilizers at the tip of the section.
1. The lift distribution of the outboard wings were calculated by merging the two outboard sections sides of wing and considering them to act as one continuous wing.

The equation employed to obtain average C_L max over total wing is

$$C_{L\,\max} = \frac{S_i C_{L\,\max,i} + S_o C_{L\,\max,o}}{S} \qquad (2)$$

where

S	total wing area (ft^2)
S_i	inboard wing area (ft^2)
S_o	outboard wing area (ft^2)
$C_{L\,\max}$	average maximum lift coefficient
$C_{L\,\max,i}$	inboard maximum lift coefficient
$C_{L\,\max,o}$	outboard maximum lift coefficient

The maximum lift coefficients of GA (W)-1 airfoil were different for each flight condition due to Reynolds number effects as listed in Table 3.

Table 3: 2-D Maximum Lift Coefficient of GA(W)-1 for Different Flight Conditions [2]

Flight condition	Max 2-D lift coefficient
Cruise	2.02
Takeoff and landing	1.95
Stall speed	1.75

For the GA (W)-2 airfoil, maximum lift coefficients also varied with the Reynolds Numbers for different flight condition.

Table 4: 2-D Maximum Lift Coefficient of GA(W)-2 for Different Flight Conditions

Flight condition	Max 2-D lift coefficient
Cruise	2.08
Takeoff and landing	1.97
Stall speed	1.84

From an approach in Nicolai[6], demonstrated in Appendix B, the 3-D maximum lift coefficients were found and are given in Tables 5 and 6.

Table 5: 3-D Maximum Lift Coefficient of GA(W)-1 for Different Flight Conditions

Flight condition	Max 3-D lift coefficient
Cruise	1.818
Takeoff and landing	1.755
Stall speed	1.575

Table 6: 3-D Maximum Lift Coefficient of GA(W)-2 for Different Flight Conditions

Flight condition	Max 3-D lift coefficient
Cruise	1.872
Takeoff and landing	1.773
Stall speed	1.656

When higher lift is needed a plain flaperon is used on the outboard sections with an airfoil chord ratio of 0.5 and a flapped wing area ratio of 0.65. The flaps deflect 20 degrees for takeoff and 40 degrees for landing. Thus, the total maximum lift coefficient, calculated based on Nicolai [6] is presented in Table 7

Table 7: Total Maximum Lift Coefficient for Different Flight Conditions

Flight condition	Flap deflection	Max 3-D lift coefficient
Cruise	0	1.850
Takeoff and landing	20	1.982
Stall speed	40	1.995

Power Selection

Performance of the resized Pegasus was assessed using several different values for engine horsepower were studied when the design still employed a telescoping outer wing. A diesel-reciprocating engine in the same category as the original design still appeared to be a good choice. Table 8 shows the performance results.

Table 8: The Effect of Engine Power Variation on the Performance of the First Version of the Resized Pegasus

Description	250 HP	200 HP	150 HP	120 HP
Takeoff gross weight (lbs)	2314	2219	2125	2103
Fuel weight (lbs)	342	328	314	311.5
Wing area (ft^2)	131.91	131.91	131.91	131.91
Engine HP	250	200	150	120
Wing loading (lb/ft^2)	17.5	16.8	16.1	15.9
Power loading (lb/hp)	9.3	11.1	14.2	17.5
Takeoff with 50 ft clear (ft)	873	1025	1299	1658
Landing with 50 ft clear (ft)	1044	1001	959	949
Service ceiling (ft)	28003	24895	20426	16139
Absolute ceiling (ft)	29514	26573	22325	18250
Max cruise at 80% power (kts)	158	144	124	105
Stall speed w/flap at sea level (kts)	45	44	43	43
Stall speed clean at cruise alt. (kts)	62	61	59	59
Max rate of climb (fpm)	2399	1894	1342	953

After the change in wing model, the vehicle encountered problems in takeoff performance and stall speed suggesting a need for a more powerful engine. A preferred engine would have a light weight with high power. The NASA sponsored GAP turboshaft engine was the final selection.

Pusher Propeller

In designing any aircraft one must make many decisions regarding the choice of propulsion systems. These include choosing between propeller and jet systems and selecting the best location for the system on the vehicle. The choice between prop and jet is usually based on desired speed and altitude of operation and on the cost of the system, both initially and over the life of the aircraft. Simple momentum theory essentially dictates that for a given amount of desired thrust, the larger the "disk" through which the propulsive flow must pass (jet engine inlet or fan area or propeller

disk area) the more efficient the device will be. Hence, propeller systems, whether turbine or piston engine driven, are inherently more efficient than a jet or fan jet. A turbine based propulsion system is, however, generally more dependable and needs less maintenance over its lifetime and may be less expensive to operate in the long run although its initial cost may be higher.

The NASA sponsored General Aviation Propulsion (GAP) project has led to the development of prototype engines such as the Williams jet or turboshaft engines, and Williams proposes to manufacture turbine based propulsion systems of comparable cost to many current piston engines, making the above choice less simple. Even so, the basics that determine system efficiency dictate that, as long as speeds are to be below about Mach 0.5, the turbine driven propeller is a better choice than even a high-bypass-ratio fan jet.

The turbofan engine, on the other hand, may offer a wider range of choice of propulsion system locations on the vehicle. A single propeller generally must be located either in front or behind the fuselage unless some kind of split tail boom system is used to place the tail behind the prop. Twin props are usually placed on the wing but can be located in a combined pusher/puller arrangement. Jets, however, can be placed at various locations along the fuselage or wings, giving somewhat more flexibility in creating a desirable weight and balance situation for the aircraft.

In designing the Pegasus and the Pegasus II consideration was given to several propulsion arrangements. An early Pegasus design employed twin ducted props placed over the inboard wings. Another Pegasus concept used twin non-ducted propellers with the inboard wing wrapped around them emulating a “channel wing” arrangement. In the final Pegasus design it was concluded that a larger diameter single propeller offered greater propulsive efficiency than two smaller diameter ducted or non-ducted propellers. Shrouding was considered for the single propeller but was ruled out because, on this size propeller, the ducting might introduce more drag than was warranted by its improved propulsive efficiency.

The choice of the aft or pusher prop configuration as opposed to a more “normal” nose mounted prop or tractor system was dictated partially by esthetic concerns but mainly because of the protection it gave the propeller blades from damage which might result from a “fender-bender” type of accident while operating in the roadable mode. It is also generally thought that if a roadable aircraft employs a tractor prop there must be a provision made for complete removal of the prop for roadway use. The use of the pusher prop eliminates these problems.

The pusher propeller does introduce its own set of problems, primarily due to the need for the propeller to operate in the non-uniform wake of the vehicle fuselage. If a pusher prop is to be used the design must be such that the flow from the upstream fuselage is not separated and that any wake is minimal. This was investigated in wind tunnel tests of the Pegasus design.

Figure 12 shows the Pegasus model in the Virginia Tech Stability Wind Tunnel. Tufts were placed on the model’s wing, tail and fuselage and the model was tested through a wide range of angle of attack, both with and without a motor driven propeller. Figure 13 shows that the flow over the aft portion of the fuselage, just in front of the prop location, is smooth and attached even when the wings are beginning to stall and there is no propeller in use. The propeller will further enhance the behavior of this flow, pulling the air around the fuselage and reducing the chances for flow separation.

There will always be a wake from the fuselage below the propeller hub and this will disturb the flow through the prop. The result of this disturbance will be increased noise from the propeller and

the need to design the prop and its shaft to take the periodic loads resulting from blades moving through that wake. The resulting noise and vibration can be reduced and tuned to a more desirable frequency by varying prop diameter, rotational speed, and the number of propeller blades. Hence, the optimum prop configuration needs to be studied and determined for this design but there is no reason that a reasonably quiet, low vibration, pusher prop system cannot be developed which will be more efficient and no noisier than the use of a turbofan system of comparable thrust. Furthermore, the placement of the propeller disk over the inboard wing and between the two vertical fin/winglets allows significant shielding of the propeller noise from the surrounding environment and the addition of suitable sound absorbing materials to the inner surfaces of the fins and upper surface of the inboard wing will further lower the noise signature of the design.

Calculations of propeller noise were done to investigate the design changes which must be made if the 75 pndb requirement is to be met at 500 feet from the vehicle. We wanted to address the noise issue which is inherent to pusher props. To assess the quantity of noise that the Pegasus II would create we used a prediction procedure for propeller noise as outlined by Roskam[5]. The goal for perceived noise level was 75 PNdB as outlined by the PAVE project guidelines.

The perceived noise level was reduced by lowering the tip speed of the propeller, that was accomplished by reducing the RPM. In order to maintain the same thrust output from the prop the number of prop blades was increased in inverse proportion to the reduction in RPM. The final results from Roskam's procedure for the Pegasus II are shown in the following calculations:

Predicted Noise Calculation

Input:

Propeller diameter (D)	5.71	ft
Number of blades (B)	6	
Power input to the propeller (SHP)	250	
RPM	1350	rpm
Number of propellers	1	
Airplane speed (V)	80	kts
Ambient temperature (T)	537	˚R (25 ˚C)
Distance	500	ft
Azimuth angle	0	degree

Solution:

Step 1 $$M_{rot} = \frac{\pi nD}{V_a} = \frac{\pi \, x \, 22.5 \, x \, 5.71}{\sqrt{1.4 \, x \, 32.2 \, x \, 53.35 \, x \, 537}} = 0.35$$

Step 2 From chart D1, FL1 = 68 dB

Step 3 From chart D2, FL2 = 3 dB

Step 4 From chart D3, FL3 = 0 dB

Step 5 From chart D4, DI = 0 dB

Step 6 NC = 0 dB (for 1 propellers)

Step 7 OSPL = FL1 + FL2 + FL3 + DI + NC = 71dB

Step 8 PNL = OSPL + _PNL

$$J = \frac{V}{nD} = \frac{80\,x\,1.688}{22.5\,x\,5.71} = 1.05$$

$$Mtip = M\infty\sqrt{1 + (\pi\ /J)\text{^}2} = \frac{80 * 1.688}{\sqrt{1.4x32.2x53.35x537}}\sqrt{1 + (\pi\ /J)\text{^}2} = 0.37$$

From chart D6, ΔPNL = 4 dB

PNL = 75 dB

In addition to reducing tip speed we also have added noise dampening features in the design which have not been accounted for in the calculations. These include the ducting effect the box wing will provide and the addition of sound deadening material to the inner sides of the box wing.

Component Weight Analysis

It was initially assumed that the weight estimation of roadable aircraft would follow different trends than that for conventional aircraft. There are a number of factors in statistical-base weight analysis for component weight that need to be examined. To achieve a close approximation real weights are applied as often as possible whereas other weights such as structural weights, which are more dependent on dimensions, were assumed to have the same variations as on conventional general aviation aircraft. Additionally, the weight of some components that were similar to the original Pegasus were assumed to weigh the same as found in Reference 2.

Based on component weight estimation methods of Raymer[7], the components that have a fixed weight are listed below.

- Transmission
- Engine
- Avionics
- Propeller
- Landing gear
- Furnishings

The breakdown of component weights is shown in Table 9. As a result, the takeoff gross weight of the vehicle is 1594

Table 9: Component Weights of Pegasus I and II

component	Weight (lb)	
	Original Pegasus	Pegasus II
Structure		
Wing	215.00	118.00
Horizontal Tail	30.00	23.00
Vertical Tail	50.00	38.20
Fuselage	350.00	222.14
Nose Gear	85.00	85.00
Main Gear	85.00	85.00
Total	815.00	571.34
Propulsion		
Engine	400.00	170.00
Transmission	305.00	305.00
Propeller	50.00	32.93
Fuel System	45.00	45.80
Total	800.00	553.73
Systems		
Flight Control	20.00	11.47
Electrical	190.00	159.53
Avionics	100.00	100.00
AC/anti-ice	80.00	82.83
Total	390.00	353.83
Cabin		
Furnishings	115.00	115.00
Variable Weights		
Fuel	480.00	372.00
Payload	700.00	800.00
Total	1180.00	1172.00
Grand Total	3300.00	2765.90

Performance Estimates

The Pegasus II performance was recalculated and shown to meet all requirements of PAVE as shown in Table 10.

Table 10: Calculated Flight Performance of the Final Design of the Pegasus II

Range (nm)	400	Landing ground roll (ft)	731
Takeoff weight (lbs)	2766	Landing, clear 50’ (ft)	1730
Engine HP	360	Service ceiling (ft)	18435
Fuel weight (lbs)	372	Absolute ceiling (ft)	19395
Payload (lbs)	800	Cruise speed (TAS)	180
Wing loading (lb/ft^2)	24.8	Stall speed w/flap (TAS)	60
Power loading (lb/hp)	7.7	Stall speed clean (TAS)	71
Takeoff ground roll (ft)	473	Max rate of climb (fpm)	2259
Takeoff, clear 50’ (ft)	1033	PNL at 500 ft	75

ROADABILITY

Some of the roadability concerns of a dual-mode vehicle have been discussed previously. In the road mode the vehicle must fit within dimensional limits (PAVE limits are more restrictive than DOT requirements) and it must meet DOT and EPA safety and environmental emission restrictions. As important as the above are the design's ability to approximate the normal road handling and stability behavior of an automobile. Finally, the need to provide power to either the propeller, fan, or jet, or to the drive wheels of the vehicle in highway mode must be addressed.

Numerous ways have been suggested for supplying power to both a propeller or fan and drive wheels. Many of these assume the use of a proven and reliable automobile engine with some type of transaxle which is capable of sending power to two different drive shafts. It has been suggested that an "all-wheel" drive system which can supposedly provide power on demand to the drive shaft most in need could automatically send power to either prop or wheels as needed. Most such concepts ignore the difference between aircraft engines and car engines.

Automobile engines are designed for operation over a wide range of RPM and for stop-and-start driving while aircraft engines are designed for continuous operation over a very narrow range of RPM. While a car engine can work in an aircraft and many have done so they are really not designed for aircraft operating requirements. The Pegasus design used a diesel aircraft engine with a unique transmission system developed by Audi. The Audi Multitronic CVT is designed for use with an engine which, like that of an aircraft, operates at near constant RPM. The CVT provides a smooth transfer of power through a continuous range of drive ratios and its weight, including transmission fluid, is approximately 220 pounds. It is recommended that this type of transmission be used to take power from an engine which is normally coupled to a propeller or fan and transfer it to the drive wheels in highway operation.

Vehicle stability on the highway is another major concern since the normal center of gravity location relative to the vehicle rear wheels is very different for an airplane and a car. As discussed earlier, the normal aircraft location of the CG just ahead of the main gear (needed to allow ease of rotation on takeoff) would result in a very unstable automobile. The Pegasus design, like that of many other PAV concepts, opts for a more standard automobile CG location and addresses the takeoff rotation need with variable height front and rear wheels. A complete analysis of the suspension system dynamics of the Pegasus was done in its design report[2] and the relevant section of that report is included here as Appendix C.

CONCLUSIONS AND RECOMMENDATIONS

It is easy to look at studies like this and say that the conclusions were obvious, that findings which show that weight and wing aerodynamic efficiency (aspect ratio) are important issues when comparing single and dual mode vehicles are not surprising. Indeed, these conclusions are obvious, but that does not make them unimportant.

The three main considerations one must include when looking at the design of any dual mode vehicle (roadable aircraft) are size (to fit roadway widths, garage dimensions, overpass clearances), center of gravity placement and its relation to takeoff rotation dynamics and highway driving stability, and the weight penalty paid for meeting DOT requirements and for automation of any transformation process between road and flight modes.

The center of gravity placement concern will, in all probability, have to be addressed by providing the dual mode vehicle with a non-aerodynamic takeoff rotation capability for CTOL operation. The vehicle must meet automobile rollover and handling stability needs when on the ground if it is to be used for reliable and safe highway transport. The center of gravity/wheel placement needed to meet this requirement is simply not consistent with the needs for aerodynamically driven rotation to a desired lift-off angle of attack during a takeoff run unless tail or canard control surface areas and/or moment arms are much larger than required for normal in-flight performance. Non-aerodynamic devices needed for takeoff rotation include hydraulic or screw driven actuators used to extend or retract the front wheel struts or axles from their "normal" in-flight or on-highway positions.

The other two considerations mentioned above, weight and aerodynamic efficiency are very much dependent on each other in several ways. As weight increases due to the need for airbag systems, automobile drive systems, pollution control systems, etc., the needed for wing area and/or high lift coefficient and aerodynamic efficiency increase. And the demands for complex, automated wing folding systems, in turn, drive the wing and vehicle weight higher, increasing the aerodynamic demands on the wing.

There is simply no way around some of the weight penalties of the dual mode vehicle, however, some are avoidable. The systems needed for crashworthiness and environmental protection which are required on an automobile but not for an aircraft must be a part of the dual-mode vehicle. On the other hand there is a very real need to investigate the conflicts inherent in two philosophies with which one may design a dual mode wing concept. The simplicity of a manual road/flight mode transition design will require less weight and will in turn, require less wing.

It is appealing to insist that any wing folding, retraction, etc. system on a dual-mode concept must be automated for ease of transformation between travel modes. Obviously, an automated system is desirable but, in our view, an assessment of the tradeoffs involved needs to be conducted to find the true costs of satisfying that desire. During the operational lifetime of a dual-mode vehicle only a very small fraction of time will be spent in the transition mode but the penalties associated with automation of transition apply to the long term and short term costs of operation of the vehicle in both modes of travel and these penalties may be significant.

In the design of a wing system for a dual-mode vehicle one must start by asking how much lift can one get from that portion of the vehicle which can fit the road mode sizing "box"; i.e., how much lift and aerodynamic performance can one get from a seven foot wide wing or wing/fuselage combination. At its simplest this is a question of the optimum aerodynamic performance of a very low aspect ratio wing (AR < 1.0). Studies by Kroo[1] for moderate aspect ratio wings conclude that a box wing configuration optimizes the performance of a wing with a set wing span. The box wing appears superior to any other non-planar wing configuration in aerodynamic efficiency. A study needs to be done to see if this holds for wings with very small aspect ratios.

Since it is almost inconceivable that even the most efficient ultra-small aspect ratio wing will be capable of supporting a dual-mode vehicle in flight with a reasonable amount of power, there will almost certainly have to be additional wing area added to the vehicle when it transitions from road to flight mode. The tradeoffs involved in the design of this "extension" to the base, ultra-low aspect ratio, inboard wing concept need to be thoroughly examined. Since there are many, many ways that "outboard" wings may be attached to the vehicle and folded, retracted, or otherwise stowed (not to

mention removed and towed), several concepts need to be examined and assessed for aerodynamic efficiency, structural integrity, and long term operational cost. The cost of operation will be based not only on the complexity of the mode transition process itself but also on the cost of the weight penalty inherent in the system in both on-road and in-flight operation. In other words, the true costs of automating the wing transition process need to be assessed and understood before declaring automation the only way to proceed within the PAVE program. For example, if automatic transition saves 30 minutes per flight but increases the cost of both ground and air travel by 10% and lowers the flight speed by 5 kts (due to extra weight), is it worth it? The expected reliability of such a system in contrast with an almost fail safe manual transition system also needs to be evaluated.

We would therefore propose that a systematic study be conducted of the wing needs for a CTOL dual-mode vehicle, starting with a look at the best low aspect ratio "inboard" or basic wing which will be a fixed part of the vehicle in both travel modes, and extending to an examination of the best (simplest?) addition or extension to that base wing needed to provide acceptable flight performance. Accompanying this study should be a thorough examination of the real costs of automation in transitioning between road and flight travel modes.

REFERENCES:

1. Kroo, Llan, and McMasters, John, "Highly Nonplanar Lifting Systems", Transportation Beyond 2000, NASA Conference Publication 10184, pp 331 - 370, February 1996
1. Gassler, R, et.al., "Pegasus", A report to the AGATE NASA/FAA General Aviation Design Competition, Virginia Tech Aerospace & Ocean Engineering Department, May 2000
1. Stiles, Palmer, *Roadable Aircraft: From Wheels to Wings,* Custom Creativity, Inc., Melbourne, FL, August 1994
1. LaBiche, M., "LaBiche Aerospace, FSC-1", www.labicheaerospace
1. Roskam, J., *Airplane Aerodynamics and Performance*, DAR Corporation, 1997
1. Nicolai, Leland M., *Fundamentals of Aircraft Design*, Domicone Printing Services, Fairborn, Ohio, 1975
1. Raymer, Daniel P., Aircraft Design: A Conceptual Approach, American Institute of Aeronautics and Astronautics, Inc., Washington, D.C., 1989

FIGURES

Figure 2: 1938 "Dual-Mode Vehicle" Concept
[Mechanics and Handicraft magazine, January 1938]

- Range 400 nm
- Loiter 45 min
- Takeoff/landing distance to clear 50’ <3,000ft
- Payload 800 lbs
- Cruise speed >100 kts
- FAR part 23 compliance

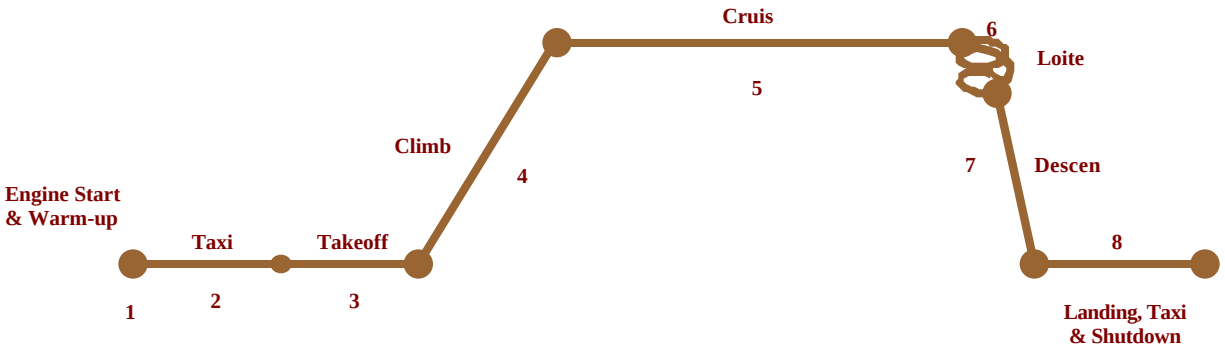

Figure 3: PAVE Mission Profile

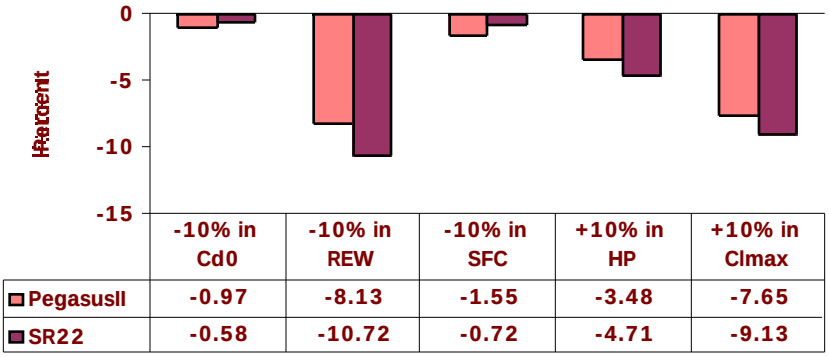

Figure 4: Takeoff Distance Sensitivity

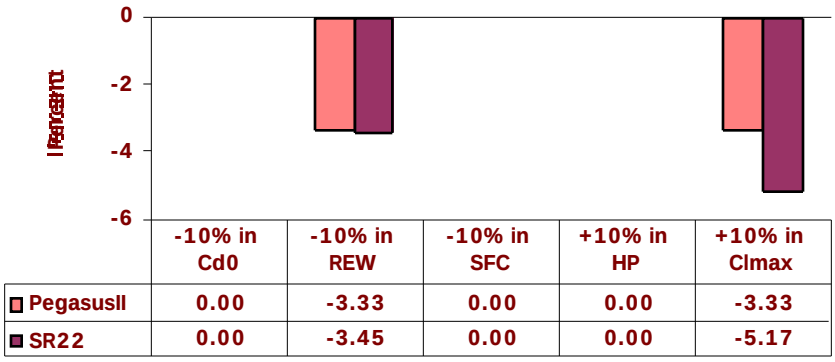

	-10% in Cd0	-10% in REW	-10% in SFC	+10% in HP	+10% in Clmax
PegasusII	0.00	-3.33	0.00	0.00	-3.33
SR22	0.00	-3.45	0.00	0.00	-5.17

Figure 5: Stall Speed Sensitivity

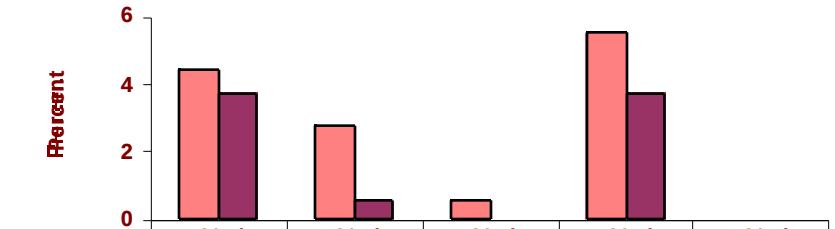

	-10% in Cd0	-10% in REW	-10% in SFC	+10% in HP	+10% in Clmax
PegasusII	4.44	2.78	0.56	5.56	0.00
SR22	3.78	0.54	0.00	3.78	0.00

Figure 6: Cruise Speed Sensitivity

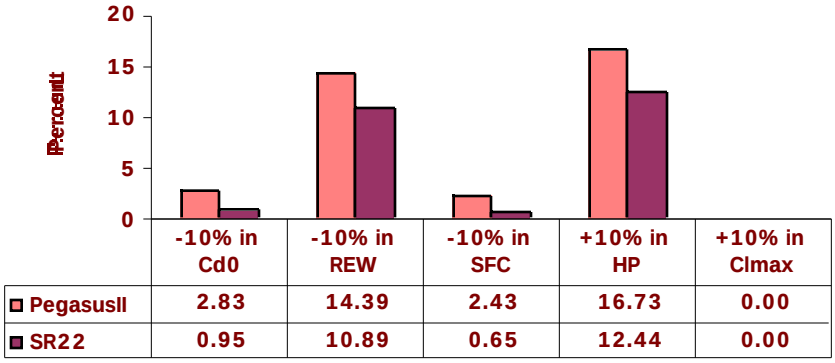

	-10% in Cd0	-10% in REW	-10% in SFC	+10% in HP	+10% in Clmax
PegasusII	2.83	14.39	2.43	16.73	0.00
SR22	0.95	10.89	0.65	12.44	0.00

Figure 7: Rate of Climb Sensitivity

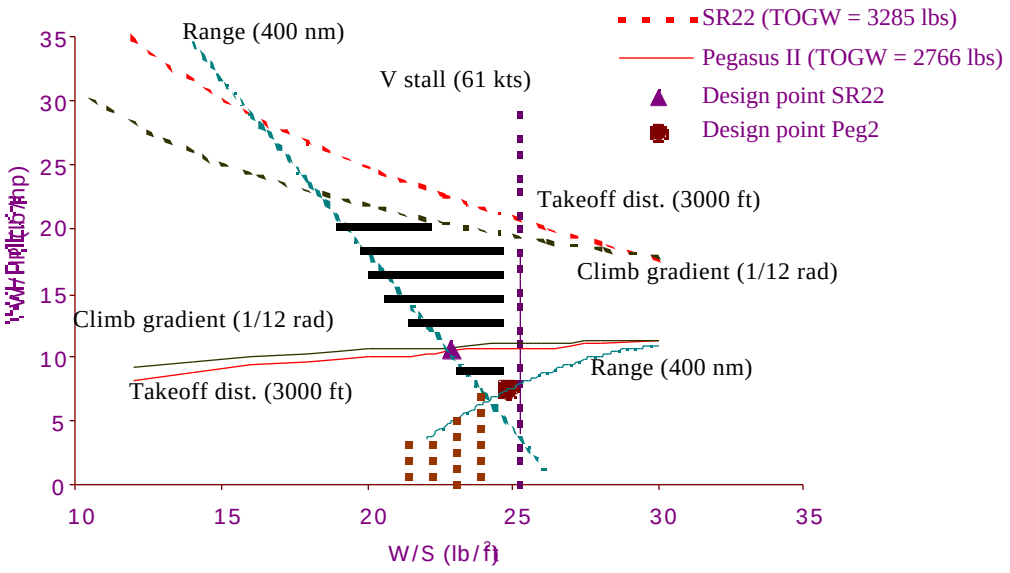

Figure 8: Pegasus II and SR22 Constraint Comparison

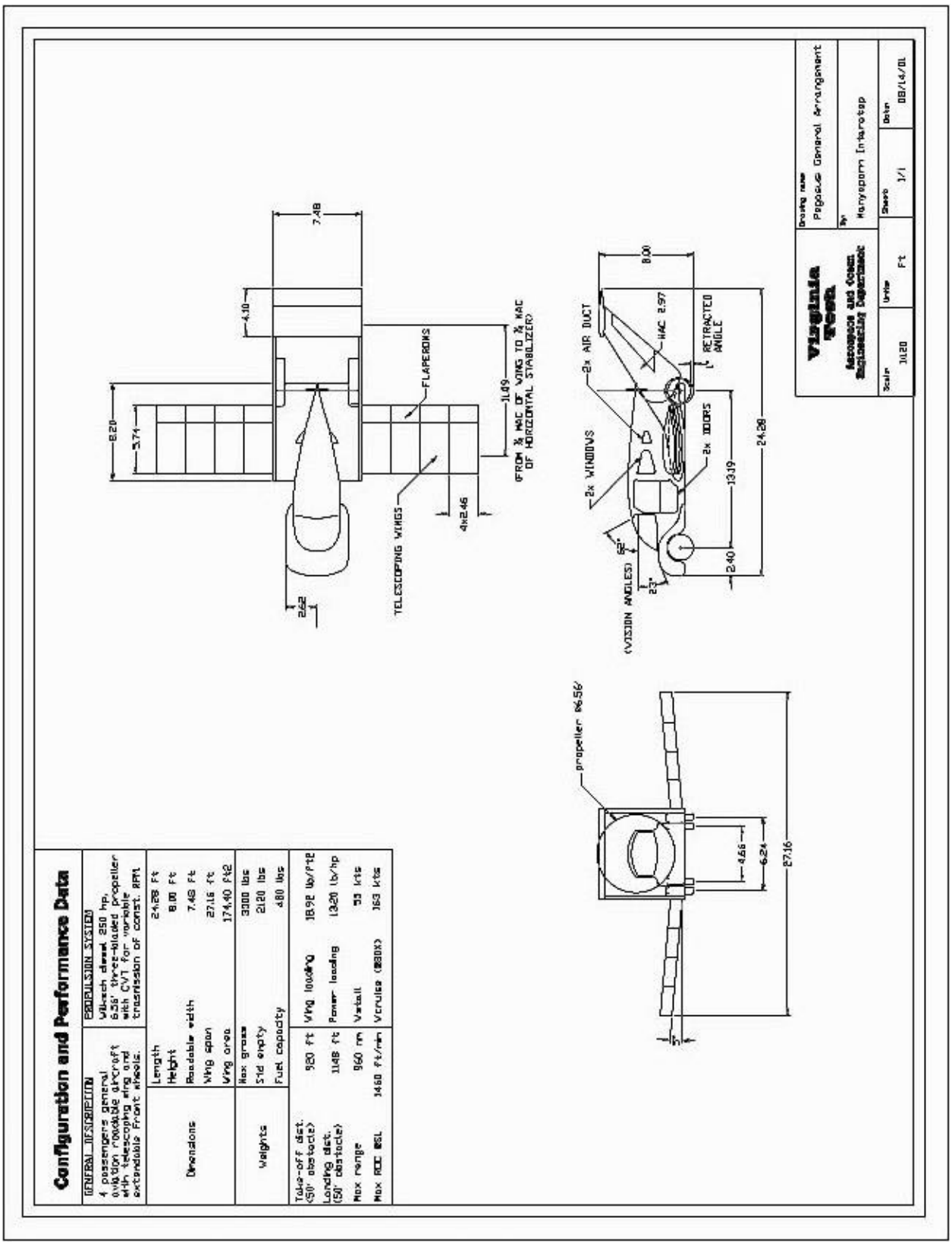

Figure 9: Original Pegasus Design

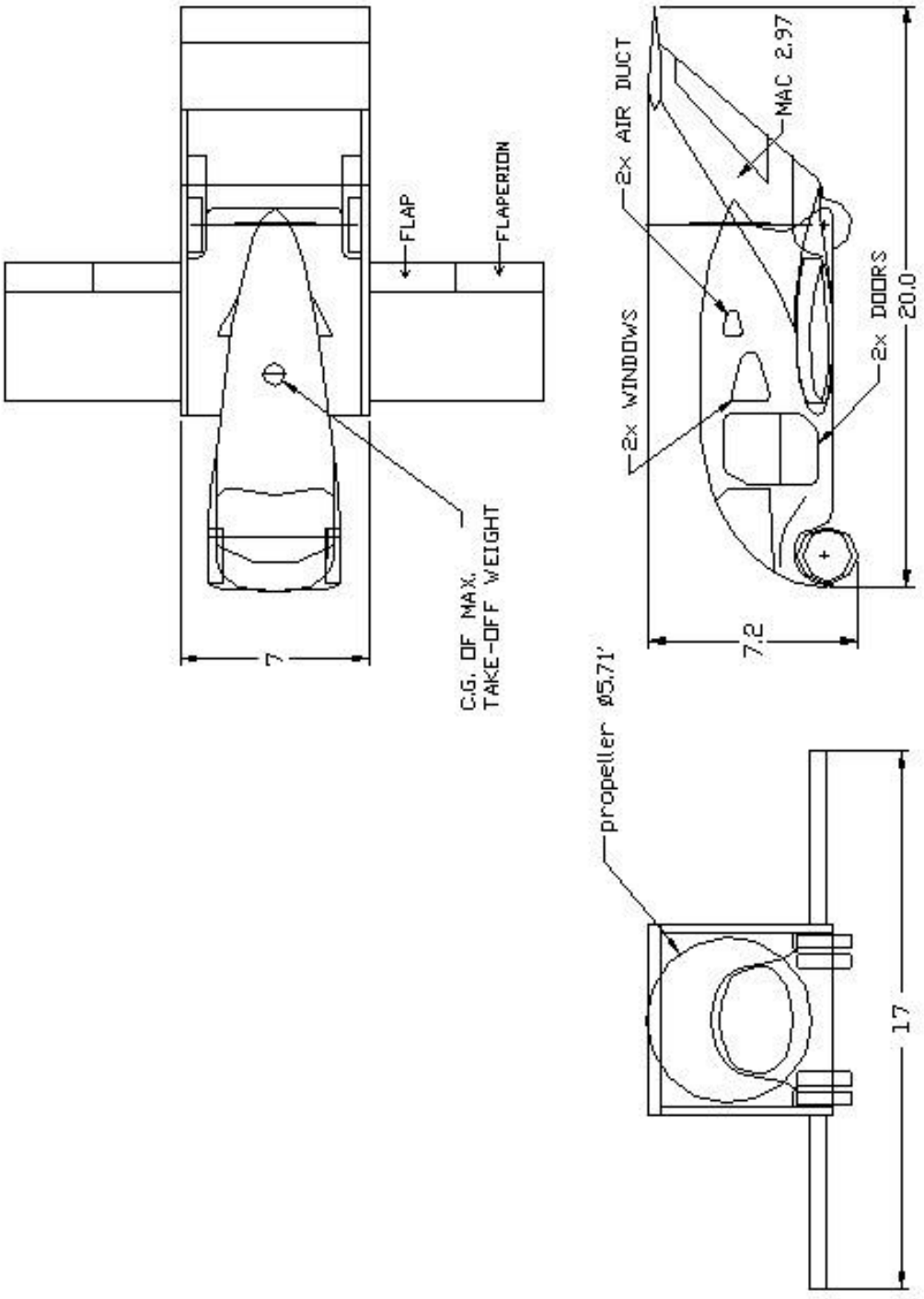

Figure 10: Pegasus II Design

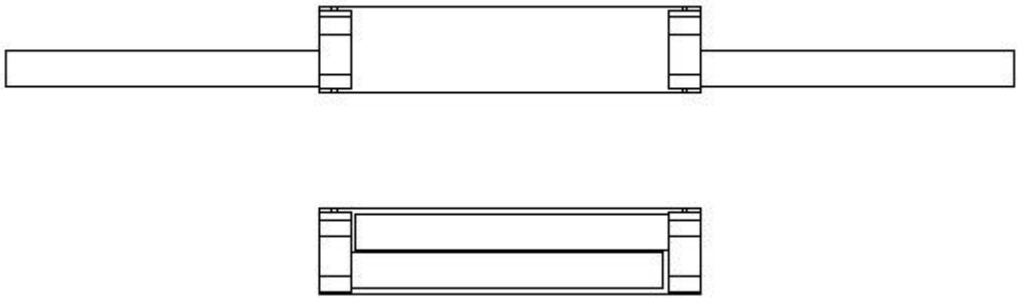

Front View

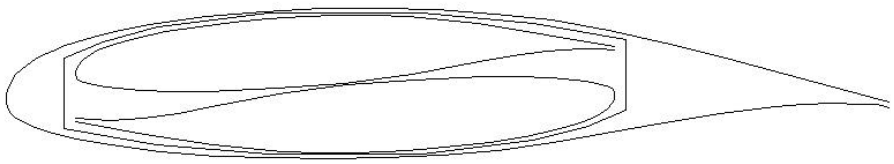

Side View

Figure 11: Outboard Wing Stowage Concept

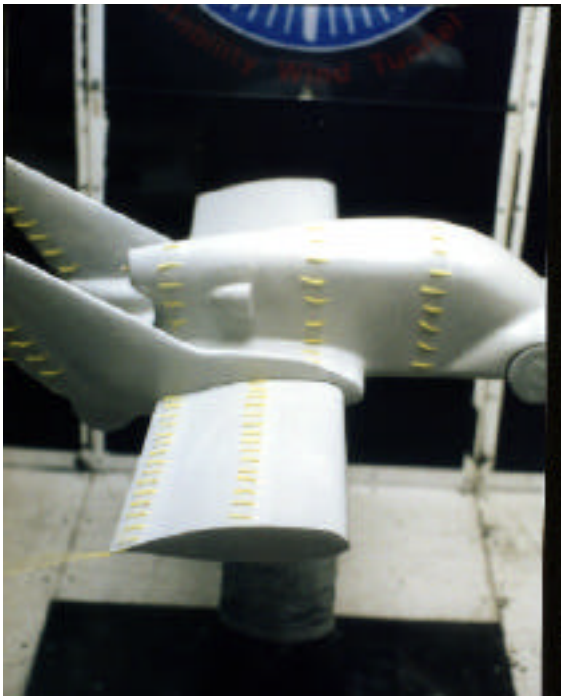

Figure 12: Flow Over Pegasus in Normal Flight

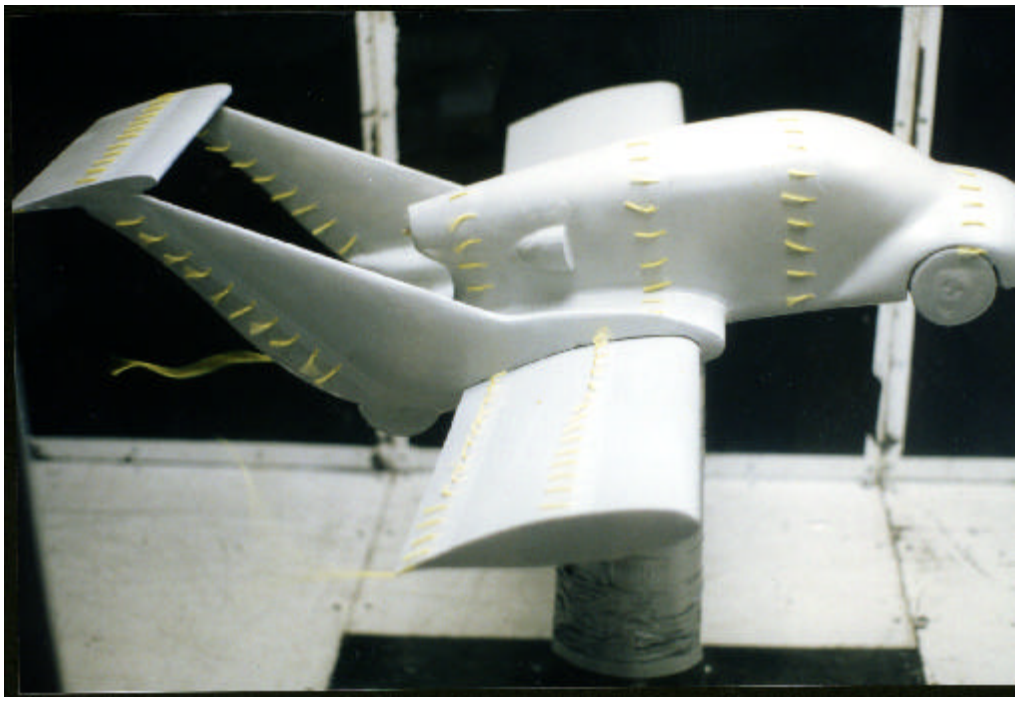

Figure 13: Flow over Pegasus with Wing Stall

APPENDIX A

COMPARATOR AIRCRAFT PERFORMANCE AND SIZING DATA

Table A-1: CTOL Aircraft Data

Manufacturer		Requirement	Cirrus	Cirrus	Lancair	Cessna
Model			SR20	SR22	Columbia 300	172R
Engine	Model	-	Continental IO-360-ES	Continental IO-550-N	Continental IO-550-N	Lycoming IO-360-L2A
	HP	-	200	310	310	160
Passengers		4	4	4	4	4
Max Range(nm)		400	800	>1000	1280	580
Take-off (ft, 50' obstacle)		< 3000	1865	1575	1250	1685
Landing (ft, 50' obstacle)		< 3000	1960	2325	2350	1295
Cruise speed (ktas)		> 100	160(@75%)	180(@75%)	190(@75%)	122(@80%)
Stall speed (kias, flap down/up)		< 61(FAR 23)	54/65	59/-	57(landing)/-	47/-
Max rate of climb (ft/min) @ SL		(FAR 23)	900	1400	1340	720
Operation Ceiling		-	17500	17500	18000	13500
Dimension (ft)	Length	-	26.25	26	25.17	27.17
	Height	-	9.25	9.2	9	8.92
	Wing span	-	35.58	38.5	36	36.08
	Wing area (ft^2)	-	135	144.9	141.2	174
	Max Gross Wt	-	2900	3400	3400	2457
	Std Empty Wt	-	1950	2250	2200	1620
	Max Useful Load	800 + fuel	950	1150	1200	837
	Fuel capacity (gals,usable/max)	-	56 (336 lbs) /-	81(486 lbs) /-	98/-	53/-
Power loading (lb/hp)		-	14.5	10.9	10.97	15.3
Wing loading (lb/ft^2)		-	21.4	23.5	24	14.1
High lift devices		-	single-slotted flaps	single-slotted flaps	flower flaps	electronically actuated single slotted, Para Lift flaps
Landing gear		-	fixed	fixed	fixed	fixed
Min cost		-	197600	276600	299700	144900

Manufacturer		Requirement	Cessna	Diamond	Luscombe Spartan	Luscombe Spartan
Model			182T	DA40 180	Model 11E 185	Model 11E 210
Engine	Model	-	Lycoming IO-540-AB1A5	Lycoming IO-360-MIA	Continental IO 360-ES	Continental IO 360-ES
	HP	-	230	180	185	210
Passengers		4	4	4	4	4
Max Range(nm)		400	845(@75%)	600	460.55	809
Take-off (ft, 50' obstacle)		< 3000	1514	1985	1250	925
Landing (ft, 50' obstacle)		< 3000	1350	-	900	500
Cruise speed (ktas)		> 100	144(@80%)	147(@75%)	113	113
Stall speed(kias, flap down/up)		< 61(FAR 23)	49/-	49 (kts)	43/47	43/47
Max rate of climb (ft/min) @ SL		(FAR 23)	924	1070	950	950
Operation Ceiling		-	18100	-	18000	18000
Dimension (ft)	Length	-	29	26.25	23.75	23.75
	Height	-	9.33	6.6	8.83	8.83
	Wing span	-	36	39.4	38.5	38.5
	Wing area (ft^2)	-	174	145	167	167
Weight (lbs)	Max Gross Wt	-	3110	2535	2280	2280
	Std Empty Wt	-	1897	-	1350	1450
	Max Useful Load	800 + fuel	1213	992	930	830
	Fuel capacity (gals,usable/max)	-	88/-	41	40	40
Power loading (lb/hp)		-	13.5	13.49	12.3	12.3
Wing loading (lb/ft^2)		-	17.8	17.6	13.7	13.7
High lift devices		-	electronically actuated single slotted, Para Lift flaps	slotted flaps	three - position flaps	three - position flaps
Landing gear		-	fixed	fixed	fixed	fixed
Min cost		-	242000	179900	155900	26323

Manufacturer		Requirement	Piper	Piper	Socata Aircraft	Socata Aircraft
Model			Archer III	Warrior III	Tampico	Tobago
Engine	Model	-	Lycoming O-360-A4M	Lycoming O-320-D3G	Lycoming O-320-D2A	Lycoming O-360-A1AD
	HP	-	180	160	160	180
Passengers		4	4	4	4	4/5
Max Range(nm)		400	444(@75%)	513(@75%)	591	508(@75%)
Take-off (ft, 50' obstacle)		< 3000	1608	1620	1870	1657
Landing (ft, 50' obstacle)		< 3000	1400	1160	1378	1509
Cruise speed (ktas)		> 100	128(@75%)	115(@75%)	115(@70%)	127(@75%)
Stall speed(kias, flap down/up)		< 61(FAR 23)	45/-	44/50	48/58	53(landing)
Max rate of climb (ft/min) @ SL		(FAR 23)	667	644	665	787
Operation Ceiling		-	14100	11000	11000	13000
Dimension (ft)	Length	-	24	23.8	25.33	25.33
	Height	-	7.3	7.3	9.91	9.83
	Wing span	-	35.5	35	32.87	32
	Wing area (ft^2)	-	171.8	170	131.81	128
Weight (lbs)	Max Gross Wt	-	2550	2440	2337	2535
	Std Empty Wt	-	1689	1533	1426	1543
	Max Useful Load	800 + fuel	861	907	911	992
	Fuel capacity (gals,usable/max)	-	48	48	40.2/41.7	53.9/55.5
Power loading (lb/hp)		-	14.2	15.52	14.64	14.08
Wing loading (lb/ft^2)		-	15	14.35	18.25	19.8
High lift devices		-	four-position manually operation flaps	four-position manually operation flaps	electronically actuated flaps	electronically actuated flaps
Landing gear		-	fixed	fixed	fixed	fixed
Min cost		-	188900	161000	190390	223980

Manufacturer		Requirement	Tiger	commander	Mooney	Mooney	Piper
Model			AG-5B	115	Eagle2	Ovation2	Arrow
Engine	Model	-	Lycoming O-360-A4K	Lycoming IO-540-T4B5	Continental IO-550-G	Continental IO-550-G	Lycoming IO-360-C1C6
	HP	-	180	260	244	280	200
Passengers		4	4	4	4	4	4
Max Range(nm)		400	572	855(@75%)	908(@75%)	1020(@75%)	880(@55%)
Take-off (ft, 50' obstacle)		< 3000	1550	1985	2550	2500	1600
Landing (ft, 50' obstacle)		< 3000	1120	1200	2400	2350	1520
Cruise speed (ktas)		> 100	134(@75%)	160(@75%)	178(@75%)	189(@75%)	137(@75%)
Stall speed (kias, flap down/up)		< 61 (FAR 23)	53(w/flaps)	54(landing)	59(landing)	59(landing)	55/60
Max rate of climb (ft/min) @ SL		(FAR 23)	850	1070	1150	1250	831
Operation Ceiling		-	13800	16800	18500	20000	16200
Dimension (ft)	Length	-	22	24.92	26.75	26.75	24.7
	Height	-	7.58	8.42	8.33	8.33	7.9
	Wing span	-	31.5	32.75	36.08	36.08	35.4
	Wing area (ft^2)	-	140.12	152	175	175	170
Weight (lbs)	Max Gross Wt	-	2400	3260	3300	3368	2750
	Std Empty Wt	-	1398	2102	2200	2225	1790
	Max Useful Load	800 + fuel	1002	1158	1100	1143	960
	Fuel capacity (gals,usable/ max)	-	51/52.6	88/90	75/-	83/-	72/-
Power loading (lb/hp)		-	-	12.5	13.5	12	13.75
Wing loading (lb/ft^2)		-	-	21.4	18.9	19.3	16.18
High lift devices		-	-	-	electronically actuated single-slotted flaps	electronically actuated single-slotted flaps	four-position manually operation flaps
Landing gear		-	fixed	retractable	retractable	retractable	retractable
Min cost		-	-	349500	360000	445000	249700

Table A-2: Dual-Mode Vehicle Data

Manufacturer		Requirement for airplane	Aeromaster Innovations	Virginia Tech	AFA (Sarh)	LaBiche AEROSPACE
Model			SYNERGY	PEGASUS	SOKOL A400	FSC-1
Engine	Model		Mazda 13B Rotary	Wilksch diesel	reciprocative	Porche 3.6L
	HP		220	250	400	445
Drive	Air	-	72" variable pitch propeller	6.56' three-bladed propeller	4.5' pusher propeller	Dual-in-Line counter rotating propeller
	Ground	-	main wheel drive through VW bug transaxle	using CVT, for vriable transmission of constant RPM	-	6 Speed Manual Transmission
Passengers		4	2+2	4	2+2	4
Max Range(nm)		400	1000	960	434.5	912
Take-off (ft, 50' obstacle)		< 3000	-	920	2300	1400
Landing (ft, 50' obstacle)		< 3000	-	1148	1500	1001
Cruise speed (ktas)		> 100	169.45	163 (@80%)	156.4	270(@75%)
Stall speed (kias, flap down/up)		< 61(FAR 23)	52.14/-	55	-	78/-
Max rate of climb @ SL (ft/min)		(FAR 23)	-	1460	800	-
Operation Ceiling		-	-	-	12000	18000
Dimension (ft)	Length	22	19	24.28	18	-
	Height	7	5.3	8	-	-
	roadable width	7	7.5	7.48	-	6.67
	Wing span	-	28.4	27.16	28	32.13
	Wing Area (ft^2)	-	103	174.4	130	130.34
Weight (lbs)	Max Gross Wt	-	1950	3300	3200	3600
	Std Empty Wt	-	1250	2120	2000	2455
	Max Useful Load	800 + fuel	700	1280	1200	1145
	Fuel capacity (gals, usable/max)	-	65	(480 lbs)	40	102

Manufacturer	Requirement for airplane	Aeromaster Innovations	Virginia Tech	AFA (Sarh)	LaBiche AEROSPACE
Model		SYNERGY	PEGASUS	SOKOL A400	FSC-1
Wing loading (lb/ft^2)	-	18.93	18.92	21.40	27.62
Power loading (lb/hp)	-	8.86	13.20	9.60	8.09
wing retraction	-	hydraulically foldable wing	telescoping wing	telescoping wing	folding wing
conversion time (s)	-	25	-	-	
Landing gear/wheels	-	main-partially retraction nose-fully retraction	4 wheels with extended front wheels for take off position	4 wheels with retracted rear wheels for take off position	4 wheels extend 20" for take off and landing
Min cost	-	30000 (kit)	324173	-	

APPENDIX B

ANALYSIS OF COMPARATOR AIRCRAFT

Appendix B List of Symbols

AR_e	Effective aspect ratio
b	Wing span (ft)
c_p	Specific fuel consumption (lb/(hp.hr))
C_{D0}	Parasite drag coefficient
$C_{D,mp}$	Drag coefficient at minimum power
C_{l_α}	Section lift curve slop (per radian)
$C_{L,A}$	Approached lift coefficient
$C_{L\ \max}$	Maximum lift coefficient
$C_{L\ \max,i}$	Inboard maximum lift coefficient
$C_{L\ \max,o}$	Outboard maximum lift coefficient
$C_{L,mp}$	Lift coefficient at minimum power
$C_{L,TO}$	Takeoff lift coefficient
d	Fuselage width (ft)
D	Drag (lbs)
E	Endurance (hrs)
F	Fuselage lift factor, $F = 1.07\left(1+\frac{d}{b}\right)^2$
g	Acceleration of gravity (ft/s^2)
h_{cr}	Cruise altitude (ft)
h_{SL}	Sea level altitude (ft)
h_{TR}	Transition altitude (ft)
K	Induce drag factor
K'	Correction for non-linear effects
L	Lift (lbs)
(L/D)	Lift to drag ratio at climb angle
M_{ff}	A ratio of takeoff gross weight to empty weight
n_{FL}	Flare load factor
N_n	Nose-gear normal force (lbs)
P_A	Power available (ft.lb/s)
P_R	Power require (ft.lb/s)
R	Range (mph)
R_{FL}	Flare radius (rad)
R_{TR}	Transition radius (rad)
$RoC_{\max}$	Max rate of climb (fpm)
S	Wing area (ft^2)
S_{CL}	Climb takeoff distance (ft)
$S_{\exp}$	Exposed wing area (ft^2)
S_i	Inboard wing area (ft^2)

S_{LA}	Landing air distance (ft)
S_{LR}	Rotation landing distance (ft)
S_{LNGR}	Nose-wheel-ground-run landing distance (ft)
S_{NGR}	Nose-wheel-ground-run takeoff distance (ft)
S_o	Outboard wing area (ft^2)
S_R	Rotation takeoff distance (ft)
S_{TR}	Transition takeoff distance (ft)
T	Thrust (lbs)
$TOGW$	Takeoff gross weight (lbs)
V_A	Approached velocity (mph)
V_{CL}	Climb velocity (mph)
V_{FL}	Flare velocity (ft/s)
V_{mp}	Velocity at minimum power (mph)
V_s	Stall velocity (ft/s)
V_{TD}	Touch down velocity (ft/s)
V_{TO}	Takeoff velocity (ft/s)
W_f	Required fuel weight (lbs)
$W_{f,actual}$	Actual-used fuel weight (lbs)
$W_{fi1,2...8}$	A fuel fraction of each phase (final/initial)
α_{0L}	zero-lift angle of attack
α_{stall}	3-D stall angle of attack
β	$\sqrt{1-M^2}$
γ_A	Flare angle (rad)
δ_f	Flap deflected angle (deg)
$\Delta C_{l\max}$	Change in $C_{l\max}$ with δ_f flap deflection
Δy	Leading edges shape parameter
η	$\frac{dC_l}{d\alpha}\frac{\beta}{2\pi}$, $\frac{dC_l}{d\alpha}$ = 2-D lift curve slope
η_p	Propeller efficiency
θ_{CL}	Climb angle (rad)
Λ_t	Sweep of wing at maximum thickness (deg)
μ	Ground fiction coefficient
μ_{break}	Ground fiction coefficient with break
ρ	Density ($slug/ft^3$)
σ	Density ratio (relative to density at sea level)

Analysis of Comparator Aircraft

As illustrated in Tables A-1 and A-2, various CTOL single and dual-mode vehicle data were generally reviewed for a selection of comparator models in this study. Each model was analyzed against PAVE requirements and for study in a sensitivity evaluation. The final four selected vehicles include two successful general aviation designs, the Cessna 182 and Cirrus SR22, and two proposed roadable aircraft, the Pegasus II and LaBiche FSC-1. These base models were reevaluated using the eight phase PAVE mission profile shown below in Figure B.1.

1. Engine start and warm-up
2. Taxi
3. Takeoff
4. Climb and accelerate to cruise altitude
5. Cruise for 400 nm
6. Loiter for 45 min
7. Descent
8. Landing, taxi and shutdown

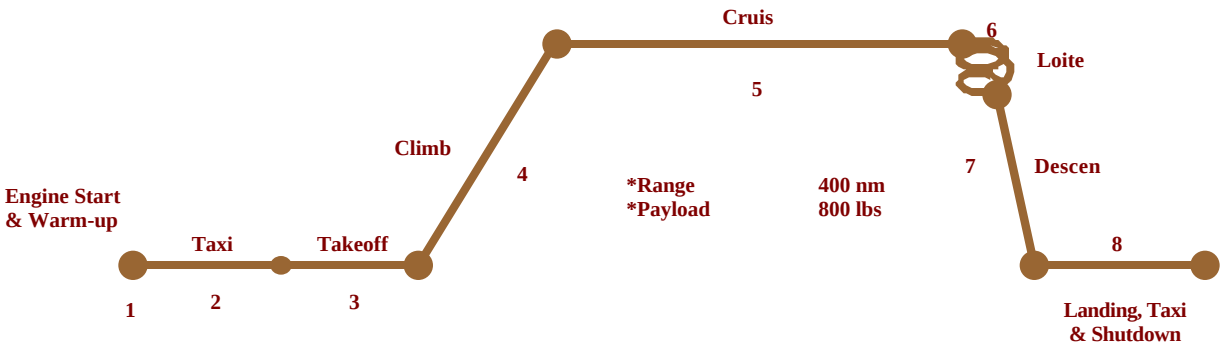

Figure B.1: Mission profile

Takeoff and fuel weight estimation

An evaluation of mission fuel weight was based on a fuel-fraction method for propeller-driven airplane in Ref. B1. The vehicle's initial configuration was input in this calculation.

$$M_{ff} = W_{fi1} x W_{fi2} x W_{fi3} x W_{fi4} x W_{fi5} x W_{fi6} x W_{fi7} x W_{fi8} \qquad \text{(B.1)}$$

In phases 1, 2, 3, 7, and 8 (W_{fi1}, W_{fi2}, W_{fi3}, W_{fi7}, W_{fi8}), the assumed phase weight ratio for a single-engine general aviation are 0.995, 0.997, 0.998, 0.993 and 0.993 respectively. These approximations are based on conventional statistics while the rest are results of performance calculations as explained below.

Phase 4: Climb and accelerate (W_{fi4})

The fuel fraction was estimated from the time used to climb at maximum rate of climb conditions to cruise altitude and using the endurance equation for propeller-driven airplanes (B.2). Also used is an assumption that an engine is operated at the maximum constant power rating.

$$E = 375\left(\frac{1}{V}\right)\left(\frac{\eta_p}{c_p}\right)\left(\frac{L}{D}\right)\ln\left(W_{if\,4}\right) \tag{B.2}$$

To gain a maximum rate of climb, an airplane must fly at its minimum power required condition. From the parabolic drag assumption, aerodynamic coefficients for this state are calculated from C_{d0} and K in Eqn. (B.3) and (B.4).

$$C_{L,mp} = \sqrt{\frac{3C_{D0}}{K}} \tag{B.3}$$

$$C_{D,mp} = 4C_{D0} \tag{B.4}$$

Then, the time to climb at maximum rate of climb is approximated from Eqn. (B.6) with an assumption of constant climb rate.

$$RoC_{\max} = 33000\left[\left\{\frac{\eta_p\sigma}{\left(TOGW/P\right)}\right\} - \left\{\frac{\left(TOGW\ /\ S\right)^{0.5}}{19\left(C_{L,mp}{}^{1.5}\ /\ C_{D,mp}\right)\sigma^{\,0.5}}\right\}\right] \tag{B.5}$$

$$E_{CL} = \frac{h_{cr} - h_{SL}}{RoC_{\max}} \tag{B.6}$$

And V_{CL} equals takeoff velocity, usually assumed to be 1.2 times of stall velocity.

Phase 5: Cruise (W_{fi5})

To determine the minimum fuel use in 400-nm cruise, Breguet's range equation, Eqn. (B.7), is evaluated at a minimum drag condition to provide a higher lift to drag ratio for the propeller-driven airplane.

$$R = 375\left(\frac{\eta_p}{c_p}\right)\left(\frac{L}{D}\right)_{\max}\ln\left(W_{if\,5}\right) \tag{B.7}$$

$$\left(L\ /\ D\right)_{\max} = \frac{1}{2\sqrt{C_{D0}K}} \tag{B.8}$$

Phase 6: Loiter (W_{fi6})

A 45-minute loiter time is required for an airplane. Eqn (B.2) is applied at the minimum power required condition.

$$V_{mp} = 0.68 \cdot \sqrt{\frac{2 \cdot TOGW}{\rho \, SC_{L,mp}}} \tag{B.9}$$

After calculating all fuel fractions and applying them to Eqn. (B.1), the weight of fuel actually used is obtaind from Eqn. (B.10)

$$W_{f,actual} = (1 - M_{ff}) TOGW \tag{B.10}$$

In this case, the total fuel required for this mission must include 5% reserve and 1% trapped fuel in the calculation.

$$W_f = 1.06 W_{f,actual} \tag{B.11}$$

Since a takeoff gross weight is unknown in the beginning, the fuel fraction estimation is reevaluated until a calculated fuel weight corresponds to the input takeoff gross weight from a summation of empty weight, payload and fuel weight. The resulting fuel weight and takeoff gross weight are essential for the performance calculations

Aircraft Performance Estimations

1. Takeoff performance [B.2,B.3]

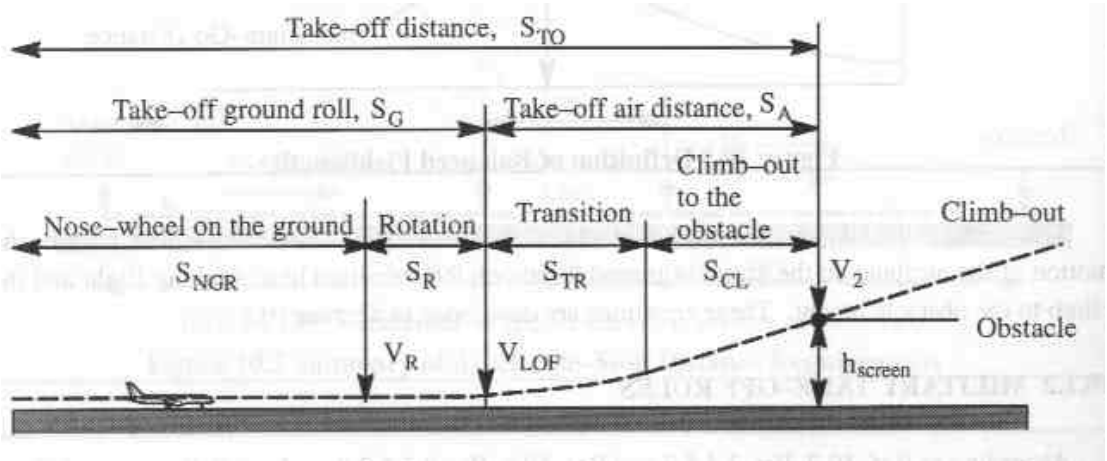

Figure B.2: Geometry of Takeoff distances [B.2]

Takeoff distance prediction starts by examining the different flight segments which make up takeoff. In general, an airplane accelerates to a takeoff velocity (V_{TO}), approximated to be 120% of a stall velocity (V_s) in takeoff configuration, and then it rotates to an angle of attack that provides a takeoff lift coefficient ($C_{L,TO}$) which equals 80% of a maximum lift coefficient ($C_{L\,\max}$). At that point, an airplane starts to lift off the runway and transitions to a climb angle until it reaches desired altitude.

$$V_{TO} = 1.2 \cdot V_s \tag{B.12}$$

$$C_{L,TO} = 0.8 \cdot C_{L\,\max} \tag{B.13}$$

For the ground roll distance, there are several approaches to estimate the ground run acceleration of these vehicles. According to a force diagram during ground roll, 5 forces dominate the calculation; lift, drag, thrust, weight, and friction force, all of which may vary with velocity. Therefore, in this case, it is assumed that overall accelerating velocities are approximately equal to steady 70% of V_{TO}. The calculation of those forces is based on this assumption without including any aerodynamic ground effect. A ground friction coefficient (μ) of 0.025 for concrete and macadam was applied. The distance while the nose-wheel is on the ground is indicated in Eqn. (B.14).

$$S_{NGR} = \frac{1.44 \cdot (TOGW\ /S)_{TO}}{g\rho\ C_{L\,\max}\left[\frac{T-D}{TOGW} - \mu\left(1 - \frac{L}{TOGW}\right)\right]} \tag{B.14}$$

For general aviation, a rotation distance is approximated to have a constant takeoff velocity for 1 second.

$$S_R = V_{TO} \tag{B.15}$$

In a transition distance, an airplane completely lifts off a ground and gradually changes to a climb angle by a constant-velocity arc (θ_{CL}) of a radius (R_{TR}) in Eqn. (B.16), (B.17) and (B.18) wherein the load factor on the airplane is assumed to be 1.15

$$R_{TR} = \frac{V_{TO}^2}{0.15g} \tag{B.16}$$

$$\theta_{CL} = \sin^{-1}\left(\frac{T-D}{TOGW}\right) \tag{B.17}$$

$$S_{TR} = R_{TR} \cdot \sin(\theta_{CL}) \tag{B.18}$$

$$h_{TR} = R_{TR}\left[1 - \cos(\theta_{CL})\right] \tag{B.19}$$

The field length definition of FAR Part 23 states that it includes the distance needed to clear an altitude 50 ft above the ground. If the transition height in Eqn (B.19) is less than that, the airplane climb distance to over 50 ft must be considered as indicated in Eqn. (B.20)

$$S_{CL} = \frac{50 - h_{TR}}{\tan(\theta_{CL})} \tag{B.20}$$

However, if the final transition height already exceeds the restriction, the takeoff distance is considered up to the point where the airplane reaches 50 ft height above the ground in transition mode.

The takeoff ground roll is a summation of S_{NGR} and S_R whereas the takeoff distance covers both takeoff ground roll and takeoff air distance.

2. Landing distance [2]

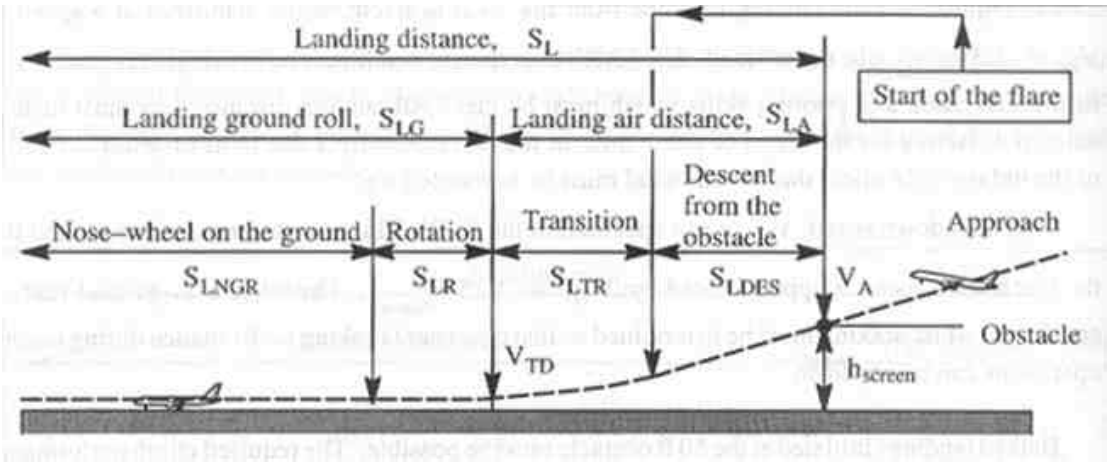

Figure B.3: Geometry of Landing Distances [B.2]

Similar to the takeoff distance, the landing distance from FAR part 23 includes the ground distance required for the airplane to clear a 50 ft obstacle and to come to a complete stop. An approach speed (V_A) is required to be 130% of V_s in landing configuration while an approach lift coefficient ($C_{L,A}$) is defined by V_A.

$$V_A = 1.3 \cdot V_s \tag{B.21}$$

$$C_{L,A} = \frac{C_{L\,\max}}{1.69} \tag{B.22}$$

With an assumption that the engine is at idle thrust, a flare angle (γ_A) is determined from Eqn. (B.23). To acquire a flare radius in Eqn. (B.24), an approximation of a flare velocity (V_{FL}) is 0.95

times of V_A is used and a load factor is 1.08 is used due to a steep flight path angle. Therefore, the landing air distance is a combination of 2 segments, approach and flare, as indicated in Eqn. (B.25).

$$\gamma_A = \sin^{-1}\left(-\frac{T}{TOGW} + \frac{L}{D}\right) \tag{B.23}$$

$$R_{FL} = \frac{V_{FL}^2}{g(n_{FL} - 1)} \tag{B.24}$$

$$S_{LA} = \frac{50}{\tan(\gamma_A)} + R_{FL}\,\frac{\gamma_A}{2} \tag{B.25}$$

The FARs require a touch down velocity (V_{TD}) must be 1.15 V_s. After that the airplane rotates to a level position. An assumption of a rotation time is 1 second.

$$V_{TD} = 1.15 \cdot V_s \tag{B.26}$$

$$S_{LR} = V_{TD} \tag{B.27}$$

With brakes activated on the main gear, ground friction coefficients are 0.4 at the main gear and 0.025 at the nose gear. the weight ratio at the nose gear is assumed to be 0.08. The landing distance when the nose-wheel on the ground is calculated in Eqn. (B.28).

$$S_{LNGR} = \left\{\frac{TOGW\ /\ S}{g\rho\left(C_D - \mu_{break}C_L\right)}\right\}\ln\left[1 + \frac{\left(V_{TO}\right)^2\rho\left(C_D - \mu_{break}C_L\right)}{2\cdot\frac{TOGW}{S}\left\{\left(\mu_{break} - \frac{T}{TOGW}\right) - \frac{N_n}{TOGW}\left(\mu_{break} - \mu\right)\right\}}\right] \tag{B.28}$$

Thus, a landing ground roll is obtained from adding S_{LR} to S_{LNGR}. Total landing distance is a summation of the landing ground roll to S_{LA}.

3. Maximum cruise speed [B.4]

Only 80% of engine horsepower was assumed used at maximum cruise speed. It is defined as the velocity where power available (P_A) equals power require (P_R) at cruise altitude.

$$P_A = 0.8 \cdot 550 \cdot \eta_p \cdot hp \cdot \sigma \tag{B.29}$$

$$P_R = \frac{1}{2}\rho V^3 S C_{D0} + \frac{K \cdot TOGW^2}{\frac{1}{2}\rho VS} \tag{B.30}$$

Figures B.4 – B.7 show the power required and power available curves and intersections of them for these vehicles.

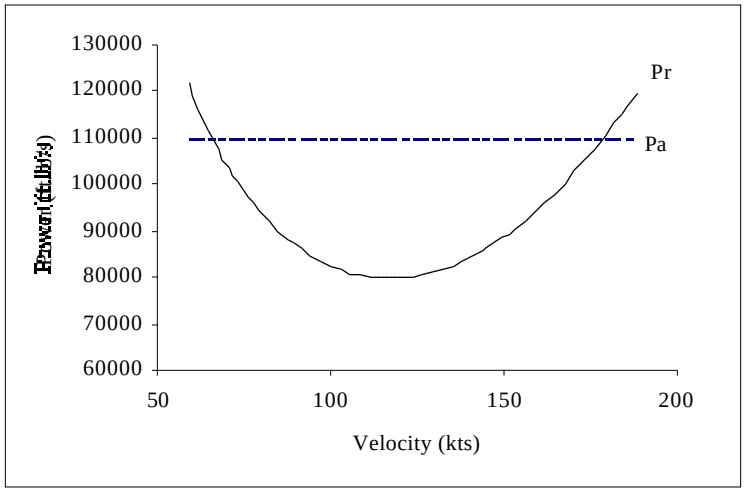

Figure B.4: Power Required and Power Available for the Pegaus II

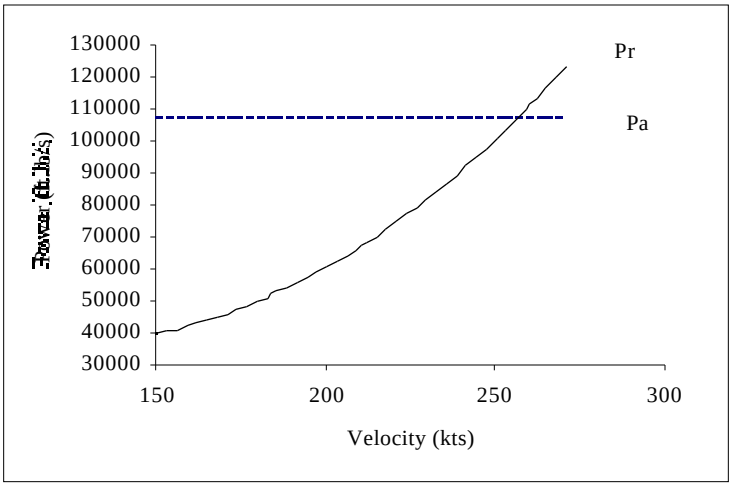

Figure B.5: Power Required and Power Available for the LaBiche

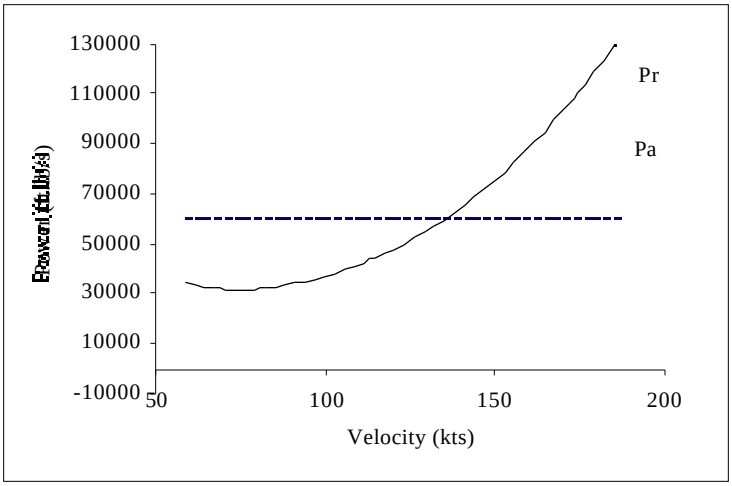

Figure B.6: Power Required and Power Available for the Cessna 182

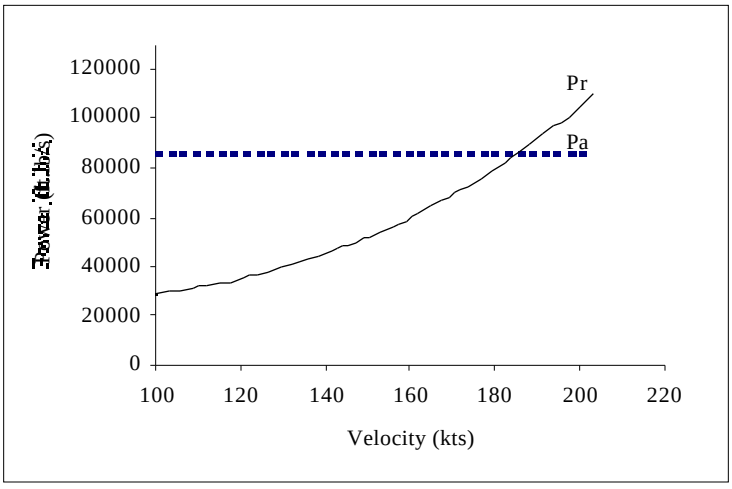

Figure B.7: Power Required and Power Available for the SR22

4. Stall speed [B.4]

The stall velocity for each airplane is determined by its takeoff gross weight and maximum lift coefficient, which varies with an application of high-lift devices and altitude. All velocities shown are true air speed.

$$V_S = \sqrt{\frac{2 \cdot TOGW}{\rho \, SC_{L\max}}} \tag{B.31}$$

5. Service and absolute ceiling [B.2]

At the service ceiling the minimum rate of climb at that altitude is defined as 100 fpm, while for absolute ceiling it is 0 fpm. By applying the rate of climb equation, Eqn. (B.5), the densities at the state of 0 and 100 fpm rate of climb can be calculated to get standard atmosphere altitudes.

A performance comparison of these vehicles was shown in Table 1 of the main report. It indicated that all four aircraft meet PAVE and FAR requirements. For the Pegasus dual-mode vehicle issues of roadability and highway use regulations will be analyzed further in Appendix C.

Lift Coefficient for Pegasus II Wing Concept

A new approach to a roadable aircraft wing structure was employed in the Pegasus II design. A new method of manually storing the outboard wing component within the inboard section was used instead of the telescoping wing concept. Both outboard wings would be put into the slot inside the inboard section in reverse as indicated in Figure B.8. The 17-percent thick of GA (W)-1 section is used for the inboard wing and a 13-percent thick , GA (W)-1, airfoil section was used for the outboard wing segments. A method of analysis of the aerodynamics of this three section wing had to be developed. There are 2 primary assumptions used in these calculations.

1. The lift distribution of inboard section was considered to resemble a 2-dimensional airfoil due effect of the vertical stabilizers at the tip of the inboard section.

2. The lift distribution to the “fence” of outboard wing was calculated by merging 2 sides of wing together as one continuous wing.

The equation employed to obtain average C_L max over total wing is

$$C_{L\max} = \frac{S_i C_{L\max,i} + S_o C_{L\max,o}}{S} \tag{B.32}$$

Figure B.8: Diagram of the Wing Stowage Design

The maximum lift coefficients of GA (W)-1 airfoil were different for each flight condition Reynolds number as listed in Ref. B.5.

Table B.1: 2-D Maximum Lift Coefficient of a GA(W)-1 for Different Flight Conditions

Flight condition	Max 2-D lift coefficient
Cruise	2.02
Takeoff and landing	1.95
Stall speed	1.75

For the GA (W)-2 airfoil maximum lift coefficients also varied with the Reynolds Numbers for different flight condition.

Table B.2: 2-D Maximum Lift Coefficient of a GA(W)-2 for Different Flight Conditions

Flight condition	Max 2-D lift coefficient
Cruise	2.08
Takeoff and landing	1.97
Stall speed	1.84

Using the following equation in Ref. B.3, 3-D maximum lift coefficients were estimated.

$$C_{L\,\max} = \left(\frac{C_{L\,\max}}{C_{l\,\max}} \right) C_{l\,\max} \qquad \text{(B.33)}$$

where $\left(\frac{C_{L\,\max}}{C_{l\,\max}} \right)$ was given in Figure B.9, which was 0.9 for 0 Λ_{LE}.

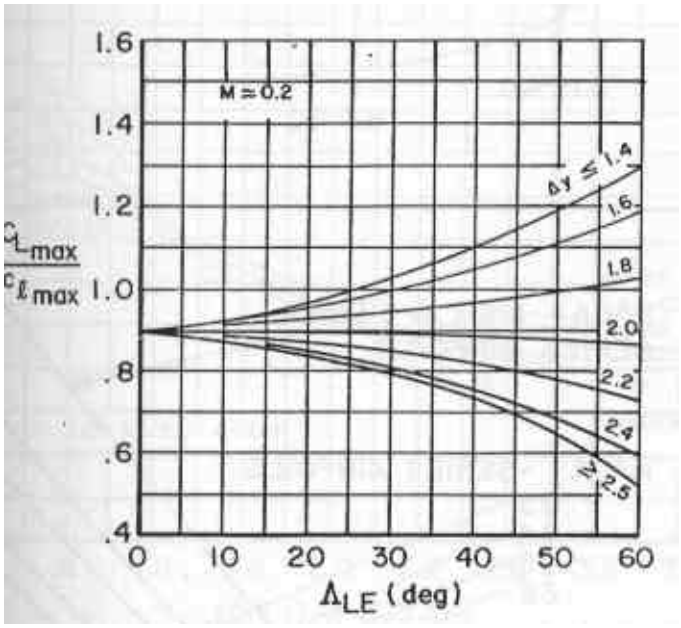

Figure B.9: Variation of $\left(\frac{C_{L\max}}{C_{l\max}}\right)$ with Λ_{LE} [B.3]

The resulting estimated 3-D maximum lift coefficients are shown in Table B.3.

Table B.3: 3-D Maximum Lift Coefficient of the GA(W)-2 for Different Flight Conditions

Flight condition	Max 3-D lift coefficient
Cruise	1.872
Takeoff and landing	1.773
Stall speed	1.656

The estimated 3-D lift cure slope was found by applying the equation from Ref. B.6. to the wing design of outboard section.

$$\frac{dC_L}{d\alpha} = \frac{2\pi\ AR_e}{2+\left[4+\frac{AR^2\beta^2}{\eta^2}\left(1+\frac{\tan^2\Lambda_t}{\beta^2}\right)\right]^{0.5}}\frac{S_{\exp}}{S}F \qquad \text{(B.34)}$$

In this case, the effective aspect ratio was assumed to be that of the straight outboard wing with 17-feet span and 5.2 feet chord since some of the lift in inboard section should affect the total lift curve slope of the outboard section. Hence, AR_e equaled 3.269. With 3.7 ft for fuselage width, F was calculated to be 1.5865 and $S_{\exp}$ was 69.16 ft^2. The 3-D lift curve slope of the GA (W)-2 section was approximated to be 0.0764 per degree.

To obtain the 3-D stall angle of attack, the following equation was applied

$$\alpha_{stall} = \frac{C_{L\max}}{C_{L_\alpha}} + \alpha_{0L} + \Delta\alpha_{C_{L\max}} \qquad \textbf{(B.35)}$$

The relationship of $\Delta\alpha_{C_{L\max}}$, taper ratio and Δy is shown in Figure B.10

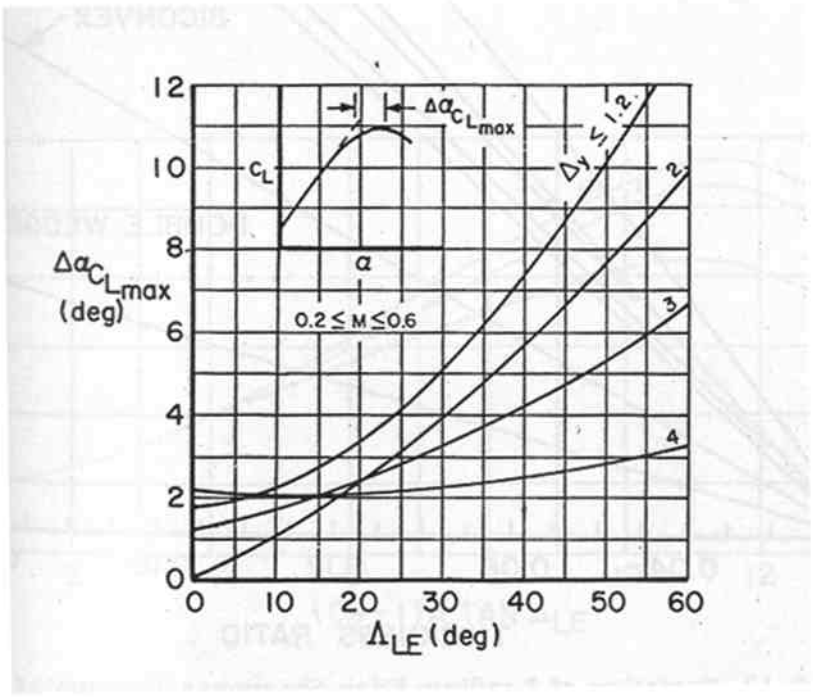

Figure B.10: Variation of $\Delta\alpha_{C_{L\max}}$ with Λ_{LE} [B.3]

The application of high-lift devices was evaluated by using the approach found in Ref. B.3. The modified Pegasus employed flaperons of the plain flap type to enhance the lift during takeoff and landing. The flap chord ratio ($\frac{c_f}{c}$) is 0.2 and the flap span ratio ($\frac{S_{wf}}{S_w}$) is 0.65.

The change in zero-lift angle of attack (α_{0L}) was found by

$$\Delta\alpha_{0L} = -\frac{dC_l}{d\delta_f}\frac{1}{C_{l_\alpha}}\delta_f K' \qquad \text{(B.36)}$$

Figure B.11 gives the variation of K' which is 1, 0.87, 0.6 for 10, 20, 40 degree flap deflections respectively. Figure B.12 shows that $\frac{dC_l}{d\delta_f}$ is approximately 3.65 for the flap chord ratio of 0.2.

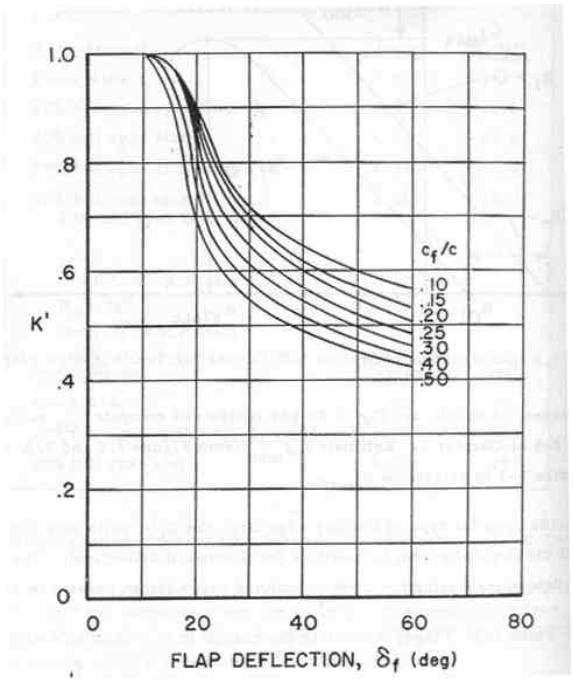

Figure B.11: Non-Linear Correction for Plain T.E. Flaps [B.3]

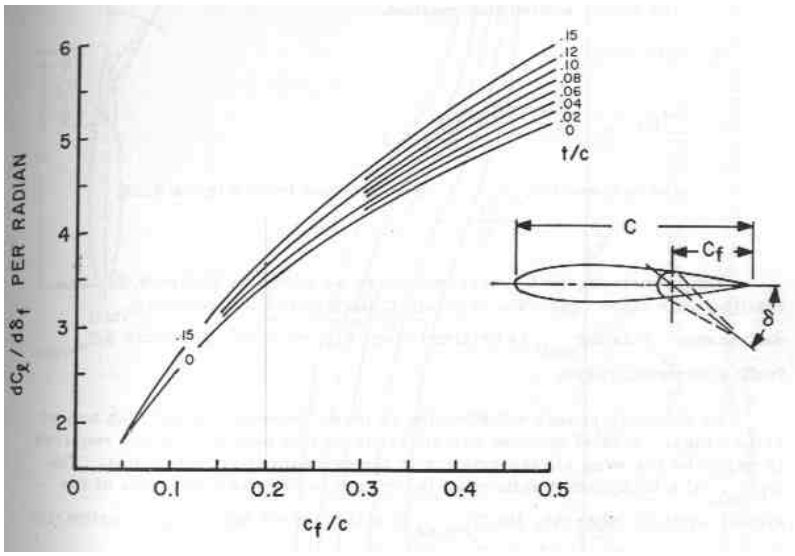

Figure B.12: Variation of $\frac{dC_l}{d\delta_f}$ with Flap Chord Ratio [B.3]

The variation in 2-D stall angle of attack for δ_f flap deflection was obtained from Figure B.13. for the desired flap chord ratio. Afterward, the 2-D lift curve with flap deflection was constructed following Figure B.14 based on the lift curve from experimental data for the GA (W)-2 airfoil in found in Ref B.7.

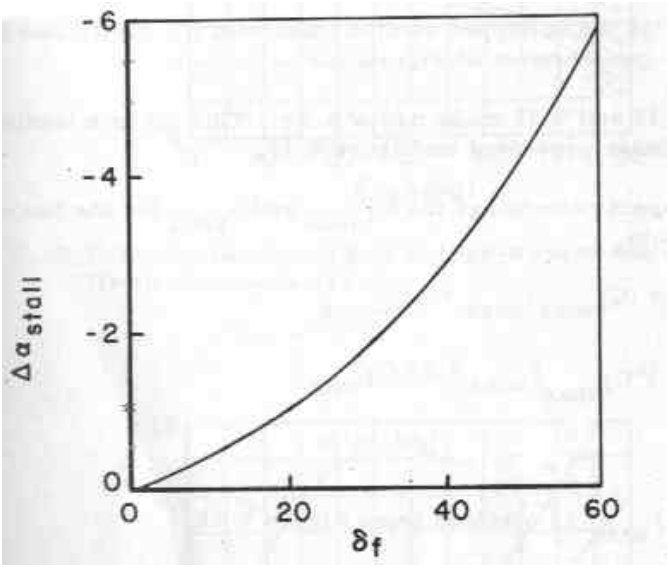

Figure B.13: Decrease in Stall Angle with Flap Deflection [B.3]

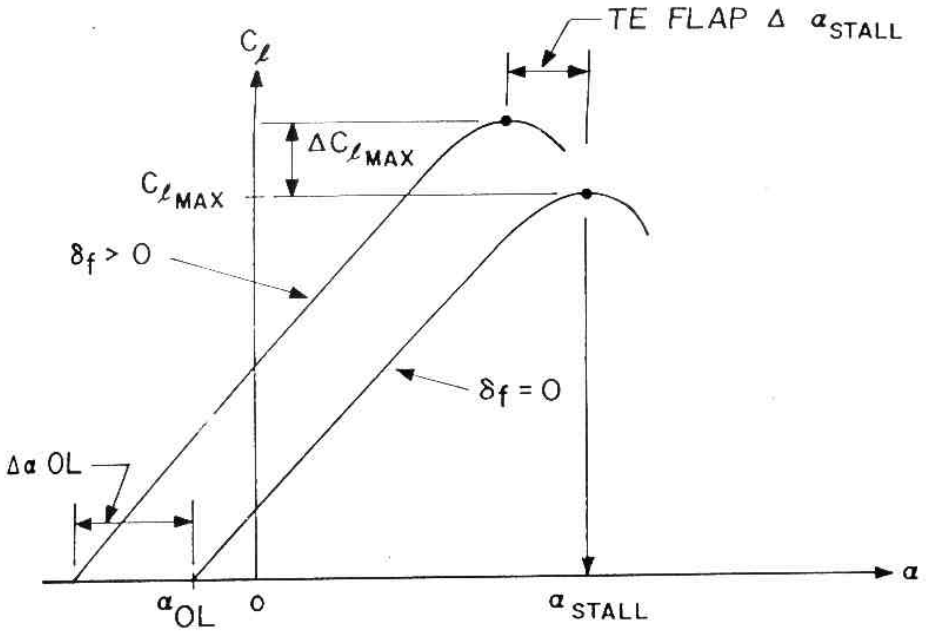

Figure B.14: Construction of Section Lift Curves for Trailing Edge Flaps [B.3]

The previous calculations of $C_{L\,\max}$, $\frac{dC_L}{d\alpha}$ and α_{stall} provided a 3-D lift curve without flap deflection. The effect of plain flap deflection on the 3-D lift curve is a change in zero-lift angle of attack that was the same as the change for the 2-D case. Also there was an increase in $C_{L\,\max}$.

$$\Delta C_{L_{\max}} = \Delta C_{l\max} \frac{S_{Wf}}{S_w} K_\Lambda \qquad \textbf{(B.37)}$$

For a non-taper wing, K_Λ equals 0.92.

This calculation was used in the construction of a 3-D lift curve with flap deflection having the same lift curve slope as the one without flap. Figure B.15 shows the resulting graph of lift curves for GA (W)-2

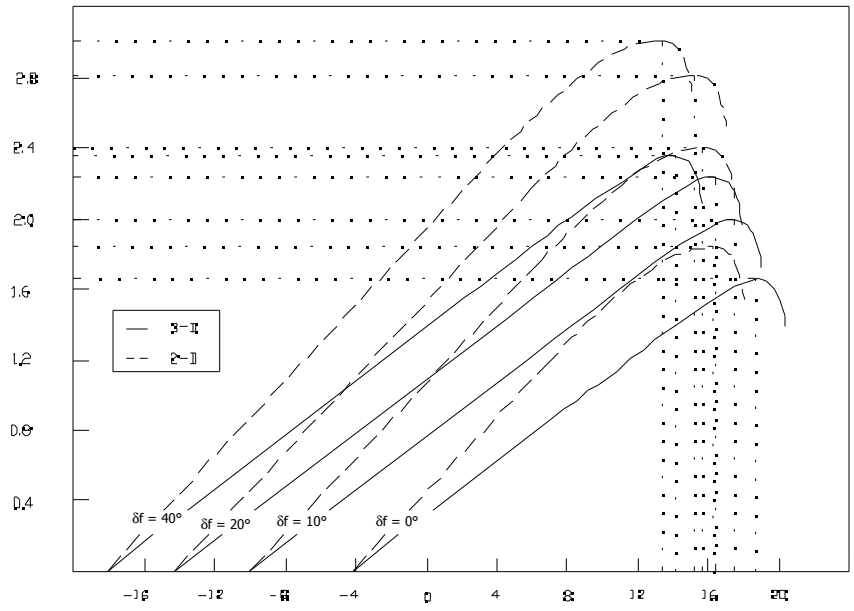

Figure B.15: Plot of the Lift Curve for the GA (W)-2 for 2-D and 3-D

The $C_{L\max}$ and α_{stall} for flap deflection of 10 – 40 degrees is shown in Table B.4

Table B.4: 3-D Maximum Lift Coefficient of the GA(W)-2 for Different Flight Conditions

Flap deflection	$C_{L\max}$	α_{stall}
10	1.9952	17.48
20	2.2378	16.37
40	2.3563	14.09

Thus, the calculation from Eqn. B.32 for total lift coefficient of this wing concept is illustrated in Table B.5.

Table B.5: 3-D Maximum Lift Coefficient of the Combined Inboard/Outboard Wing

Flight condition	Lift coefficient for entire wing
Cruise	1.850
Takeoff and landing	1.982
Stall speed	1.995

References

B.1 Roskam, Jan, *Airplane Design Part 1: Preliminary Sizing of Airplanes*, DARcorporation, Lawrence, Kansas, 1997

B.2 Roskam, Jan, Lan, Chuan-Tau E., *Airplane Aerodynamics and Performance*, DARcorporation, Lawrence, Kansas, 1997

B.3 Nicolai, Leland M., *Fundamentals of Aircraft Design*, Domicone Printing Services, Fairborn, Ohio, 1975

B.4 Anderson, John D., JR., Introduction to Flight, International 3rd edition, McGraw-Hill Book Company, Singapore, 1989

B.5 Gassler, R, et.al., *Pegasus, A report to the AGATE NASA/FAA General Aviation Design Competition*, Virginia Tech Aerospace & Ocean Engineering Department, May, 2000

B.6 Raymer, Daniel P., *Aircraft Design: A Conceptual Approach*, American Institute of Aeronautics and Astronautics, Inc., Washington, D.C., 1989

B.7 McGhee, Robert J., Beasley, William D., and Somers, Dan M., *Low-Speed Aerodynamic Characteristics of A 13-Percent-Thick Airfoil Section Designed for General Aviation Applications, NASA TM X-72697*, Langley Research Center, Hampton, VA, May, 1977

APPENDIX C

ROADABILITY EVALUATION
(FROM ORIGINAL VIRGINIA TECH PEGASUS REPORT[2]

(NOTE: THIS SECTION WAS “APPENDIX M” IN THE PEGASUS REPORT AND IS STILL SO NOTATED ON THE FOLLOWING PAGES WHICH ALSO RETAIN THEIR NUMBERING FROM THAT REPORT.)

Appendix M. Roadability

M.1. Introduction

The Road Vehicle Design Specification addresses all issues that affect the ability of the designed vehicle to travel safely and legally on the road, meeting or exceeding all regulations and requirements.

Given that the design is for a roadable aircraft, a concern for the roadability of the vehicle must underlie all design activities. This underlying concern is clearly evident in the evolution of the vehicle configuration to a baseline level; the baseline design was arrived at as a result of continuous trade-offs between road and air vehicle requirements.

Upon progression from the baseline to the detailed design stage, the project group formed a number of sub-groups with specific objectives. Each of these sub-groups was responsible for addressing both the air and the roadable components of their agenda. The roadability sub-group was responsible for developing all components of the vehicle relating specifically to travel on the road. The Road Vehicle Design Specification can be sub-divided into three main areas:

- Design and integration of the road systems of the vehicle including steering, brakes, and suspension / landing gear.
- Calculation of the vehicle performance in terms of velocities, acceleration, braking, handling, and rollover.
- Proof that the vehicle will meet US and EC transport regulations and standards.

M.2. Road Systems Design

The road systems are those components that directly affect the ability of the vehicle to drive safely on the road; namely the steering, suspension, and brakes.

The road systems serve a dual purpose; firstly as the vehicle suspension, steering and braking systems when in road configuration, and secondly as the vehicle undercarriage when in flight configuration. In order to meet the requirements of both cases it was necessary to make trade-offs in order to optimize the system to provide adequate performance in both configurations. The main considerations for each configuration are tabulated below in table M.2-1.

Table M.2-1 Configurations Considerations

ROAD CONFIGURATION	FLIGHT CONFIGURATION
Safety	Absorption of landing loads
Stability & Handling	Ground Stability
Passenger Comfort (ride)	Ground Clearance
Vehicle Lift	Wing Incidence on take-off

The road systems design is biased towards the road configuration due to the complex loadings that must be accounted for in this configuration. In most cases, such as braking and steering, the design for the road exceeds the similar requirements for the air. The suspension represents the greatest challenge and this has been the object of a large proportion of the design efforts.

M.2.1. Wheels/Tires Selection

The tire selection was based on a hybrid between car and aircraft tires. Major considerations were the package size and weight, cornering stiffness (for road handling), and tire deflection (for landing load absorption).

In order to provide suitable performance in the road configuration it was necessary that the rear tires had greater cornering stiffness than the front tires; this was achieved by increasing the rated load index of the rear tires through increasing the section width. This led to section widths of 165mm at the front, and 175mm at the rear. The aspect ratio was a compromise between a low aspect ratio for good cornering stiffness and low rolling friction, and a high aspect ratio to provide maximum tire deflection for landing (Eqn M-1):

(M-1) Aspect Ratio, AR = (Section Height / Section Width) * 100

An aspect ratio of 75% was chosen as a compromise, based on an analysis of car and aircraft tires. To keep the rolling radius of front and rear tires as close as possible, the rear tires have a rim diameter of 13", and the front tires a rim diameter of 14". The tire construction is radial, as radial tires represent "the only means of satisfying the increasingly variegated range of operating capabilities demanded of the tires used on today's passenger cars and heavy commercial vehicles"[1]. This leads to a tire designation of P165/75 R14 (Load Index = 81) for the front tires, and P175/75 R13 (Load Index = 85) for the rear tires (based upon Pirelli P2000's). The tire pressure was designated as 24psi, front and rear.

The wheels were chosen on the basis of minimum weight and hence TSW Imola alloy road wheels were selected.

M.2.2. Suspension Design Requirements

The suspension was designed according to the following requirements :

- Provide adequate wheel clearances across the load range, in all modes,
- Provide adequate clearance for the flaperons at full deflection,
- Limit package size,
- Maintain minimal wing incidence in road configuration, especially at low weights,

- Provide adequate load absorption for road and landing cases,
- Give good ride response, with similar frequencies front and rear
- Optimize cornering performance to produce understeer across all loading conditions.

The design process was iterative, with minor modifications being made to the geometry and spring design to optimize the vehicle and suspension performance according to the above requirements.

The suspension system operates in four modes; the suspension configuration for each mode is:

Road : The suspension is optimized for road travel.

Take-Off : Rear wheels retract slightly to increase wing incidence by 1°.

Flight : The suspension semi-retracts into the fuselage to reduce drag, whilst still allowing a small amount of the wheel to protrude in case of an emergency landing scenario.

Landing : The suspension fully extends due to the force of the spring and the variable damper is set to provide optimal shock absorption for touch-down.

M.2.3. Suspension Configuration

The front suspension is of an upper wishbone configuration with the lower arm attached to a longitudinal torsion bar (see Figure M.2-1). The two prongs of the upper wishbone and the torsion bar are attached to the vehicle structure. The stub axle / steering swivel are connected to the arms by ball joints. The damper is located on the lower arm and runs between the two prongs of the upper wishbone to attach to the vehicle structure, via a screwjack.

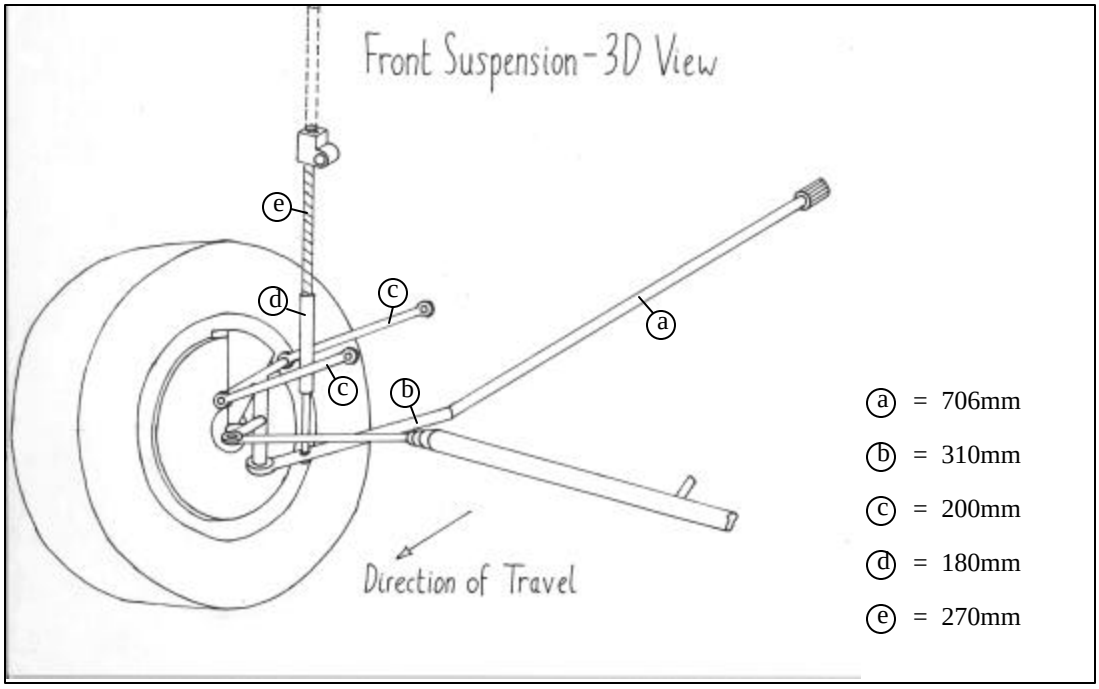

Figure M.2-1 Front Suspension

The rear suspension is of a trailing arm configuration (see Figure M2-2) with a spring/damper unit attached close to the wheel. Given the limited package requirements at the rear wheels the trailing arm attachment is mounted as low as possible. For take-off the rear suspension retracts by 70mm to provide an additional 1° of wing incidence.

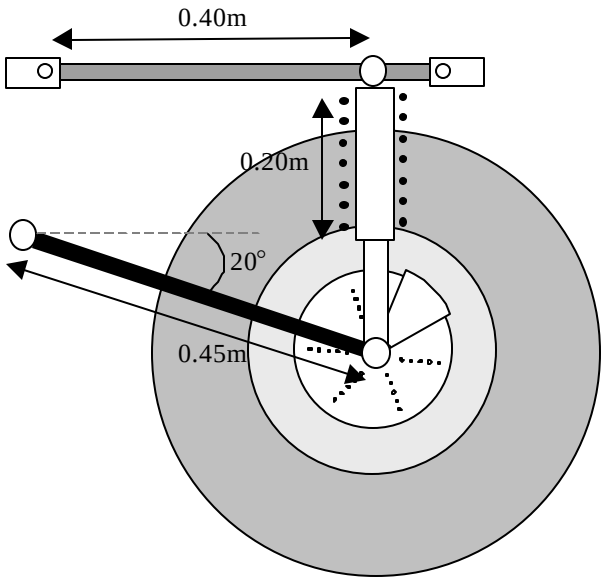

Figure M.2-2 Rear Suspension

The ground clearances, across the load range, in the different modes are as follows in table M.2-2:

Table M.2-2 Ground Clearences

GROUND CLEARANCES		
Mode	**Front (mm)**	**Rear (mm)**
Road	349 – 400	368 – 400
Take-Off	349 – 400	298 – 330
Flight	200	200
Landing	470	500

M.2.4. Damping

Active dampers provide variable damping for the front and rear suspension. This system operates by using a solenoid valve to control the rate of flow of damping fluid and hence alter the damping ratio. The variable damping ratio allows the performance of the vehicle to be optimized when in the road configuration. More importantly, the active damping allows the damping ratio to be varied between the different requirements of the road case and the landing case.

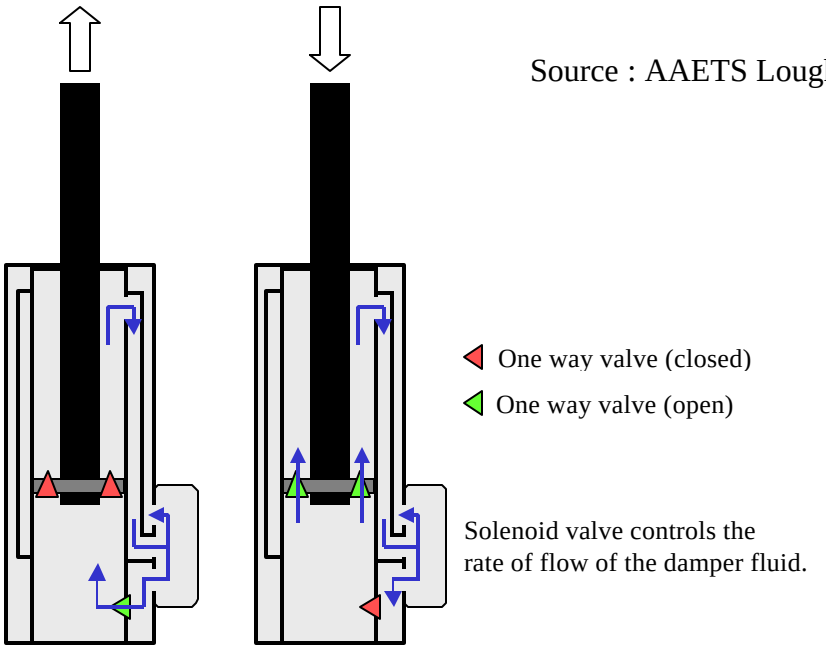

Figure M.2-3 Front and Rear Dampers

The front and rear dampers are used to semi-retract the wheels in flight (refer to figures M2-1 and M2-2). The dampers are connected to the vehicle structure via screw jacks, which allows the damper, and hence the whole wheel unit, to be semi-retracted. The screw jacks are electrically powered with a manual back-up. Each front damper is connected to a single screw

jack mounted close to the vertical. Each rear damper is mounted to a longitudinal sliding arm, operated by the screw jack.

The damper lengths may be determined from the maximum suspension deflection divided by the spring ratio (for the damper), giving lengths 0.18m (front) and 0.20m (rear).

M.2.5. Landing Deflection

The aircraft is designed to touch down rear wheels first. The minimum leg deflection was calculated using Eqn's M-2 to M-4:

(M-2) $$KE = Wv^2/2g = \eta nW\delta$$

(M-3) $$\eta\delta = v^2/2ng$$

(M-4) $$\eta\delta = \eta_{tyre}\delta_{tyre} + \eta_{leg}\delta_{leg}$$

A maximum descent velocity for a civil aircraft of 3.05 m/s[XXXM5], and a minimum value for n of 3, were used. The tire efficiency η_{tire} = 0.47[XXXM5,] and damper efficiency η_{leg} = 0.65 (estimated). Hence, the vertical travel for the rear suspension arm is required to be at least 0.14m (5.5 in.) to absorb the kinetic energy of landing; given that the damper length is 0.20m this is ample.

M.2.6. Front Geometry and Spring Design

The suspension was optimized through varying the deflection (and hence the wheel rate), and the lower arm length and angle. An initial evaluation, based upon a maximum bump acceleration of 0.5g @MTOW[3] and a maximum shear stress of 800N/mm^2 [4], gave an optimal value for the lower arm length of 0.31m (12.2 in). A ground clearance of 400mm (15.7 in) was chosen as a compromise between the opposing requirements of road and flights operations. Using the values for ground clearance and lower arm length the lower arm angle was determined

as 33°. A negative swing arm suspension geometry[3] was initially chosen to reduce the loads on the torsion bar. However, in order to provide good cornering performance it was necessary to raise the front roll center, and hence the geometry was modified to inclined parallel links[3]. With this information the geometry was defined, as shown in the following diagram :

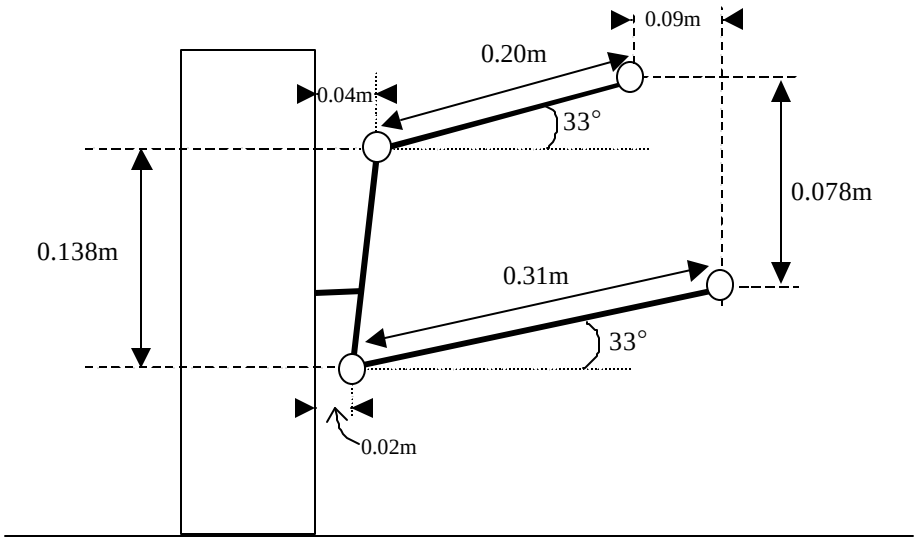

Figure M2-4 (not to scale)

A target value for the wheel rate was estimated from the lateral load transfer performance calculations (see Section M3.9). The suspension static deflection was then optimized, front and rear, to reach a compromise between this requirement and the ground clearance requirements.

The torsion bars were designed using the method described by Dunn[2], summarized in Eqn's M-5 to M-11:

(M-5) $$k_w = \frac{W}{\delta}$$

(M-6) Ride Frequency, $$\lambda = \frac{1}{2\pi}\sqrt{\frac{g k_w}{W}} = \frac{1}{2\pi}\sqrt{\frac{g}{\delta}}$$

(M-7) $$\frac{T}{J} = \frac{Gq}{L} = \frac{t}{r}$$

(M-8) $$d = \sqrt[3]{\frac{16T}{pt}}$$

(M-9) $$L = \frac{Gq \ \ pd^4/32}{T}$$

(M-10) $$T_{SL} = R_L a = W_{SL} R_{S.SL}$$

(M-11) $$k_q = k_W R_{S.SL}{}^2 + T\frac{dR_S}{dX}$$

Based upon this method, the wheel rate k_w of the front suspension is 29.43N/mm giving an acceptable ride frequency of 1.44Hz, at MTOW, and the following deflections:

Min Operating Weight	-	70.0mm (2.76 in.)
Max Take-Off Weight	-	120.5mm (4.92 in.)
0.5g Bump Acceleration	-	180.7mm (7.13 in.)

Given the geometry of the front suspension the force diagram is as follows (not to scale):

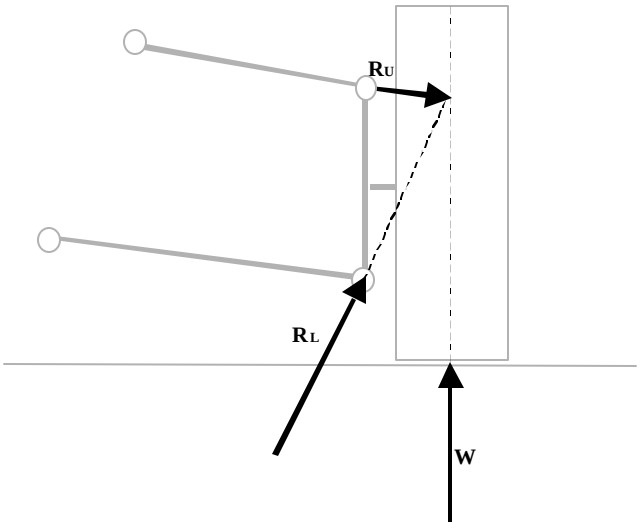

Figure M.2-5 Front Suspension

From the above diagram the angles between the force lines, termed α,β, and δ may be determined. The static deflection at MTOW is used to calculate the suspension geometry for this condition :

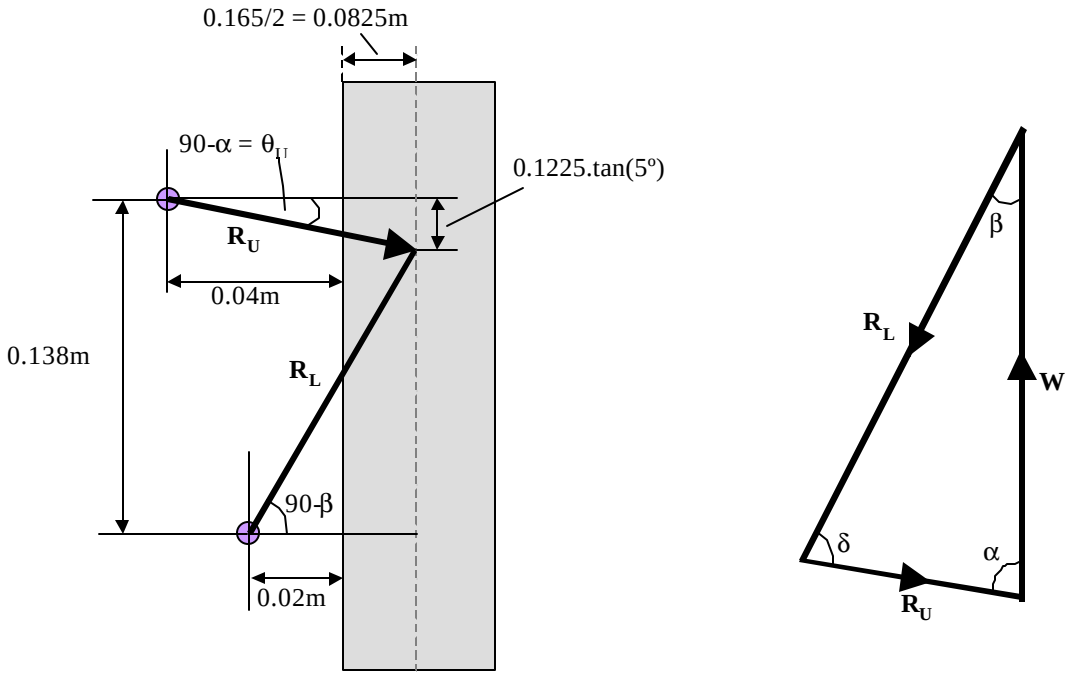

Figure M.2-6 Front Suspension Loading

Using the sine rule :

$$\frac{W}{\sin \boldsymbol{d}} = \frac{R_L}{\sin \boldsymbol{a}} = \frac{R_U}{\sin \boldsymbol{b}}$$

The dimension, a, may be determined:

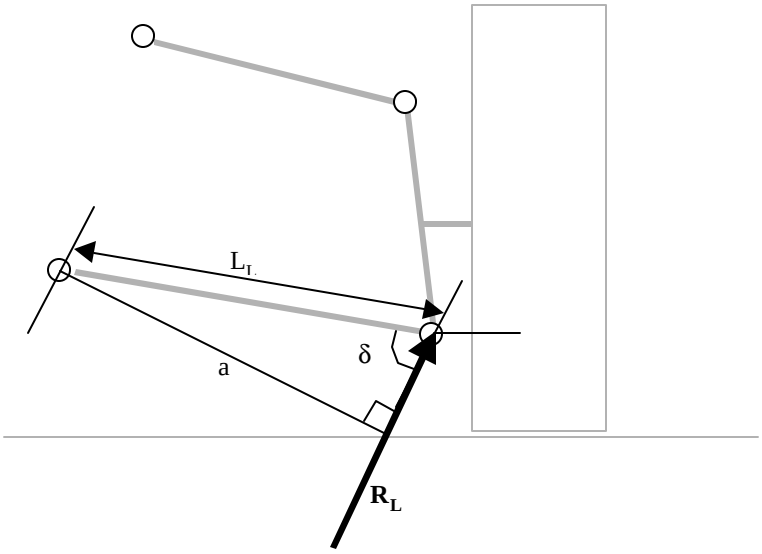

Figure M.2-7 Normal Force on the Front Suspension

Eqn's M-10 and M-11 now give the torsion bar rate k_θ as 2.42 x 10^6 N/rad, leading to a torsion bar diameter of 22.0 mm (0.87 in.) and a length of 706mm (27.8 in.) - based upon a maximum shear stress of 800N/mm^2.

M.2.7. Rear Suspension and Spring Design

The rear suspension geometry is outlined in the following figure :

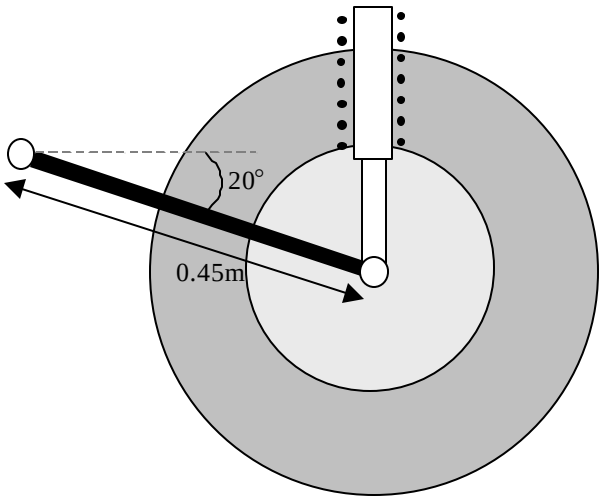

Figure M.2-8 Rear Suspension

The coil springs were designed using the method described by Dunn[2], summarized in Eqn's M-12 to M-15:

(M-12) $$k_s = k_w R^2$$

(M-13) $$t = k\frac{2.55SD}{d^3}$$

(M-14) $$k = \frac{4C-1}{4C-4} + \frac{0.615}{C}$$

(M-15) $$n_a = \frac{Gd^4}{8k_s D^3}$$

Based upon this method, the wheel rate k_w of the rear suspension is 24.87N/mm, giving an acceptable ride frequency of 1.37Hz @MTOW within 5% of the value for the front suspension, and the following deflections:

Min Operating Weight	-	100mm (3.94 in.)
Max Take-Off Weight	-	132mm (5.20 in.)
0.5g Bump Acceleration	-	197mm (7.76 in.)

The spring rate k_s is 24.9 N/mm, leading to a coil diameter of 100mm (3.94 in.), a wire diameter of 12mm (0.47 in.), and a requirement for 8 turns (based upon a maximum shear stress of 800N/mm^2).

For the maximum bump case (0.5g@MTOW) the ground clearance is 303mm (12.04 in), or 233mm (9.26 in) with the rear suspension lowered for take-off. The maximum possible flaperon deflection is 60%, giving a vertical distance of 300mm (11.92 in) downward. Given that the outer wing is mounted approximately 100mm (3.97 in) from the bottom of the fuselage it can be shown that in the worst case scenario the flaperon is 33mm (1.31 in) above the ground.

This state requires a combination of extremes (max. bump, full flap and full control deflection) and will be reached only occasionally and for brief periods; when it is the suspension stops will prevent the flap impacting with the ground.

M.2.8. Steering System

The steering system is operated by a simple rack and pinion arrangement, with the pinion being driven by an electric motor. No mechanical back-up is provided, allowing the vehicle electronics to disconnect the steering from the controls when the wheels are retracted. This system causes a concern over safety and reliability, as the system is not yet certified. Mercedes are pioneering drive-by-wire electronics and it is likely to receive certification within the next decade.

The steering geometry is based on the Ackerman geometry, Eqn's M-16 & M-17:

(M-16) $$\delta_0 = \tan^{-1}\frac{L}{(R + t/2)}$$

(M-17) $$\delta_i = \tan^{-1}\frac{L}{(R - t/2)}$$

This gives a maximum outward angle of 30.9° and a maximum inward angle of 37.2°.

M.2.9. Braking System

The braking system architecture consists of floating caliper disc brakes on all wheels. The brakes shall be actuated electronically using electronic actuators, with a mechanical linkage from the rear brakes to the handbrake serving as the secondary and parking brake system.

M.2.10. Wheel Volumes and Attachment Points

The dimensions of the front wheels are 165mm (6.57 inches) width, 603mm (23.74 inches)diameter. The dimensions of the rear wheels are 175mm (6.89 in.), 593mm (23.33 in.) The suspension attachment points are defined using the geometric center of the wheel as a reference point (x,y,z) = (0,0,0), using the following co-ordinate system:

+ve x = longitudinal : towards front of vehicle

+ve y = lateral : towards the centerline of the vehicle

+ve z = vertical : towards the ground

The wheels are mounted 4.02m (13.19 ft) apart. The lateral distance between the centerlines of the front wheels is 1.42m (4.66 ft). The lateral distance between the centerlines of the rear wheels is 1.94m (6.36 ft). At the reference position, i.e. minimum operating weight, the front and rear wheels both provide a distance between the ground and the underbody of the vehicle of 0.4m (15.75 in.).

For the front wheels the range of angles through which the upper and lower arms travel (where +ve is a downward displacement) are:

Upper Arm : 50.4° (full downward wheel deflection) → 10.8°

Lower Arm : 50.4° → 10.8°

The front suspension has four attachment points:

Two upper wishbone attachment points

@ (0.075, 0.290, -0.201)m & (-0.075, 0.290 -0.201)m

Torsion Bar attachment point

@ (-0.706, 0.363 -0.123)m

Damper attachment point

@ (0.0, 0.144, -0.560)m

The whole front wheel has an upward displacement from the reference position of 0.11m (4.33 in.) and a downward displacement of 0.07m (2.76 in.). Throughout its travel the front of the wheel must rotate through 30.9° towards the vehicle and 37.2° away from the vehicle.

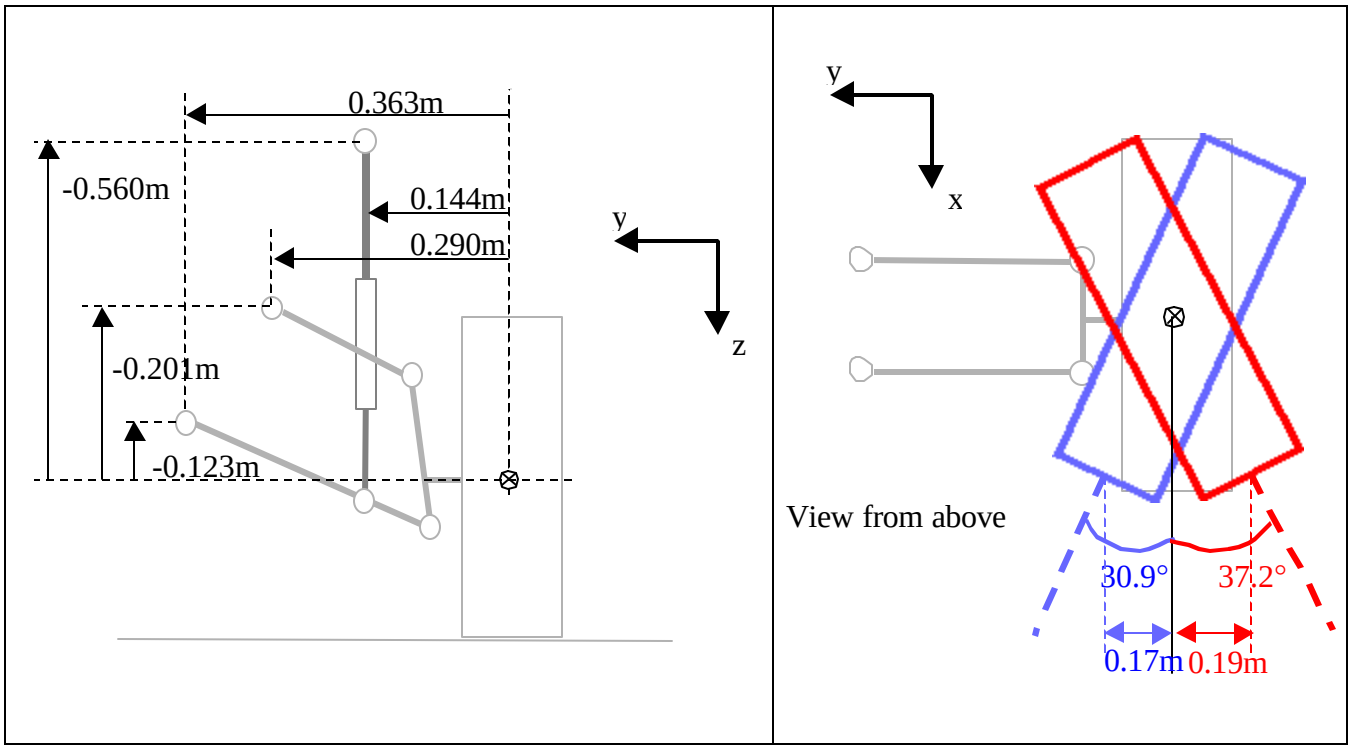

Figure M.2-9 Rear Suspension Schematic

The rear suspension has three attachment points:

Swing arm attachment point (A)

@ (0.423, 0.098, -0.015)m

Two screwjack attachment points, with 50mm clearance (B & C)

@ (0.433, 0.098, -0.394) & (-0.050, 0.098, -0.394)m

The whole rear wheel has an upward displacement from the reference position of 0.097m (3.82 in.) and a downward displacement of 0.10m (3.94 in.).

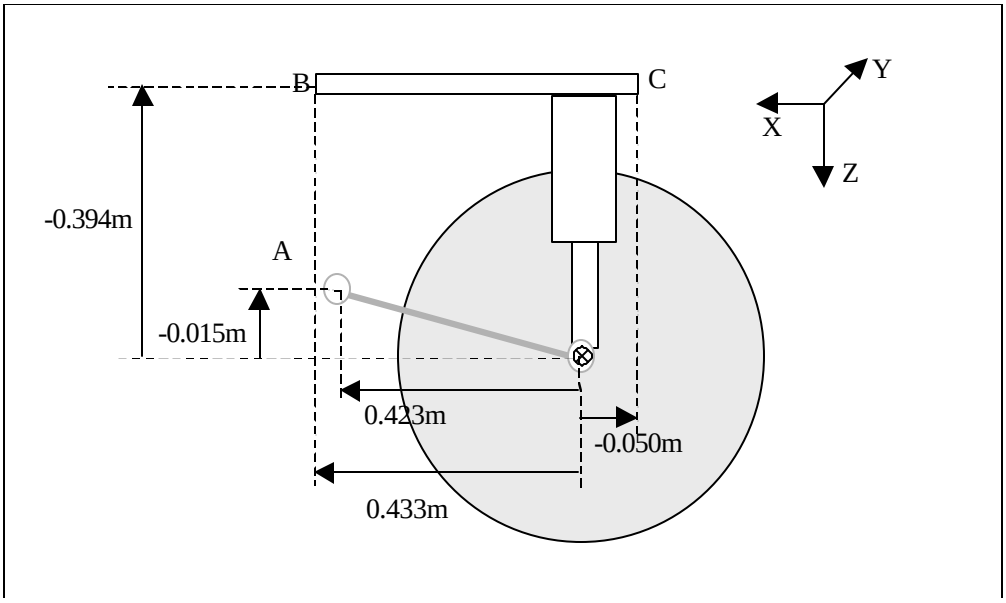

Figure M.2-10 Rear Suspension Positioning

M.3. Vehicle Dynamics

The road vehicle is *not* designed to offer a road performance comparable to modern high performance automobiles. Rather the emphasis for road performance is upon safety and predictable handling. The vehicle performance analysis is based upon Gillespie[3].

M.3.1. Vehicle Loading

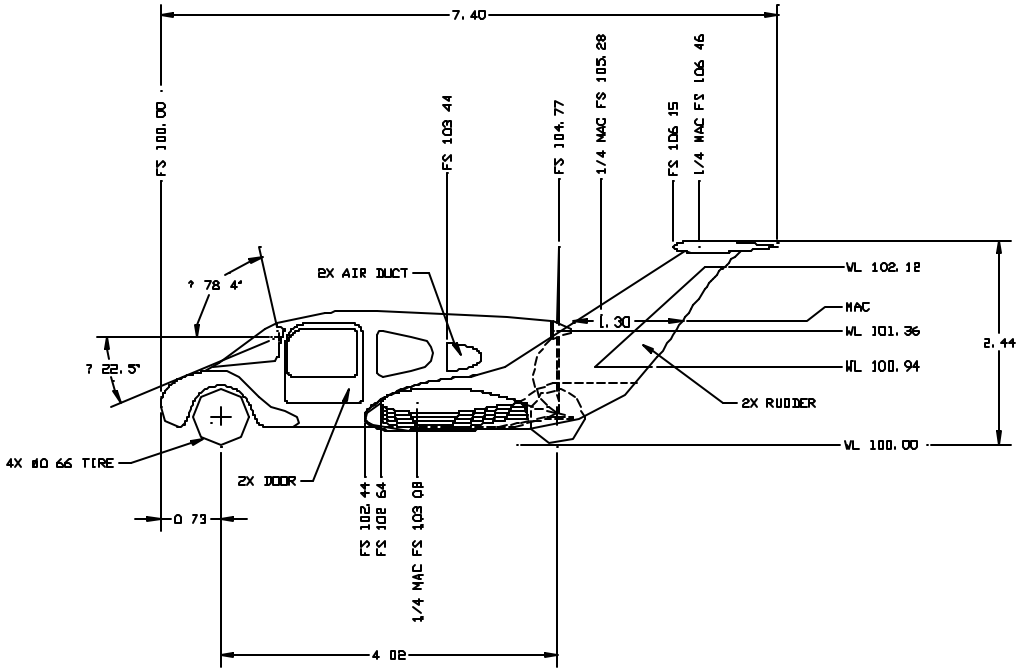

Figure M.3-1 Dimensioned Side View of the Pegasus

For suspension and ride analysis the vehicle must be separated into sprung and unsprung masses. The body is a single lumped mass and each wheel assembly is an unsprung mass of the following magnitude:

Unsprung Mass (each front wheel assembly) = 30 kg

Unsprung Mass (each rear wheel assembly) = 30 kg

Using Eqn's M-18 and M-19:

(M-18) $W_{fs} = W \cdot (c / L)$

(M-19) $W_{rs} = W \cdot (b / L)$

the static loads at MTOW, minimum operating weight, and an intermediate value (front passengers + ½ fuel) may be tabularized:

Table M.3-1 Operating Conditions

OPERATING CONDITION	**Mass (kg)**	**CG (m) *1**	**W_{fs} (N)**	**W_{rs} (N)**	**Load Distribution (F : R)**
Min Operating	1047	2.20	4650	5621	45 : 55
Front Passengers + ½ Fuel	1229	2.05	5908	6148	49 : 51
MTOW	1510	1.93	7701	7111	52 : 48

**1 From front axle.*

These operating conditions shall be used, where appropriate, throughout the vehicle performance analysis.

M.3.2. Road Loads

The total road load may be decomposed into the aerodynamic drag (Eqn M-20) and the wheel rolling resistance (Eqn's M-21 & M-22):

(M-20) $D_A = \frac{1}{2}\,\rho V^2 C_D A$

(M-21) $R_{xt} = f_r.W$

(M-22) $f_r = f_0 + 3.24 f_s (V/100)^{2.5}$

Values for the basic rolling resistance coefficient and speed coefficient may be estimated from Figure M3-2 as $f_o = 0.012$ and $f_s = 0.0075$:

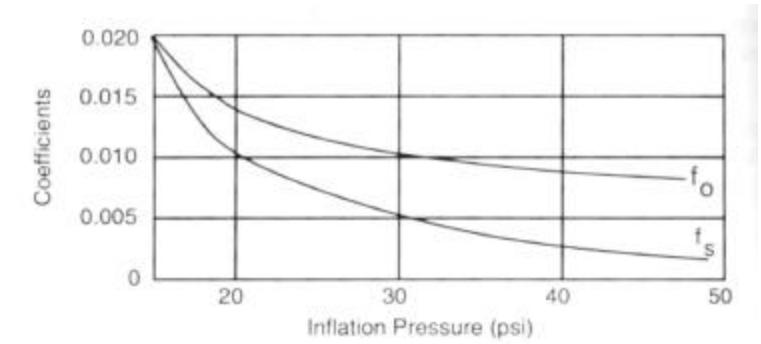

Fig. 4.34 Coefficients for Eq. (4-15).

Figure M.3-2 Tire Rolling Resistance Coefficient

Given a drag coefficient of 0.0275, based upon a 16.22m^2 (174.6 ft^2) reference area, the total road load and its components can be plotted against speed (Graph M 3-1).

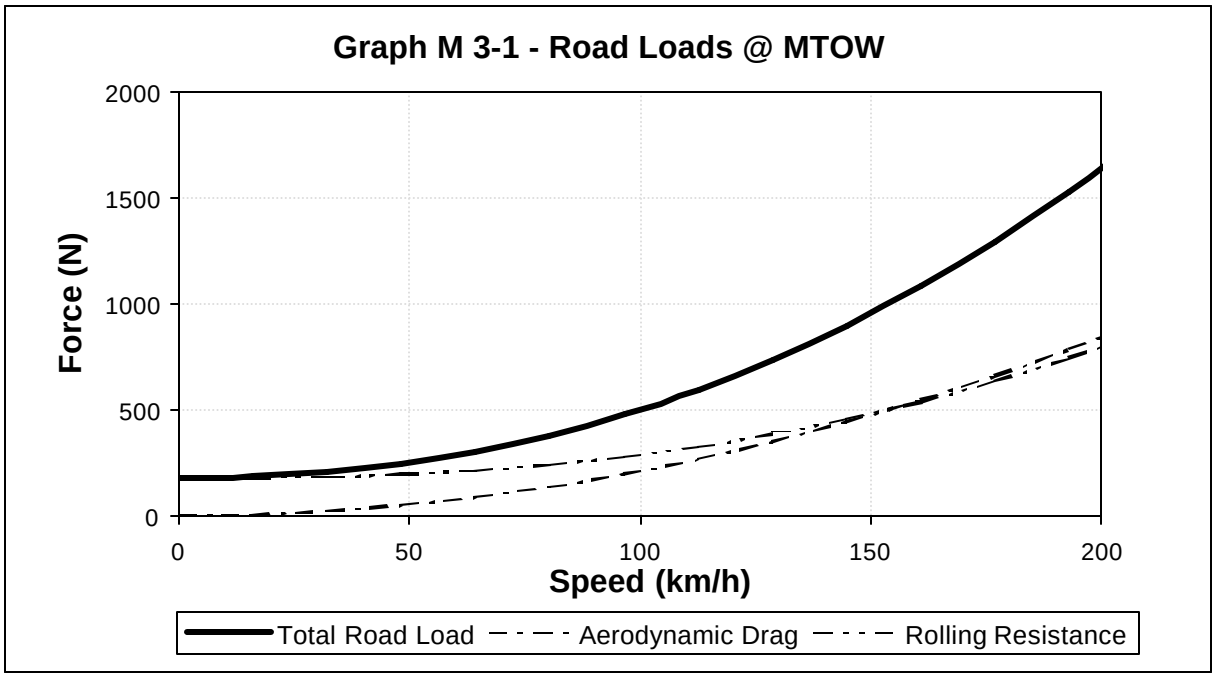

Figure M.3-3 Road Load Power vs. Speed

Using Eqn M-23:

(M-23) $$P_{RL} = R_{RL} \times V$$

the road load power may be plotted against speed (Figure M.3-3).

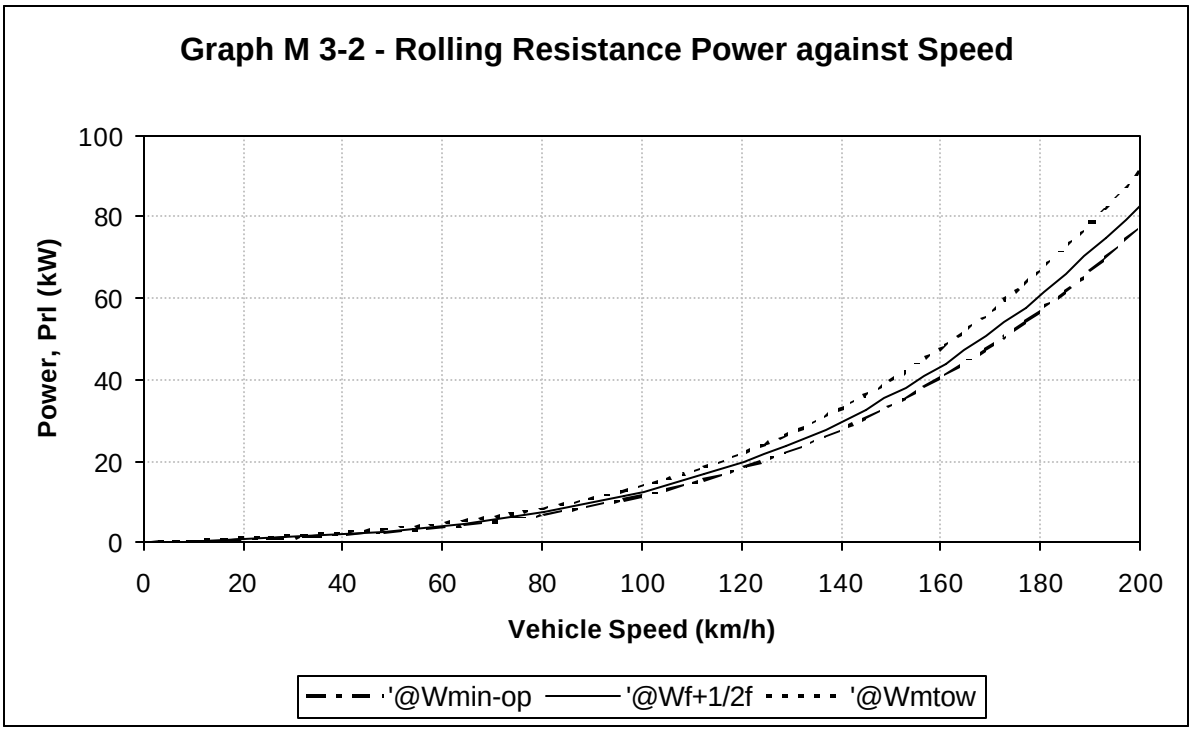

Figure M.3-4 Roling Resistance Power vs. Speed

The maximum available power can be determined from Eqn M-24:

(M-24) $$P = T\omega$$

This gives a value of 40.7kW, using a constant engine speed (due to the CVT) of 2700RPM. The maximum speed can now be read from Graph M 3-2 as 160km/h (99mph) at minimum operating weight.

Graph M 3-2 shows the power required to overcome the road load forces, and at a cruise speed 105km/h (65mph) a power of approximately 15kW is required at MTOW.

M.3.3. Aerodynamic Lift

In order to ensure the safety and stability of the vehicle it is necessary to calculate the lift force caused by the inboard wing of the vehicle. The suspension is designed such that the fuselage is at 0° incidence at the minimum operating weight, and pitches slightly nose downwards as the loading increases. Using Eqn M-25:

(M-25) $$L_A = \tfrac{1}{2}\,\rho V^2 C_L A$$

Given that the lift coefficient is 0.143 (based on 2^o wing incidence) for a stub wing reference area of $5.7m^2$ ($61.35\ ft^2$), the lift force may be calculated as 997N (224.1 lbf) at 160km/h (99.4 mph). In the worst case, with the front suspension at full rebound and the rear at full bump, the fuselage is at 2.4^o incidence and the lift coefficient is 0.204 giving a lift force of 1422N (319.7 lbf) at 160km/h (88.4 mph). The lift force therefore causes a maximum of a 14% reduction in effective body weight; this should not adversely effect the vehicle's road performance.

Given that the lift coefficient is 0.143 (based on 2° wing incidence) for a stub wing reference area of $5.7m^2$, the lift force may be calculated as 997N at160km/h. In the worse case, with the front suspension at full rebound and the rear at full bump, the fuselage is at 2.4° incidence and the lift coefficient is 0.204 giving a lift force of 1422N at 160km/h. The lift force therefore causes a maximum of a 14% reduction in effective body weight; this should not adversely effect the vehicle's road performance.

M.3.4. Acceleration

Using Eqn's M-26 & M-27:

(M-26) $$ma_x = F_x - R_x - D_A$$

(M-27) $$ma_x = \eta \frac{T_e \omega_e}{V} - \tfrac{1}{2} \rho V^2 C_D S - f_r.W$$

The acceleration over a range of speeds may be determined, using values for engine torque of 180Nm (132.7 lbf-ft), a drive efficiency of 0.8, and a constant engine speed, due to the CVT, of 2700RPM. The maximum acceleration of the vehicle is plotted in Graph M 3-3, for the specified operating conditions across a range of velocities:

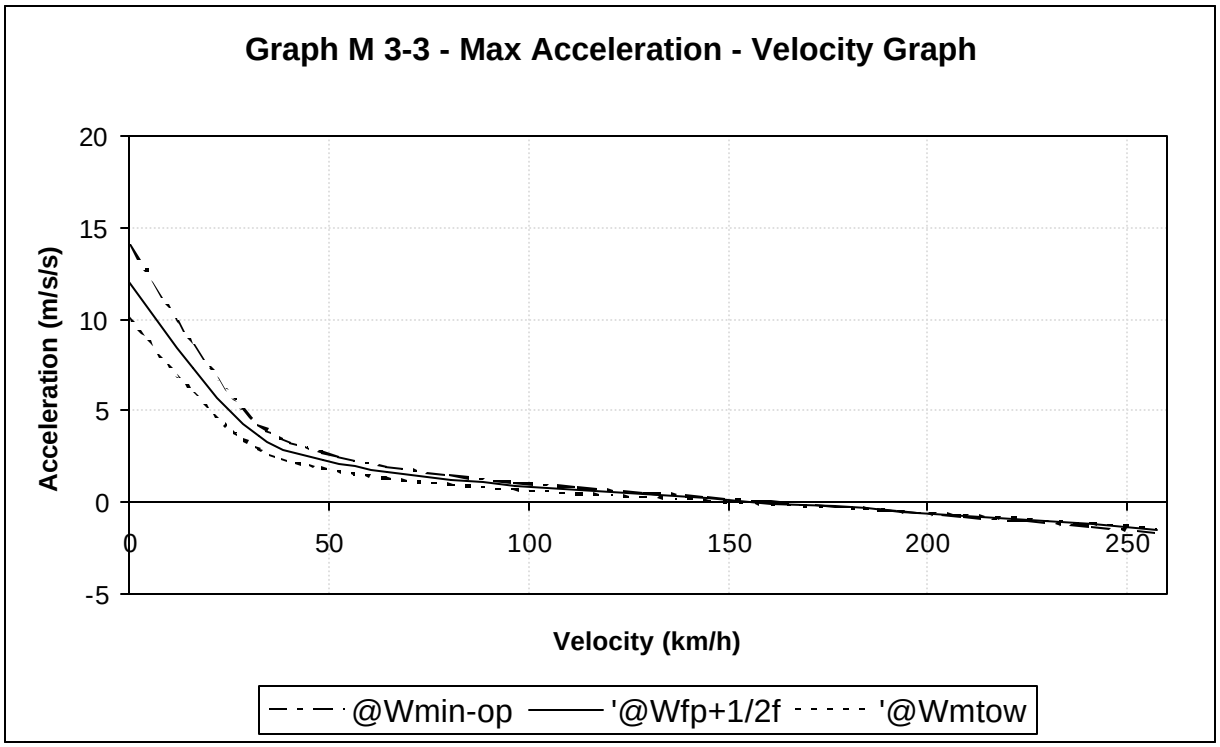

Figure M.3-5 Maximum Acceleration vs. Velocity

From Newton's Laws of Motion an acceleration-time graph may be produced (Graph M 3-4) that shows a minimum 0-100km/h (0-60 mph) time of approximately 11 seconds at minimum operating weight, and 16.5 seconds at MTOW. This model is extremely crude for

initial accelerations and does not take into account loss of traction effects; hence these values should be used for guidance only.

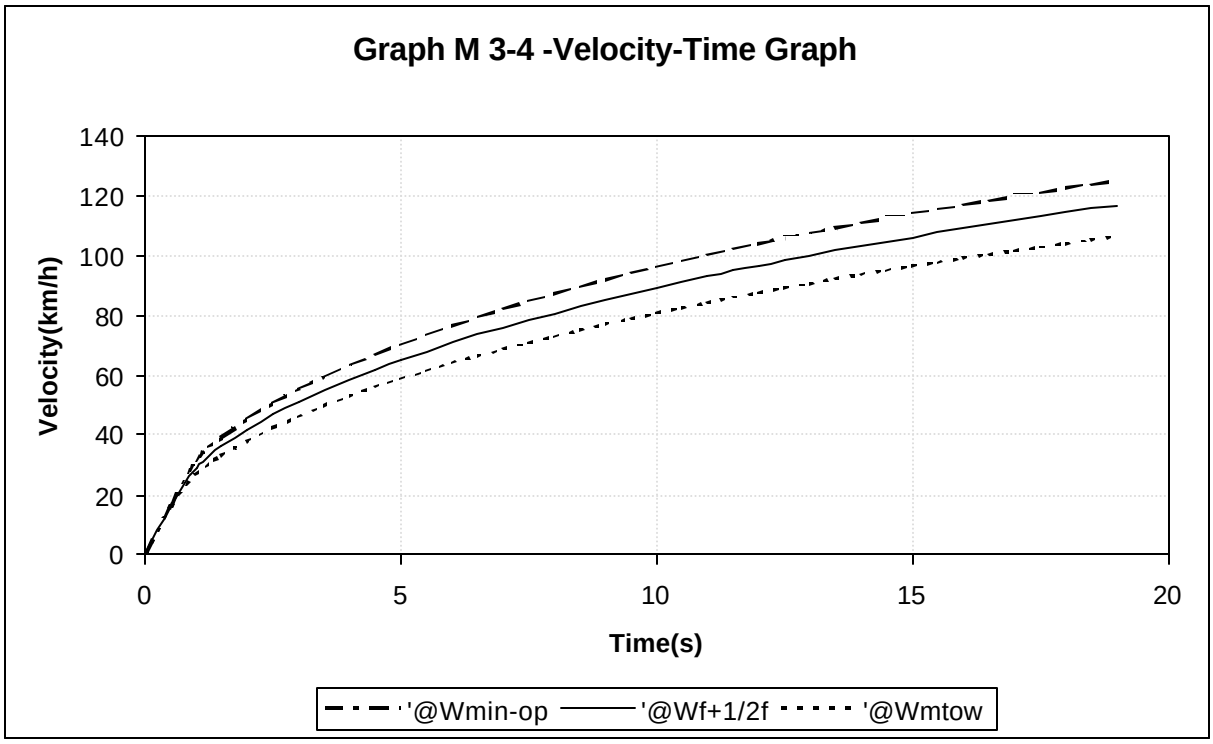

Figure M.3-5-a Velocity-Time Graph

M.3.5. Braking

The requirements of EC Directive 71/320 and ECE Directive 13 stipulate that for a M1 classified vehicle:

With the engine disengaged the required stopping distance, SD (m) may be calculated from the velocity, v (km/h) using:

$$SD = 0.1v + v^2/150$$

which at a test speed of 80km/h (49.71 mph) gives a stopping distance of 50.7m (166.3 ft). The brake control force must be no greater than 500N (112.4 lbf).

The EC requirement includes a component for driver reaction time (SD = 0.1v), hence removing this component gives the braking performance of the vehicle from the application of the brakes to a complete stop. The stopping distance of the vehicle from the application of the brakes is SD = $v^2/150$ = 42.66m (140.0 ft). Using Eqn's M-28 to M-31:

M-28) $$ma_x = -F_b - R_x - D_A$$

(M-29) $$D_x = \frac{F_{xt}}{m} = -\frac{dV}{dt}$$

(M-30) $$V_0 = \frac{F_{xt}}{M} t_s$$

(M-31) $$SD = \frac{V_0^2}{2\frac{F_{xt}}{M}} = \frac{V_0^2}{2D_x}$$

The minimum vehicle deceleration, total deceleration force, and stopping time may be calculated as:

D_x = 5.8m/s^2 (19.0 ft/s^2)

F_x = 8738N (1964.4 lbf)

t_s = 3.84s

This analysis is based upon the engine disengaged case at MTOW, with no retarding force being supplied by engine braking.

A more complex analysis, Eqn's M-28 and M-32, takes into account aerodynamic drag and rolling resistance forces, giving a retardation force from the wheel brakes of 8671 N (1949.3 lbf).

(M-32) $$SD = \frac{m}{2C} \ln\left[\frac{(F_b + R_x) + CV_0^2}{(F_b + R_x)}\right]$$

Including a margin for error and to allow for brake wear, the total braking force to be supplied by the brakes is set at 9000N (2023.3 lbf). Using Eqn M-32, and setting a constant value for the rolling resistance coefficient of 0.015 for passenger cars on a concrete surface[3], the stopping distance can be plotted against initial velocity (Graph M 3-5).

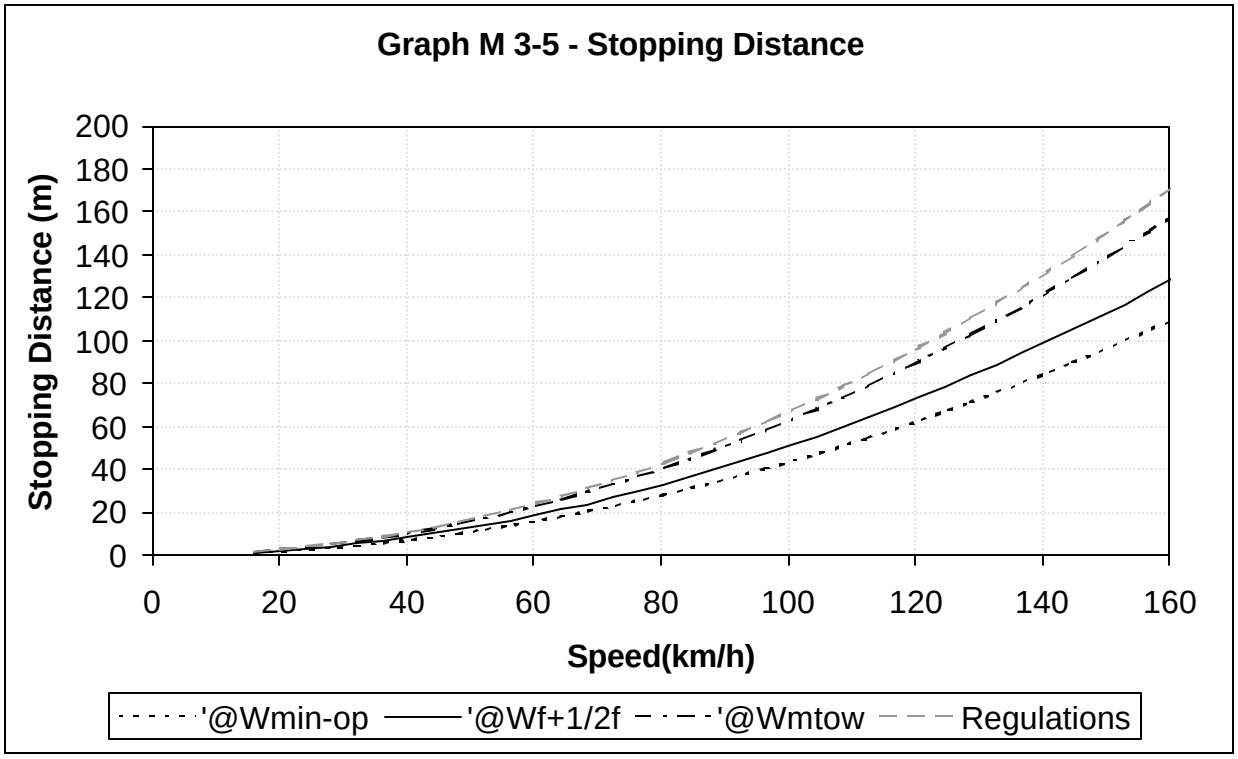

Figure M.3-6 Stopping Distance vs. Speed

M.3.6. Steady-State Cornering (Simple Analysis)

The cornering behavior of a motor vehicle is often equated with 'handling'. Handling is a loose term that refers to the subjective measurement of the vehicles response by the driver, as part of a 'closed loop' vehicle-driver system. For determining the behavior of the vehicle alone, the 'open loop' system, the vehicle's directional response may be measured. The most

commonly used measure of the vehicle's open loop response is the understeer gradient, which is a measure of steady-state performance that can be used to infer performance in quasi-steady-state conditions[3].

Eqn M-33 presents a simplified steady-state cornering model based upon a bicycle-type vehicle, and uses tire cornering stiffness to calculate the understeer gradient.

(M-33) $$\delta = 57.3\frac{L}{R} + \left(\frac{W_f}{C_{af}} - \frac{W_r}{C_{ar}}\right)\frac{V^2}{gR}$$

(M-34) $$CC_a = C_a / F_z$$

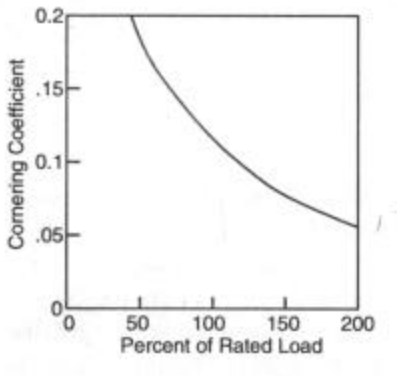

Figure M.3-7 Cornering Coefficient

The single-tire cornering stiffness' for the roadable aircraft were estimated, based on the cornering coefficient (Eqn M-34), which may be calculated using the tire load as a percentage of the rated load. Using Figure M3-3, the following values can be obtained:

Operating Condition	**Mass (kg ,lbs)**	**C_{af} (N/deg,lbf/deg)**	**C_{ar} (N/deg,lbf/deg)**
Min. Operating	1047,2308	405,91.05	479,107.7
Front passengers	1229,2709	472,106.1	507,114.0

+ ½ fuel			
MTOW	1510,3329	500,112.4	533,119.8

When using the bicycle model (Eqn M-33) the values for single-tire cornering stiffness must be doubled to obtain the tire cornering stiffness' across the front and rear axles. The understeer gradients, K, may now be determined:

$K_{min\text{-}op}$ = -0.12deg/g

$K_{f+1/2f}$ = 0.17deg/g

K_{mtow} = 0.95deg/g

The effect of the understeer gradient is as follows:

Table M.3-2 Understeer Gradient

	Understeer gradient, K	**Slip angles, a**	**Behavior on constant radius turn**
Neutral Steer	K = 0	$\alpha_f = \alpha_r$	Slip angles equal with increasing a_y hence no change in steering angle required.
Understeer	K > 0	$\alpha_f > \alpha_r$	With increasing a_y front wheel slip increases compared to back, increasing steering angles required.
Oversteer	K < 0	$\alpha_f < \alpha_r$	With increasing a_y back wheel slip increases compared to front, decreasing steering angles required.

Understeer reduces the lateral acceleration gain and the yaw velocity gain (rate of change of heading angle) and hence too much understeer will produce a sluggish vehicle response. A certain degree of understeer is favourable as it provides safe handling characteristics compared to the oversteer case in which the vehicle can become unstable, typical values are in the region 1deg/g.

M.3.7. Yaw Velocity Gain and Characteristic Speed

The yaw velocity, or yaw rate, of the vehicle is the rate of change of heading of the vehicle (deg/s). The yaw velocity gain is the ratio that represents a gain that is proportional to velocity in the case of a neutrally steered vehicle, and will effect the subjective evaluation of the vehicles handling by the driver. Using Eqn M-35:

(M-35) $$\frac{r}{d} = \frac{V/L}{1 + KV^2 \big/ 57.3Lg}$$

The yaw velocity gain may be plotted as a function of speed for the roadable aircraft across the specified load range (Graph M 3-6).

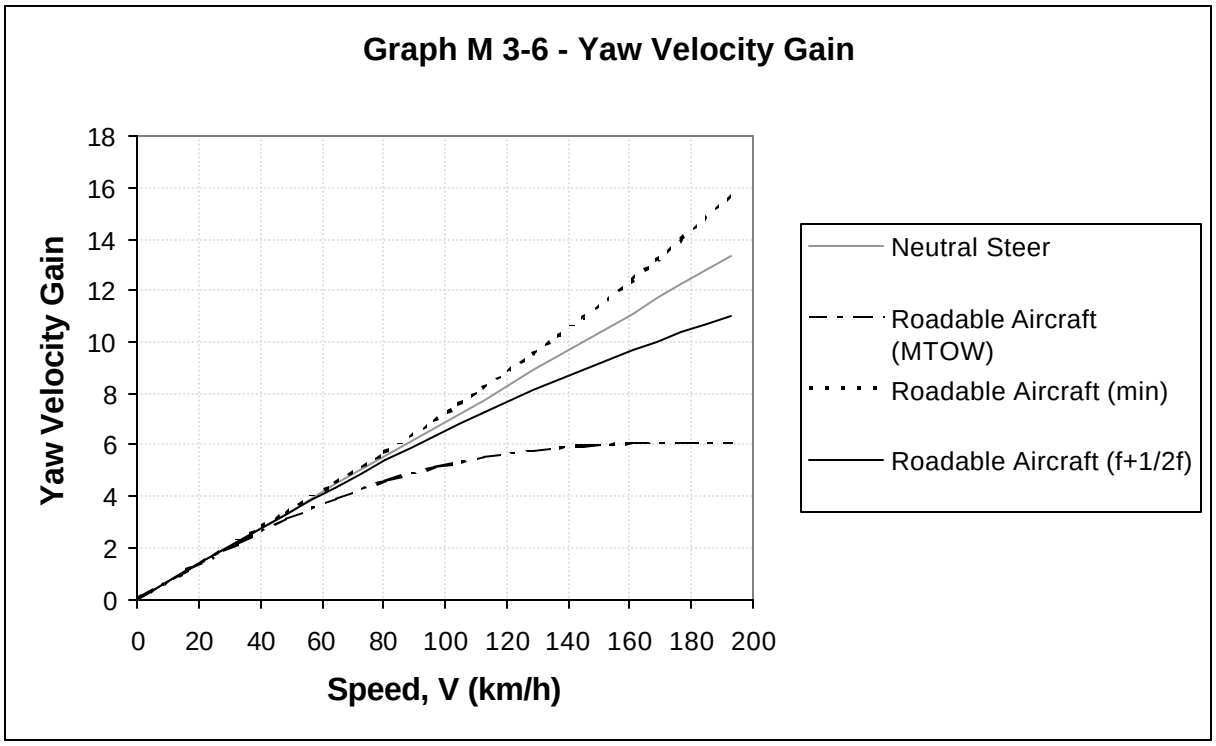

Figure M.3-8 Yaw Velocity Gain

Graph M 3-6 shows a wide variation in the Yaw Velocity Gain with vehicle weight. As a result, the handling of the vehicle will change significantly with weight, from sharp handling at the minimum operating weight to sloppy handling at MTOW.

The characteristic speed is the speed at which the vehicle is most responsive in yaw. Above the characteristic speed the vehicle has good straight line stability but its turning performance will be poor. The characteristic speed can be calculated using Eqn M-36, for MTOW, as approximately 176km/h (109.36 mph), which is above the maximum speed of the vehicle.

(M-36) $$V_{char} = \sqrt{57.3Lg/K}$$

This means that the vehicle will have good steering response across its speed range.

M.3.8. Side Slip Angle

The sideslip angle, β, is defined as the angle between the longitudinal axis and the local direction of travel, at the center of gravity. At higher cornering speeds the rear of the vehicle drifts outwards to generate the necessary slip angles on the rear tires, and this will cause the sideslip angle to move from positive (towards the turn center) to negative (away from the turn center). The speed $V_{\beta=0}$ at which this transition occurs is independent of the radius of turn and may be calculated using Eqn M-37:

(M-37) $$V_{b=0} = \sqrt{57.3 g c C_{ar} / W_r}$$

This gives a zero sideslip velocity of approximately 36km/h across all operating conditions. Above this speed the rear of the vehicle will slip outwards during turning. For a 50m (164.0 ft) radius turn the sideslip angle with a lateral acceleration of 0.4g is 4.9° at MTOW; this angle will be noticeable but not significant.

M.3.9. Steady-State Cornering (Complex Analysis)

The complex analysis of steady-state cornering uses a four-wheel model, based upon Eqn's M-38 to M-44:

(M-38) $$K = K_{tyres} + K_{llt} + K_{at}$$

(M-39) $$K_{llt} = \frac{W_f}{C_{af}} \frac{2b\Delta F_{zf}^2}{C_{af}} - \frac{W_r}{C_{ar}} \frac{2b\Delta F_{zr}^2}{C_{ar}}$$

(M-40) $$\Delta F_{zf} = \frac{1}{t_f} \left[K_{ff} \frac{Wh_1}{K_{ff} + K_{fr} - Wh_1} + W_f h_f \right] \frac{V^2}{Rg}$$

(M-41) $$\Delta F_{zr} = \frac{1}{t_r}\left[K_{fr}\frac{Wh_1}{K_{ff}+K_{fr}-Wh_1}+W_r h_r\right]\frac{V^2}{Rg}$$

(M-42) $$K_f = 0.5K_w t$$

(M-43) $$F_y = C_a \boldsymbol{a} = (aF_z - bF_z^2)\boldsymbol{a}$$

(M-44) $$K_{at} = W\frac{p}{L}\frac{C_{af}+C_{ar}}{C_{af}C_{ar}}$$

This analysis takes into account the lateral load transfer effects of the suspension, where load is shifted to the outer wheels, and also the aligning torque effects, caused by lateral forces being developed in a tire behind it's roll center. The model does not account for tire camber or steering effects.

Given an empirically estimated value for the second polynomial of cornering stiffness as 0.00036, a CoG height of 0.54m (1.77 ft) above the bottom of the fuselage, a front roll center calculated as the bisection of a line parallel to the suspension arms running through the tire contact patch with the vehicle center-line, and a rear roll center height taken as the roll center of the rear wheels, the following parameters were obtained:

Table M.3-3 Load Cases

Load Case	**h_f (m,ft)**	**h_r (m,ft)**	**CG_x(m,ft) *1**	**h_1 (m,ft)**	**DF_{zf}/a_y (N/g,lbs)**	**DF_{zr}/a_y (N/g,lbs)**
$W_{min\text{-}op}$	0.41,1.35	0.324,1.06	2.2,7.22	0.577,1.89	3012,6640	2936,6472
W_{front} + ½ fuel	0.34,1.12	0.324,1.06	2.05,6.73	0.624,2.05	3417,7533	3398,7491
W_{mtow}	0.26,0.85	0.324,1.06	1.93,6.33	0.585,1.92	3927,8657	4130,9105

**1 From the front axle*

Using these values and Eqn M-39 & Eqn M-44 and a value for the pneumatic trail of 0.01m, the understeer gradients can be recalculated:

- $K_{total} = K_{tyres} + K_{at} + K_{llt}.a_y$
- $K_{Wmin\text{-}op} = -0.12 + 0.10 + 0.72a_y$ deg/g
- $K_{Wf+1/2f} = 0.17 + 0.11 + 0.53a_y$ deg/g
- $K_{Wmtow} = 0.95 + 0.13 + 0.79a_y$ deg/g

These values show that both the effects of aligning torque and lateral load transfer contribute to increasing the total understeer gradient of the vehicle. The understeer gradient is plotted against lateral acceleration for all three operating conditions (Graph M 3-7).

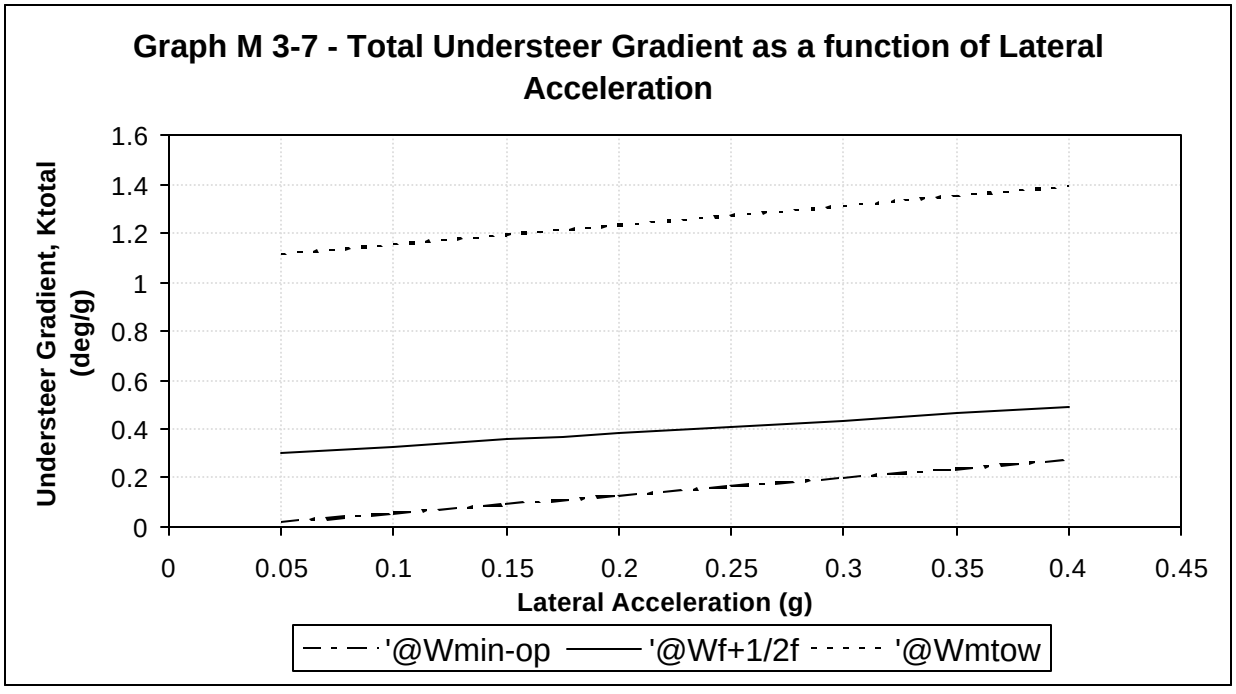

Figure M.3-9 Understeer Gradient

The graph shows steadily increasing understeer across all operating conditions. The steering angles are depicted for an example turn of 50m (164.04 ft) radius (Graph M 3-8).

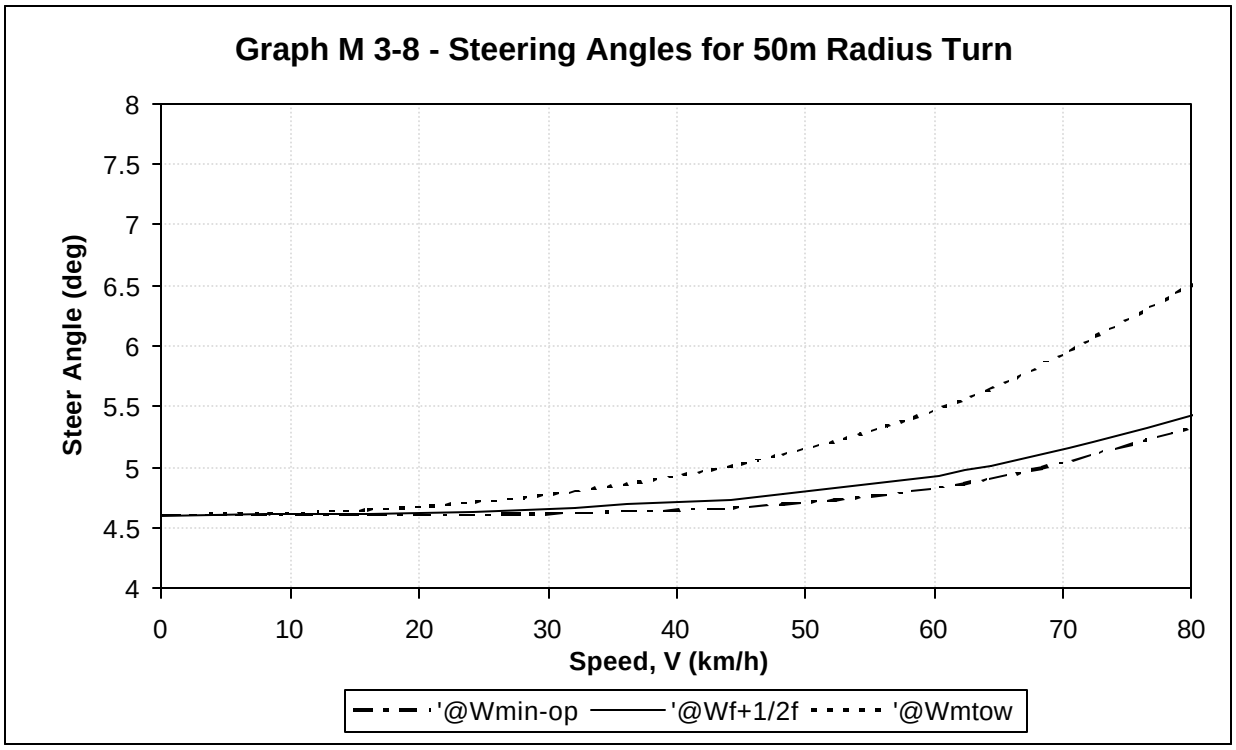

Figure M.3-10 Steering Angles for Fifty Radius Turn

M.3.10. Rollover

Using Eqn's M-45 & M-46:

(M-45) $$\frac{a_y}{g} = \frac{t}{2h}\frac{1}{\left[1+R_f\left(1-h_r/h\right)\right]}$$

(M-46) $$R_f = {d_f}\Big/{a_y} = \frac{Wh_1}{\left(K_{ff}+K_{fr}-Wh_1\right)}$$

The lateral acceleration required to induce rollover can be calculated as ranging between 0.98 to 1.00g's of lateral acceleration, from minimum operating to maximum take-off weight. Given that maximum cornering accelerations usually exceed no more than 0.4g, the rollover case presents no threat to the vehicle or it's occupants.

M.4. Transport Regulations

As a roadable aircraft, the Pegasus must meet the US and European driving regulations. Due to the similarities between these regulations, the Pegasus needed to comply with only one of these. The UK regulations were used as specifications for the design as outlined in section M.4.2.

M.4.1. Example UK/EC Regulations

The Roadable Aircraft is classified as a Motor Car, according to UK Construction & Use Regulations, and is categorized as an M1 type vehicle according to the EEC Classification, whereby:

Category M : Motor vehicles having at least four wheels, or having three wheels when the maximum weight exceeds one metric ton, and used for the carriage of passengers.

Category M1 : Category M vehicles used for the carriage of passengers having not more than eight seats in addition to the drivers seat.

The Construction & Use Regulations[1 & 6] are briefly summarized below in three categories: dimensions, performance, and required equipment. The regulations presented no major problems to the configuration chosen.

M.4.1.1. Dimensional Regulations

- Maximum Length = 11m
- Maximum Width = 2.5m
- Rear Overhang must not exceed 60% of the wheelbase.
- Exterior mirrors must not project more than 20cm from the vehicle (if placed under 2m above the road surface).
- Positioning of lights – see Toyne[XXXM6].

M.4.1.2. Performance Regulations

- Capable of powered reverse travel.
- Power must be at least 4.4kW for every 1000kg of the max. gross weight.
- Must comply with EC directives for emissions.
- Noise emission no greater than 80dB under test conditions.
- The driver must have a clear view of the road in front of him
- Must comply with the EC Directives on performance of service, secondary and parking brake systems (see Bosch Automotive Handbook[XXXM1]).

M.4.1.3. Required Equipment Regulations

- Springs must be provided between the body and the wheels.
- A protective steering mechanism must be provided.
- Door latches and hinges must be fitted and capable of absorbing crash impact
- The vehicle must be fitted with windscreen wipers & washers, a speedometer (10% accuracy), an audible warning, mirrors (interior and offside *or* two exterior), a silencer, manufacturers and ministry plates, parking brakes, seat belts and pneumatic tyres.
- The petrol tank must have national type approval.
- Specified Safety Glass must be fitted to the windows in front and either side of the driver. Other windows must be fitted with Specified Safety Glass or Safety Glazing.

1) Bosch(1996) *Automotive Handbook 4th Edition* Robert Bosch GmbH

2) Dunn (1999) *Suspension Design* AAETS, Loughborough University.

3) Gillespie (1992) *Fundamentals of Vehicle Dynamics* SAE Inc.

4) Spring Design AE-21 (1996) SAE Inc

5) Stinton (1983) *The Design of the Aeroplane* Blackwell Science Ltd

6) Toyne (1982) *Motor Vehicle Technical Regulations 3rd Edition* Ruislip Press Ltd.